Fakultät für Medizin

Optical analysis of microRNA activity and therapeutic manipulation of microRNA-29 *in vivo*

Petros Avramopoulos

Vollständiger Abdruck der von der Fakultät für Medizin der Technischen Universität München zur Erlangung des akademischen Grades eines

Doktors der Naturwissenschaften (Dr. rer. nat.)

genehmigten Dissertation.

Vorsitzender: Prof. Dr. Thomas Misgeld

Prüfer der Dissertation:

1. Prof. Dr. Dr. Stefan Engelhardt
2. Prof. Dr. Arne Skerra

Die Dissertation wurde am 15.01.2019 bei der Technischen Universität München eingereicht und durch die Fakultät für Medizin am 13.08.2019 angenommen.

Ἰθάκη

Σὰ βγεῖς στὸν πηγαιμὸ γιὰ τὴν Ἰθάκη,
νὰ εὔχεσαι νἆναι μακρὺς ὁ δρόμος,
γεμάτος περιπέτειες, γεμάτος γνώσεις.
……
Ἡ Ἰθάκη σ᾽ ἔδωσε τ᾽ ὡραῖο ταξίδι.
Χωρὶς αὐτὴν δὲν θἄβγαινες στὸν δρόμο.
Ἄλλα δὲν ἔχει νὰ σὲ δώσει πιά.

Κι ἂν πτωχικὴ τὴν βρῇς, ἡ Ἰθάκη δὲν σὲ γέλασε.
Ἔτσι σοφὸς ποὺ ἔγινες, μὲ τόση πείρα,
ἤδη θὰ τὸ κατάλαβες ἡ Ἰθάκες τί σημαίνουν.

Κ. Π. Καβάφης

Ithaka

As you set out for Ithaka
hope your road is a long one,
full of adventure, full of discovery.
……
Ithaka gave you the marvelous journey.
Without her you wouldn't have set out.
She has nothing left to give you now.

And if you find her poor, Ithaka won't have fooled you.
Wise as you will have become, so full of experience,
you'll have understood by then what these Ithakas mean.

C. P. Cavafis

Abbreviations

AAV	adeno-associated virus
AF	atrial fibrillation
Ago	Argonaute / Ago clade protein
AMCF	adult mouse cardiac fibroblasts
AMCM	adult mouse cardiac myocytes
AMI	acute myocardial infarction
AngII	angiotensin II
ASO	antisense oligonucleotide
ATP	adenosine triphosphate
bp	base pair
BW	body weight
C. elegans	*Caenorhabditis elegans*
cDNA	complementary DNA
cEt	2',4'-constrained ethyl
CF	cardiac fibroblast
CM	cardiac myocyte
CMV	Cytomegalovirus
DAPI	4', 6-diamidino-2-phenylindole
DCM	dilated cardiomyopathy
ddH2O	double-distilled water
DGCR8	DiGeorge syndrome critical region 8
DNA	deoxyribonucleic acid
dNTP	deoxyribonucleoside triphosphate
ds	double-stranded
DTT	1,4-dithiothreitol
E.coli	*Escherichia coli*
ECM	extracellular matrix
EDTA	ethylenediaminetetraacetic acid
EF	ejection fraction
eGFP	enhanced green fluorescent protein
FACS	fluorescence-activated cell sorting
FFPE	formalin-fixed paraffin-embedded
FISH	fluorescent *in situ* hybridization
FITC	fluorescein isothiocyanate
FS	fractional shortening
H. sapiens	*Homo sapiens*
HEK	human embryonic kidney
I/R	ischemia-reperfusion
IF	immunofluorescence
ISO	isoproterenol
LNA	locked nucleic acid
lncRNA	long non-coding RNA
LV	left ventricle
$LVID_d$	left ventricular internal diameter end diastole
$LVID_s$	left ventricular internal diameter end systole
MI	myocardial infarction
miRNA	microRNA
MMP	matrix metalloproteases
mRNA	messenger RNA
NRCF	neonatal rat cardiac fibroblasts
NRCM	neonatal rat cardiac myocytes
nt	nucleotide(s)
PAGE	polyacrylamide gel electrophoresis
PBS	phosphate buffered saline
PCR	polymerase chain reaction
PE	phenylephrine
PFA	paraformaldehyde
PNA	peptide nucleic analog
pre-miRNA	precursor miRNA
pri-miRNA	primary miRNA
PS	phosphorothioate
qRT-PCR	quantitative real time polymerase chain reaction
RFP	red fluorescent protein
RISC	RNA induced silencing complex
RMCE	recombinase-mediated cassette exchange
RNA	ribonucleic acid
RNAi	RNA interference
rpm	revolutions per minute
RT	room temperature
RV	right ventricle
SEM	standard error mean
siRNA	small interfering RNA
ss	single-stranded
stRNA	small temporal RNA
TAC	transverse aortic constriction
TL	tibia length
UTR	untranslated region
WGA	wheat germ agglutinin
wt	wildtype

Table of Contents

List of Figures

1 Introduction

1.1 MicroRNA biogenesis and modes of action

Until recently, 99% of the human genome, that has no protein-coding potential[1], was considered as "junk" DNA. In the meanwhile, it has become common knowledge, that the vast majority of the DNA that gets transcribed to RNA but does not get translated to proteins can have important biological functions[2]. The noncoding RNAs are divided into two classes based on their size, the long noncoding RNAs, or lncRNAs, that are longer than 200 nucleotides, and the small noncoding RNAs, that are shorter noncoding RNA molecules. Among the small noncoding RNA classes, microRNAs (or miRNAs or miRs) have received special attention the last two decades. Lee et al. first observed that the *lin-4* gene did not code for a protein, but its RNA could negatively regulate the expression of LIN14 by antisense complementarity, thereby controlling *Caenorhabditis elegans* development in a temporal manner[3]. For several years this was thought to be an exception, until 2000, when another microRNA, *let-7*, was found to also regulate the developmental timing in *C. elegans* by negatively regulating the expression of the *lin-41* gene[4]. The finding that *let-7* was conserved in a wide range of animal species, including mammals, led to the idea, that it might play a similar role there[5]. Until then, *lin-4* and *let-7* were termed small temporal RNAs (stRNAs). Several groups identified that these two molecules were part of a larger class of small noncoding RNAs that posttranscriptionally regulate the expression of genes both in invertebrates and vertebrates, now termed microRNAs[6–8]. Since then microRNAs have been found among others in plants, viruses and humans[9].

1.1.1 Biogenesis of microRNAs

In animals, microRNAs are transcribed in the nucleus as a longer primary transcript called "pri-miRNA" by RNA polymerase II[10–12]. The pri-miRNA contains a hairpin region, that gets sequestered by the microprocessor, a trimeric complex consisting of one copy of the Drosha endonuclease and two molecules of its partner DiGeorge Syndrome Critical Region 8 (DGCR8 or "Pasha" in invertebrates)[13]. The two RNase III catalytic domains of Drosha cut the pri-miRNA in a way to produce a -approximately 60-70 nucleotides long- pre-miRNA, that consist of a stem-loop with a 2 nucleotide overhang on the one strand[14]. The pre-miRNA is then exported from the nucleus to the cytosol by Exportin 5 and Ran-GTP[15,16], and get cut by another RNase III enzyme, Dicer, resulting in a duplex of the mature microRNA (miR) and its passenger strand (miR*) miR : miR* [8,17]. The cutting results in a ~22 nucleotides (nt) long duplex, with 2 nt 3' overhangs at each end, a result of the cleavage of both RNase III enzymes, Drosha and Dicer[14,18]. The mature strand gets then incorporated into the RNA-induced silencing complex (RISC)[19,20] and is then directed against complementary 3' UTRs of mRNAs, and through its

direct interaction with an Argonaute protein is guided to either the transcriptional or translational repression, or even degradation of the target mRNAs[21,22]. The strand of the miR : miR* duplex with the less tight binding at its 5' is most likely to be chosen to be the mature strand[23]. The biogenesis, as well as the modes of action of a typical microRNA are depicted in **Figure 1.1**[24].

1.1.2 MicroRNA modes of action

MicroRNAs bind to their target mRNAs by complementary pairing of the nucleotides 2-8, also known as the "seed region"[25]. If the complementarity of the rest of the molecule is of very high degree, then the target mRNA can be degraded, most of the times in animals though, the complementarity is imperfect, leading to translational inhibition, or mRNA destabilization, or both[3,22,26]. The key component of the RISC complex, the Argonaute protein, is a protein family that consists of four members (AGO1- AGO4) in mammals, out of whom only AGO2 has the ability to cleave the target mRNA at the position that corresponds to nt 10-11 of the microRNA[27,28]. The main modes of action of microRNAs in mammals are translational repression - at either the initiation step or one of the post-initiation steps- or mRNA destabilization by deadenylation and subsequent mRNA decay, and their exact mechanisms are reviewed by[29]. Because only 7-8 nucleotides are required for miRNA : target mRNA interaction, one miRNA can target multiple targets, and one mRNA can be targeted by multiple miRNAs[25,30]. For that reason, miRNA families, that is miRNAs with the same seed sequence, are expected to have the same or similar targetome. It is believed that more than half of the human genes are regulated by microRNAs[31]. It is therefore not surprising that microRNAs have been found to be involved in the control of key steps in development[3,26,32], metabolism[33,34], and a wide variety of diseases, such as multiple types of cancer[35–37], Alzheimer's Disease[38], Parkinson[39], multiples sclerosis[40], viral infections[41], and diseases of the cardiovascular system[42–47].

1.2 MicroRNAs and cardiac remodeling

Cardiovascular disease is the most prevalent cause of death worldwide[48]. Cardiac remodeling is the change of the geometry, size and function of the heart, and can be divided in physiological (due to exercise or pregnancy), and pathological remodeling. Causes for the later can be an injury, such as acute myocardial infarction, or chronic stress, such as pressure or volume overload, which can be caused by chronic hypertension, congenital heart disease, aortic stenosis, or valvular dysfunction.

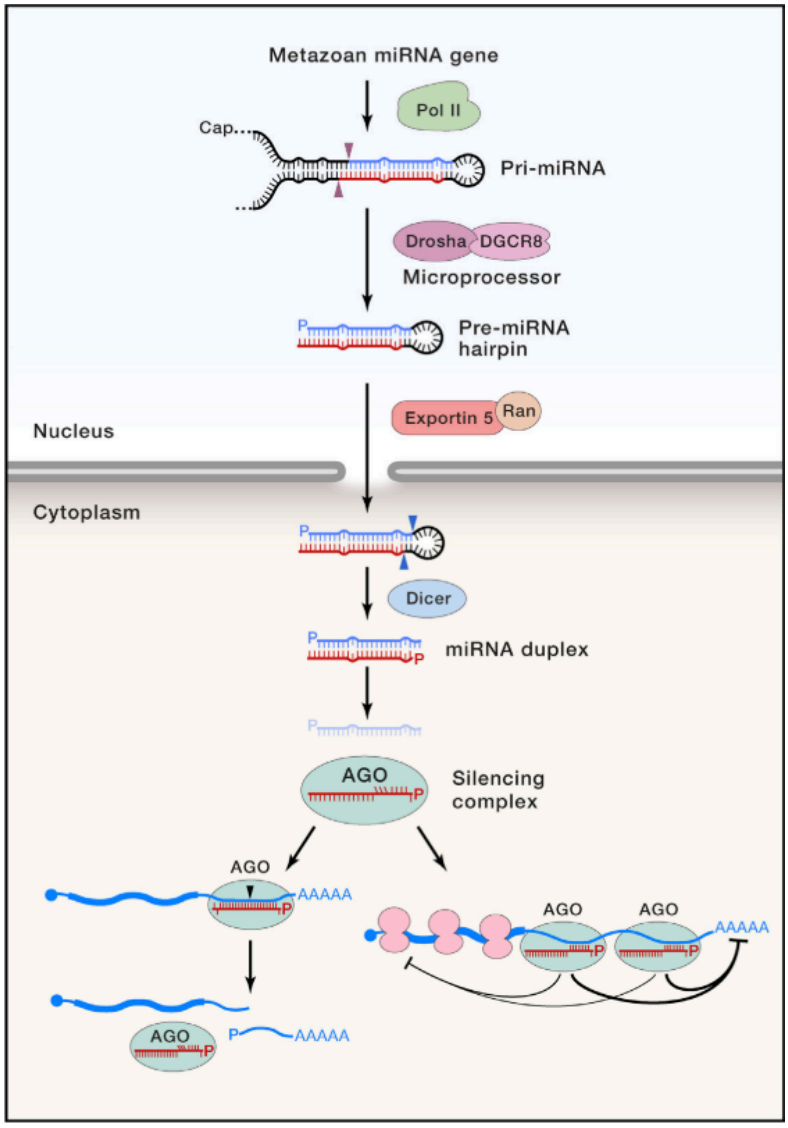

Figure 1.1. Biogenesis and modes of action of a typical miRNA

The miRNA gene is transcribed by Pol II, forming a primary transcript ("pri-miRNA") with an extensive stem-loop structure, which is then processed by Microprocessor, resulting in a pre-miRNA molecule. The pre-miRNA is then exported from the nucleus by Exportin 5 and Ran–GTP. Dicer, a second RNase III enzyme, cleaves the 60-70 nt long pre-miRNA, in a way to produce a ~22 nt long miRNA:miRNA* duplex, with 2 nt overhangs at each end. The mature miRNA strand (red), is incorporated into an Argonaute protein (AGO) to form the RISC complex, whereas the miRNA* strand (blue), is degraded. The so-called "seed region", consisting of the nucleotides 2–8 of the microRNA (upward red vertical lines) are guided to pair with complementary target mRNA. If the complementarity between the miRNA and the target is very extensive, the target can be cleaved by AGO (left; black arrowhead). In most cases concerning mammalian cells though, the complementarity is imperfect, resulting in translational repression of the target mRNA or mRNA deadenylation. Adapted from Bartel (2018)[24].

The word "remodeling" was first used with its current meaning to describe the increase in the size of the left ventricle in a rat model of myocardial infarction[49]. Unlike physiological remodeling during pregnancy or exercise, in pathological remodeling there is a worsening of cardiac function, that can result in heart failure[50]. Despite the treatment of the patients with ACE inhibitors, angiotensin II receptor blockers, aldosterone antagonists and β-blockers, the 5-year mortality of heart failure patients still remains close to 50%[51]. Therefore, there is a need

for development of new therapeutics, with microRNA manipulation strategies comprising a promising candidate for the future. Cardiac hypertrophy and fibrosis are the two hallmarks of cardiac remodeling. Several microRNAs have been implicated in cardiac hypertrophy[43,45,52] and fibrosis[42,44,53–55]. Among them, miR-29 drew our attention, because it appeared among the most potent hypertrophy-inducing microRNAs , although it was considered as an antifibrotic molecule[44]. This also points out the need for development of cell-type specific therapeutics.

1.2.1 Cardiac hypertrophy

Cardiac hypertrophy can be divided into eccentric (adaptive) and concentric (maladaptive) (**Figure 1.2**). The eccentric type is regarded as the physiological hypertrophy, such as in aerobic athletes or pregnancy[56], and is a result of volume overload. Concentric hypertrophy on the other hand, is pathological, is attributed to congenital heart defects, valvular disease, hypertensive cardiomyopathy, and comprises a response to pressure overload[57]. Pathological cardiac hypertrophy may start in order to compensate for the cardiomyocyte death and/or the improper pumping of the myocardium, but in the long term it becomes maladaptive and can lead to sudden death or heart failure[58].

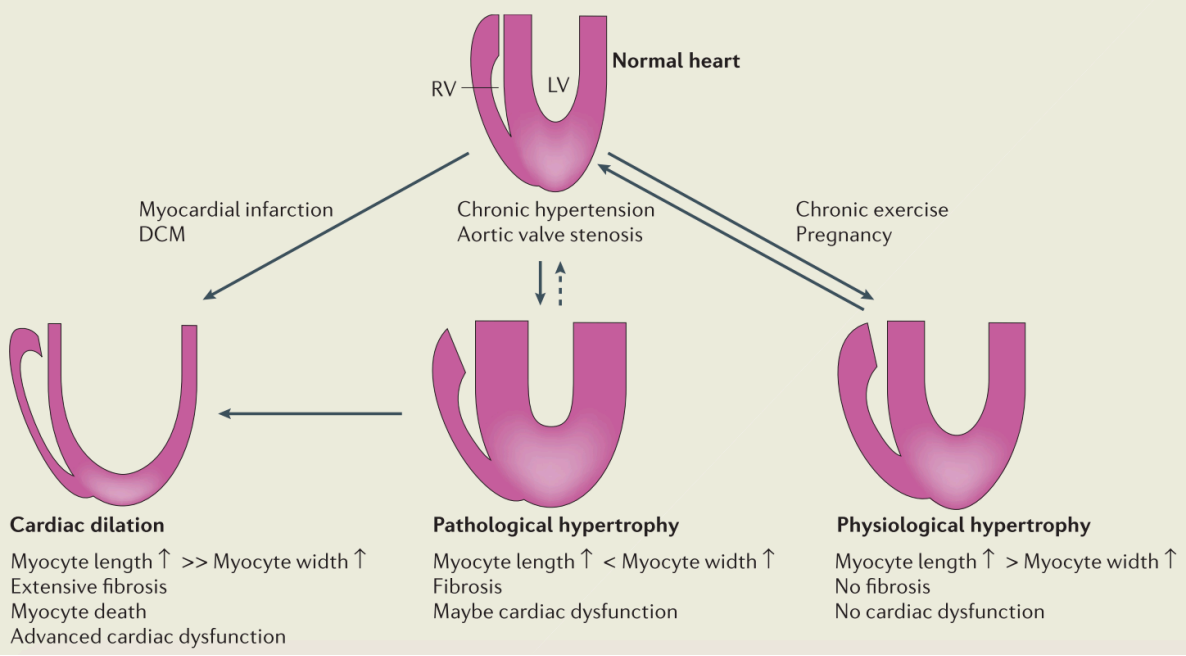

Figure 1.2. Types of cardiac hypertrophy

Chronic exercise or pregnancy can lead to physiological hypertrophy, which is characterized by a proportional increase in the cardiomyocyte width and length, that is accompanied by an increase in the ventricular chamber and normal cardiac function. Pathological hypertrophy on the contrary, is distinguished by a disproportional growth of the cardiomyocyte width than its length and decreased chamber size, that results in fibrosis and decreased cardiac function. Sometimes, in cases of extensive fibrosis, a type of remodeling called dilated cardiomyopathy can be observed, in which case the ventricular chamber is enlarged and weakened, leading to advanced cardiac dysfunction. DCM, dilated cardiomyopathy; LV, left ventricle; RV, right ventricle. Adapted from Heineke & Molkentin (2006)[57].

Pathological, in contrast to physiological hypertrophy, results in activation of the fetal gene program[59]. The two different types of hypertrophy have distinct molecular patterns and are characterized by discrete underlying signaling pathways[60].

1.2.2 Myocardial fibrosis

After an acute injury, the cardiac fibroblasts (CF) are activated, proliferate, excrete proinflammatory cytokines and ultimately turn into myofibroblasts[61,62] (**Figure 1.3**).

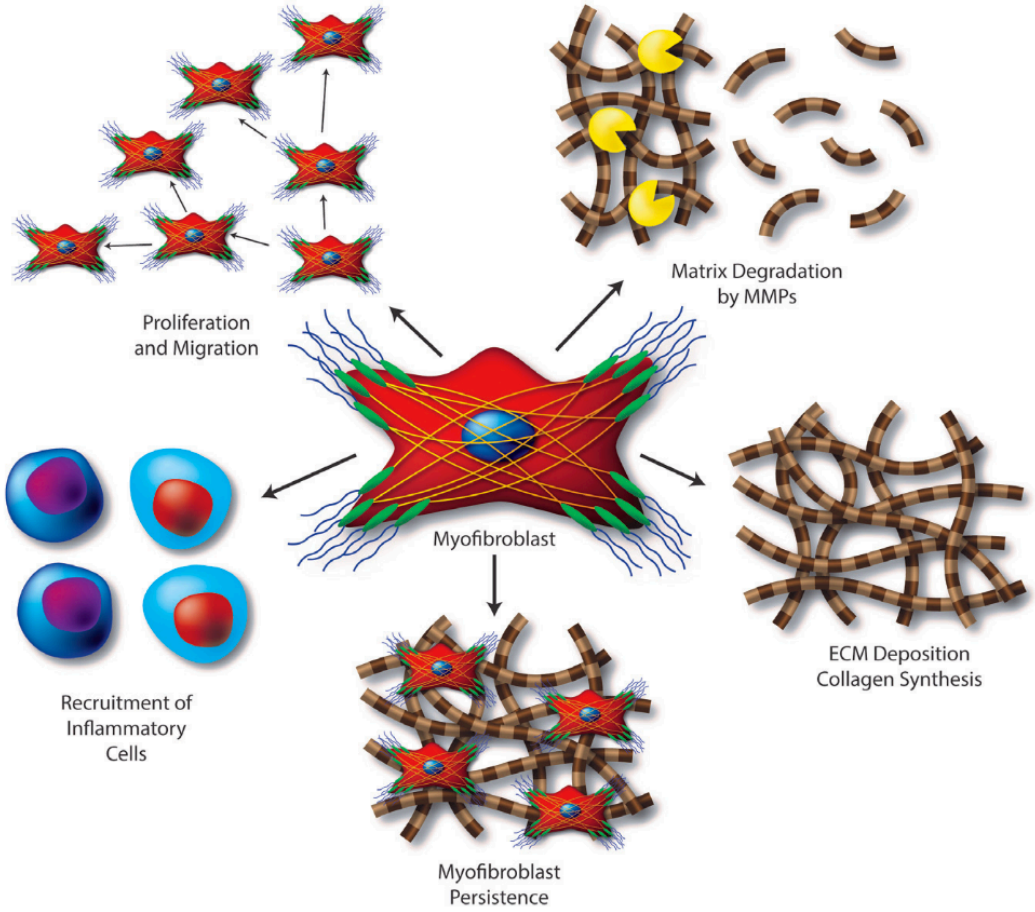

Figure 1.3. Characteristics and functions of activated cardiac myofibroblasts

During the pathogenesis of fibrosis, the cardiac fibroblasts transform into myofibroblasts, which excrete proinflammatory and profibrotic factors, produce matrix metalloproteases and other matrix degrading enzymes, which in turn leads to proliferation and migration of the myofibroblasts. Moreover, the activated myofibroblasts lead to accumulation of ECM. Persistence of myofibroblasts can lead to maladaptive fibrosis and ultimately heart failure. Adapted from Travers et al. (2016)[62].

This cell type produces collagens and extracellular matrix (ECM) in order to fill the gap of the dead cells, but long-lasting ECM deposition can lead to fibrosis, which increases the stiffness of the myocardial tissue, impairing the ventricular contraction and relaxation[63]. The fibrosis process might also induce cardiomyocyte hypertrophy via paracrine signaling[64]. Moreover, the electrical uncoupling of the cardiac fibroblasts from the cardiac myocytes can lead to arrhythmias and further cardiomyocyte (CM) dysfunctions[65]. Transverse aortic constriction

(TAC), is an animal model of pressure overload, that lead to CM hypertrophy. It also triggers a reactive interstitial fibrosis (adaptive), in order to replace the cell damage, succeeded by replacement fibrosis in areas of CM death[66].

1.2.3 Wnt signaling and its implication in cardiac hypertrophy

Cardiac hypertrophy is characterized by a plethora of underlying molecular mechanisms, such as cardiac myocyte proliferation, cell survival signaling and angiogenesis[60]. Among them, the Wnt signaling pathway possesses a pivotal role, which will be described in this chapter.

The Wnt signaling pathway is conserved from *D. melanogaster* till *H. sapiens* and was discovered in 1984 due to its involvement in carcinogenesis[67]. It has been shown to have a critical engagement in cardiac development[68,69]. Although it is quiescent under homeostatic conditions in adult mice, it gets activated upon pathological stress of the heart[70].

The Wnt signaling can be divided in canonical, which is β-catenin dependent[71] (**Figure 1.4**), and non-canonical, which is further subdivided in the Wnt/JNK (or planar cell polarity (PCP)) and Wnt/calcium pathways[72,73] (**Figure 1.5**).

Canonical Wnt signaling:

In the absence of a stimulus, that is a Wnt ligand, the “destruction complex”, composed of adenomatosis polyposis coli (APC), casein kinase 1 (CK1), AXIN, and glycogen synthase kinase 3β (GSK3β), retain β-catenin in the cytoplasm and mark it for degradation by the proteasome[74]. APC first phosphorylates Ser45 of β-catenin, which is followed by phosphorylation of β-catenin residues Ser33, Ser37, and Thr41 by GSK3β[75]. These sites are critical for the recognition by β-TrCP, a member of the ubiquitination machinery[76].

In the presence of a Wnt ligand, it binds to the extracellular domain of a seven-pass-transmembrane member of the G-protein coupled receptors (QPCRs) called Frizzled (FZD)[74], together with its coreceptors LRP5/6 (low density lipoprotein receptor-related)[77]. In humans, 19 members of the Wnt family and 10 Frizzled receptors have been identified[74]. As a result, disheveled-1 (Dvl-1) mediates the relocation of Axin from the cytoplasm to the plasma membrane, disassembling the destruction complex[78]. β-catenin is not any more tagged for degradation, accumulates in the cytoplasm and subsequently translocates to the nucleus, where it replaces GROUCHO, a transcription corepressor[74], binds to the transcription factor T-cell factor/lymphoid enhancer factor (TCF/LEF) and leads to an activation of the transcription of Wnt-responsive genes[74].

In the context of cardiac remodeling, Schans et al. showed that the onset of pressure overload-mediated cardiac hypertrophy was mitigated in mice lacking *Dvl-1*, in which the Wnt signaling was impaired[79]. In contrast, transgenic mice with a cardiac-specific overexpression of *Dvl*-1

resulted in cardiac hypertrophy by the age of 3 months and died prematurely because of cardiac dyfunction[70]. Moreover, *Wnt3a* has been found to be upregulated in ischemic cardiac myocytes[80] and *Fz2* expression was also increased in the left ventricles of rats undergone TAC[81].

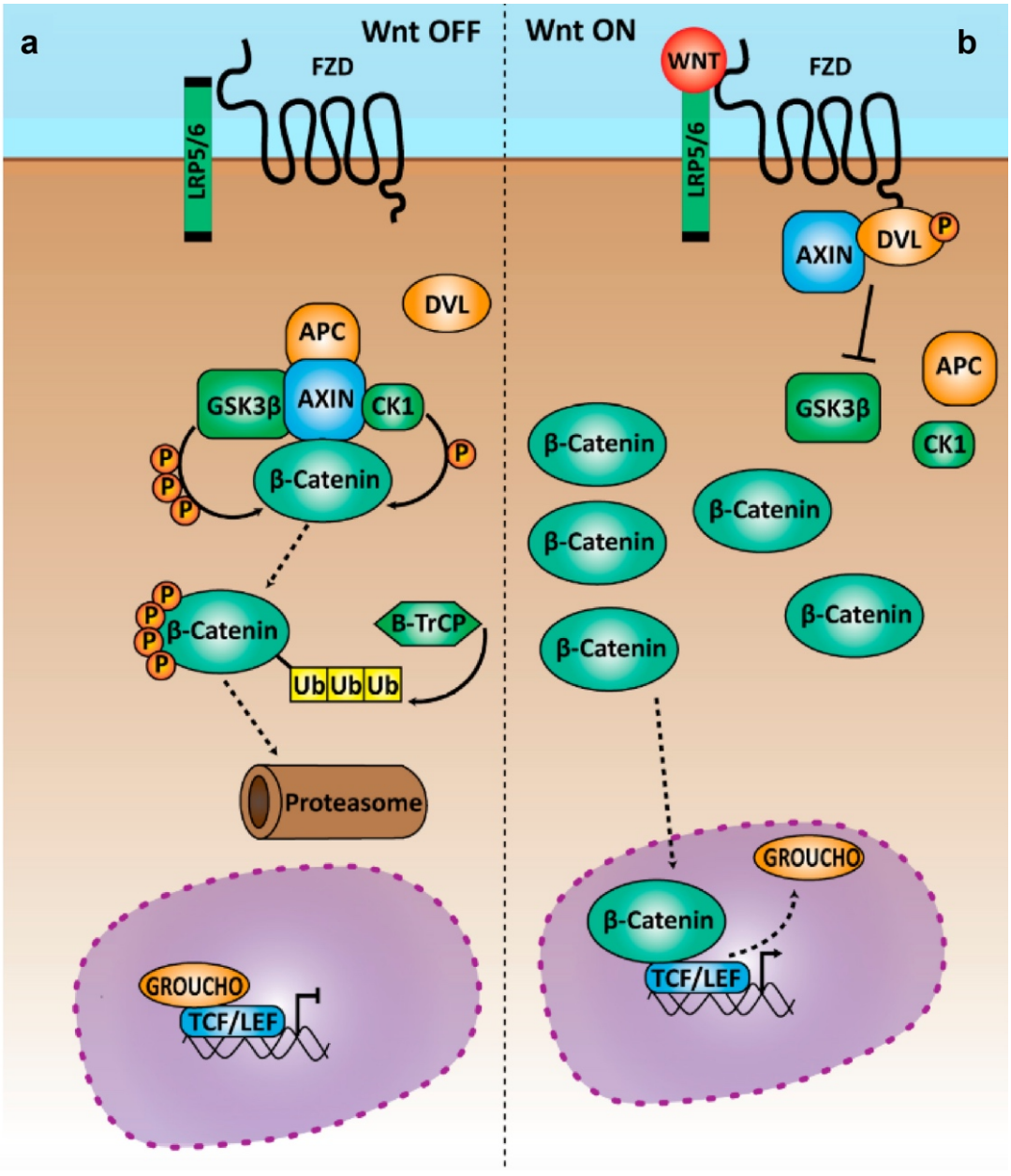

Figure 1.4. Canonical Wnt signaling

(**a**) In absence of Wnt (Wnt OFF status), the destruction complex of β-catenin phosphorylates β-catenin, leading to its ubiquitination by β-TrCP and its subsequent degradation by the proteasome. In this case, β-catenin cannot translocate to the nucleus and dispatch GROUCHO, a transcriptional repressor, so the Wnt-responsive genes do not get expressed. (**b**) In the presence of Wnt, it binds to the Frizzled-LRP5/6 coreceptors, leading to the disassembling of the destruction complex. The latter results in the accumulation of β-catenin in the cytoplasm, which then translocates to the nucleus, bind to TCF/LEF replacing the transcriptional corepressor GROUCHO. This triggers the activation of the Wnt-responsive genes. APC: adenomatous polyposis coli; CK1: casein kinase 1; DVL: dishevelled; FZD: frizzled; GSK3β: glycogen synthase kinase 3 beta; LRP5/6: lipoprotein receptor-related protein 5/6; Ub: ubiquitin. Adapted from de Jaime-Soguero et al. (2018)[82].

Wnt/ calcium signaling:

The Ca^{2+}-associated branch of the non-canonical Wnt pathway is illustrated in **Figure 1.5a**. After Wnt binding to a frizzled receptor, a trimeric G-protein activation leads to activation of Phospholipase C (PLC)[83]. PLC cleaves phosphatidylinositol-4,5-bisphosphate (PIP2) into inositol-1,4,5-trisphosphate (IP3), that triggers the release of Ca^{2+} from the endoplasmic reticulum (ER), and diacylglycerol (DAG), which stimulates protein kinase C (PKC)[84,85]. Increased Ca^{2+} concentration leads to activation of Ca^{2+}-sensitive proteins, such as calcineurin and the Ca^{2+}/calmodulin-dependent protein kinase II (CaMKII)[73]. Calcineurin then dephosphorylates the nuclear factor of activated T-cells (NFAT), whose activated form can translocate to the nucleus and drive the transcription of NFAT-responsive genes[86]. GSK3β on the other hand, can phosphorylate NFAT, inhibiting its translocation to the nucleus[87].

Wnt/ JNK signaling:

This branch of the non-canonical Wnt pathway, also known as the planar cell polarity pathway (PCP) from the early *Drosophila* studies, gets activated by binding of a Wnt ligand to a frizzled receptor independent of the LRP5/6 coreceptors[88] and is depicted in **Figure 1.5b**. Dishevelled associates with Dishevelled-associated activator of morphogenesis 1 (DAAM1) to signal to the small GTPase RhoA[89], leading to the stimulation of Rho-associated kinase ROCK, who is responsible for cytoskeleton re-organization[90]. In a parallel branch Dishevelled signals to a second small GTPase, Rac, which promotes JNK activity[91] through c-Jun, a member of the AP1 transcription factor complex[92].

In relation to cardiac remodeling, a constitutively active variant of GSK3β, where its serine-9 residue was mutated to alanine, protected the mice from cardiac hypertrophy, induced by calcineurin activation, β-adrenergic stimulation and pressure overload[93,94]. Moreover, a mutant form of NFAT lacking its regulatory N-terminal domain, where the GSK3β phosphorylation sites are located, was constitutively active in the nucleus, causing cardiac hypertrophy independent of calcineurin signaling[95].

Negative regulators of the Wnt pathway:

Except for the members of the destruction complex, that were mentioned before, there are still some molecules that are fine-tuning the activation of the Wnt pathway. The family of secreted frizzled-related proteins (sFRP) have a similar Wnt-binding domain as the frizzled receptors and are competing them for Wnt binding[96]. Wnt inhibitory factor 1 (WIF-1), can also bind to Wnt and inhibit signaling[97]. DKK1, a member of the dickkopf family, can bind to the LRP5/6 coreceptors and Kremen, internalize them and lead to their degradation, reducing the number of available receptors for Wnt signaling[96].

CTNNBIP1 (or ICAT) was shown to interact with β-catenin preventing it from binding to TCF/LEF[98]. HBP1 also binds to TCF/LEF leading to the silencing of the Wnt pathway[99]. HBP1 deficiency resulted in cardiac hypertrophy[100]. GLIS2 is also a negative regulator of the Wnt signaling by directly interacting with β-catenin[101].

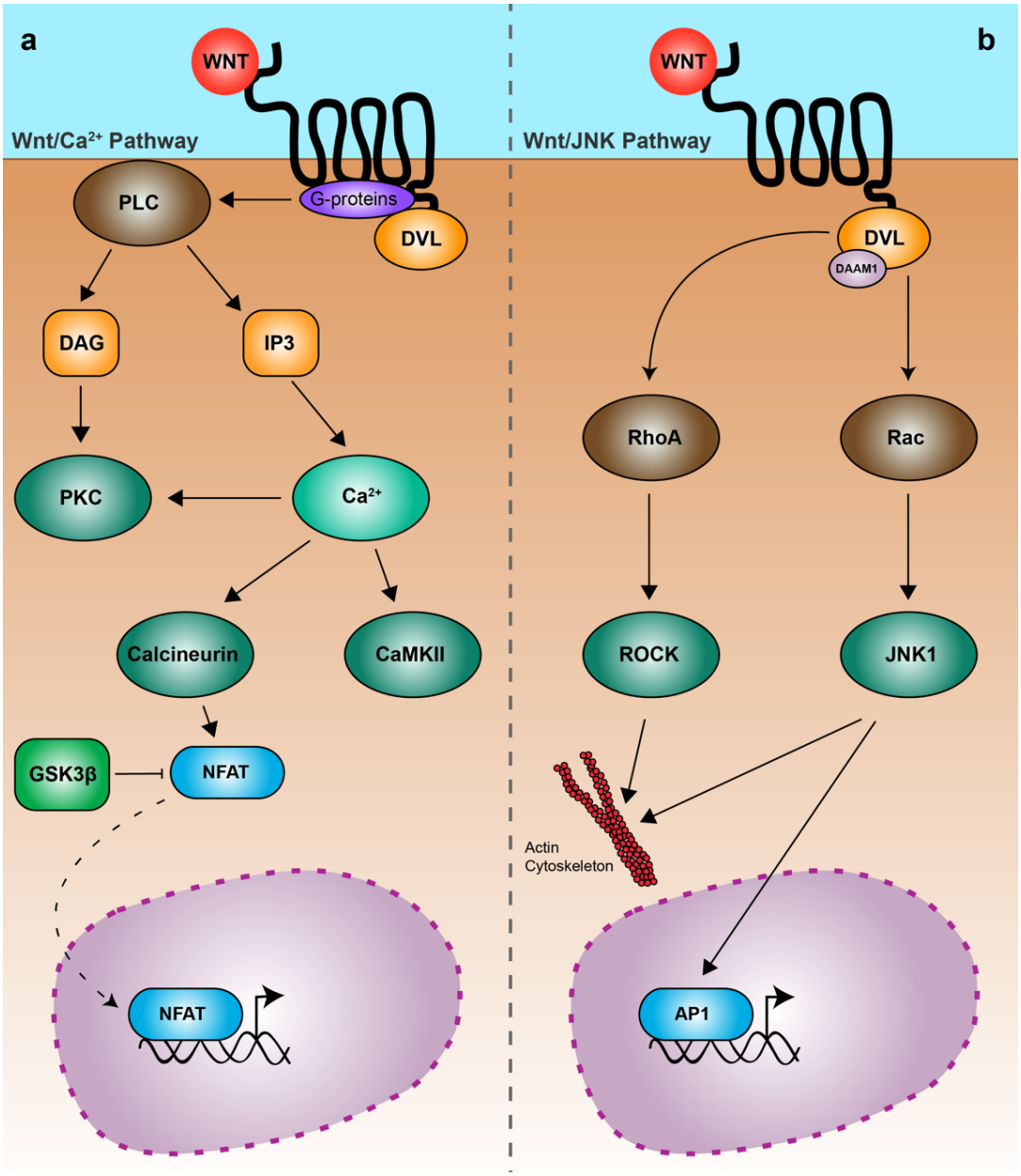

Figure 1.5. Non-canonical Wnt signaling

(**a**) Wnt/Ca^{2+} pathway. Wnt binding to a Frizzled receptor activates a trimeric G-protein, resulting in stimulation of the classical Ca2+ release pathway involving DAG, IP3 and the Ca2+-sensitive proteins CaMKII and Calcineurin. The latter dephosphorylates NFAT leading to its translocation to the nucleus and activation of NFAT-responsive genes. (**b**) Wnt/JNK pathway. Dishevelled-associated activator of morphogenesis 1 (Daam1) binds to Dishevelled (DVL) leading to Rho-associated kinase (ROCK) through the small GTPase Rho. In parallel DVL activates Rac, which signals to JNK1, that can lead to activation of the C-Jun transcription factor, that is part of the AP1 transcription factor complex. Both ROCK and JNK1 are involved in actin skeleton re-organization. Figure is drawn to match the style of **Figure 1.4**.

1.2.4 MicroRNAs implicated in cardiac hypertrophy and fibrosis

MicroRNAs in cardiac hypertrophy

MicroRNAs have been implicated in cardiac hypertrophy[43,45,52]. Among these microRNAs, miR-29 has been shown to target the expression of several profibrotic genes and to be downregulated in several fibrosis-mediating diseases[102–106]. These findings have led to the interpretation that miR-29 confers anti-fibrotic effects and that elevating the expression of this microRNA would be promising for an anti-fibrotic therapy.

MiR-1 was identified in 2002 by the group of Thomas Tuschl as a heart-specific microRNA[107]. Using a microarray, miR-1 was found to be downregulated in mice from day 1 till 1 week after TAC in comparison to sham[108]. The same study proposed Ras GTPase–activating protein (RasGAP), cyclin-dependent kinase 9 (Cdk9), fibronectin, and Ras homolog enriched in brain (Rheb), as miR-1 targets and showed miR-1 transfection *in vitro* to protect from serum- or endothelin-1 (ET-1)-induced cardiomyocyte hypertrophy. MiR-1 was also found downregulated in biopsies from hypertrophied hearts of human patients in comparison to healthy controls[43], suggesting a protective role for miR-1 against cardiac hypertrophy. In line with these data, miR-1 was shown to target a series of molecules involved in the development of cardiac hypertrophy, such as calmodulin, Gata4, Mef2a[109], insulin-like growth factor-1 (IGF-1)[110] and the cytoskeleton regulatory protein Twinfilin-1[111]. In another study, miR-1 overexpression via adeno-associated virus serotype 9 (AAV9) in rats subjected to TAC was able to reverse cardiac hypertrophy, function and decrease myocardial fibrosis[112]. The authors also suggested Fibullin-2, a secreted protein involved in ECM development, as a direct target of miR-1.

MiR-133 is clustered with miR-1 on the same chromosomal locus and are transcribed together in skeletal and myocardial tissues[113]. MiR-133 could inhibit cardiac hypertrophy *in vitro*, whereas a decoy inhibitor of miR-133 induced hypertrophy *in vitro*[43]. The same group was able to show, that *in vivo* administration of antagomir-133 stimulated cardiac hypertrophy, with direct miR-133 targets involved being RhoA and Cdc42, both regulators of cardiac hypertrophy, and Negative Elongation Factor Complex Member A (Nelf-A). Calcineurin was proposed to regulate and be regulated by miR-133 expression: both *in vitro* and *in vivo*, in cardiomyocyte hypertrophy (induced by phenylephrine and TAC, respectively), calcineurin expression was induced, whereas miR-133 levels declined[114]. In addition, cyclosporin A, a - in complex with cyclophilin - inhibitor of calcineurin could hinder the downregulation of miR-133 in cardiac hypertrophy.

MiR-208a has been shown to be necessary for cardiac hypertrophy, myocardial fibrosis, and β*MHC* expression after TAC and in hypothyroidism: importantly, genetic deletion of miR-208a, whose genetic location lies in an intron of the α*MHC* gene, prevented mice from developing cardiac hypertrophy and myocardial fibrosis after aortic banding[52]. Moreover, cardiac-specific

miR-208a knock-in was sufficient to induce pathological hypertrophy, with a simultaneous decrease in the expression of its targets Thrap1 and myostatin[115].

MiR-212/132 cluster is also necessary and sufficient to cause cardiac hypertrophy[45]. Genetic deletion of this cluster protected mice from TAC-induced heart failure, whilst its CM-specific overexpression resulted in maladaptive cardiac hypertrophy. Both microRNAs target the transcription factor Foxo3, which is known for its anti-hypertrophic and pro-autophagic properties. Of note, pharmacological inhibition of miR-212/132 after TAC prevented from pathological hypertrophy and myocardial fibrosis in mice, proposing a therapeutic potential of miR-212/132 targeting.

MiR-22 is upregulated in phenylephrine- (PE) and angiotensin II- (AngII) induced hypertrophic cardiac myocytes, transfection of it leads to increased hypertrophy, whereas its inhibition blunts the PE- or AngII-induced hypertrophy, at least in part, by targeting PTEN[116]. In a separate study, inhibition of miR-22 was also protective against cardiac hypertrophy[117]. Global and cardiomyocyte-specific miR-22 deletion, protected from cardiac remodeling induced either by isoproterenol (ISO) or a genetic model of cardiac hypertrophy caused by a CM-specific overexpression of calcineurin. Intriguing was the fact, that cardiac deletion of miR-22 resulted in dilated cardiomyopathy upon ISO treatment. Sirt1 (Sirtuin 1) and Hdac4 (histone deacetylase 4) were shown to be direct targets of miR-22 in the myocardium.

MiR-378 is substantially higher expressed in the neonatal than in fetal mice hearts, is muscle-specific and within the myocardium expressed only in cardiac myocytes[118]. Overexpression of miR-378 in cardiac myocytes leads to increased apoptosis, because of direct targeting of IGFR1 (insulin-like growth factor receptor 1) inhibiting the anti-apoptotic PI-3K (phosphatidylinositol3-kinase)/Akt pathway[118]. Our group showed, that miR-378 is anti-hypertrophic and can improve the cardiac function after pressure overload by targeting 4 key components of the MAPK signaling pathway: MAPK1, IGFR-1, GRB2 (growth factor receptor-bound protein 2), and KSR1 (kinase suppressor of ras 1)[46].

MiR-199a reduced autophagy and provoked cardiac hypertrophy by activating mTOR signaling and direct targeting of the anti-hypertrophic molecule Gsk3β[119]. MiR-199b targets Dyrk1a (NFAT kinase dual-specificity tyrosine-(Y)-phosphorylation regulated kinase 1a), thereby affecting the calcineurin/NFAT signaling pathway and leading to heart failure[120]. AntagomiR against miR-199b protected from and even reversed the cardiac hypertrophy and fibrosis caused by aortic binding in mice.

MicroRNAs in cardiac fibrosis

Our group was the first to describe the role of miR-21 in a cardiac disease model, demonstrating that it targets sprouty homolog 1 (Spry1) specifically in the cardiac fibroblasts,

thereby stimulating the ERK–MAP kinase activity pathway[42]. MiR-21 global knockout mice were not protected from pathological remodeling of the myocardium[121], whereas specific knockdown of miR-21 in the nonmyocytes could preserve the cardiac function in a pressure overload model in mice[55]. In a myocardial ischemia-reperfusion (I/R) model, miR-21 was found to directly target PTEN in cardiac fibroblasts, leading to derepression of MMP2 (matrix metalloprotein-2)[122].

MiR-30 and miR-133 both target connective tissue growth factor (CTGF), a key profibrotic molecule, protecting from extended ECM deposition[53]. In another study, miR-133a transgenic expression resulted in protection from myocardial fibrosis in a pressure overload model in mice[54].

MiR-29 was found to be downregulated after myocardial infarction in mice, but also in the border zone of the infarcted region from human patients receiving heart transplants[44]. In this study, the authors found miR-29 to be expressed higher in cardiac fibroblasts than myocytes, to target Elastin, Fibrillin and Collagens 1a1, 1a2 and 3a1, and after *in vivo* inhibition by antagomiR-29b they observed a modest derepression of the above mentioned collagens, at the mRNA level. They also observed, that treatment of cultured fibroblasts with transforming growth factor-β (TGF-β), the most important fibrosis mediator, decreased the levels of miR-29, leading the authors to the hypothesis, that after myocardial infarction, there is a TGF-β-mediated decrease of the anti-fibrotic miR-29. In a separate study, transfection of isolated cardiac fibroblasts with pre-miR-29 or antimiR-29 revealed several collagens, as well as leukemia inhibitory factor (LIF) and insulin-like growth factor 1 (IGF-1), as miR-29 targets[123]. After inhibition of miR-29b *in vivo* with antagomiR-29b after aortic constriction, the authors reported excess fibrosis without an obvious decline in cardiac function. Moreover, in an animal model of atrial fibrillation (AF) miR-29b levels were downregulated[124]. Transfection of atrial fibroblasts with miR-29b resulted in decreased expression of collagens and fibrillin, while miR-29 inhibition *in vivo* increased the mRNA level of *Col1a1*. The authors suggested miR-29b as a potential biomarker for AF, as they found it to be downregulated both in plasma and atrial tissue from AF patients.

Although circulating microRNAs in the serum had been proposed as biomarkers for some cancers, Ji et al. first proposed miR-208a, a cardiac-specific microRNA, as a marker for cardiac injury caused by isoproterenol infusion in rats[125]. More importantly, the authors found miR-208a levels in serum from rats with cardiac injury to correlate with the levels of cardiac troponin I, a well-established marker for myocardial injury. Since then, quite a few reports have suggested microRNAs as biomarkers of either myocardial infarction, heart failure, or other cardiac diseases[124,126–128].

The implications of microRNAs in cardiac remodeling are illustrated in **Figure 1.6**.

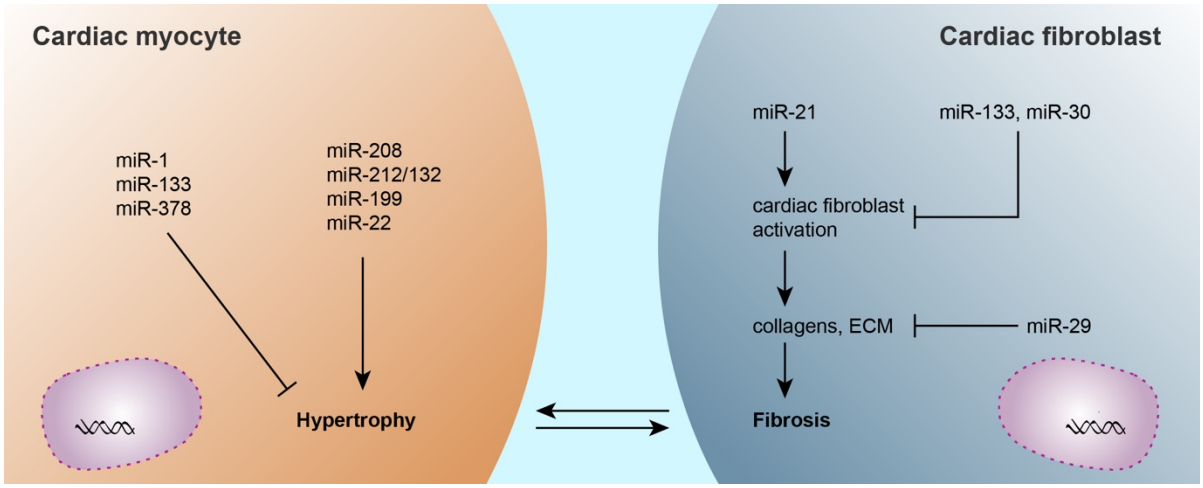

Figure 1.6. The implication of microRNAs in hypertrophy and fibrosis

In both cardiac myocytes and cardiac fibroblasts, microRNAs form complex regulatory networks, eventually leading to promotion or prevention from hypertrophy and fibrosis, respectively. The double arrows represent the interconnection between cardiac myocytes and cardiac fibroblasts.

1.2.5 Analysis of miR-29 in primary cardiac myocytes indicates a prohypertrophic role

As a validation of the surprising result of a screening from our group for hypertrophy modulating microRNAs in neonatal rat cardiac myocytes (NRCM), that found miR-29 to be among the most potent prohypertrophic microRNAs[129], Y. Sassi transfected NRCM with synthetic miR-29 molecules, that could successfully repress a luciferase reporter, indicating their activity (**Figure 1.7a**)[47]. Transfection of each one of miR-29a, miR-29b and miR-29c synthetic precursors, in the presence or absence of the α1 adrenoceptor agonist phenylephrine, led to a remarkable increase in the NRCM cell size (**Figure 1.7b**)[47]. This noteworthy finding encouraged our team to investigate the localization and expression pattern of miR-29 in healthy and diseased animals.

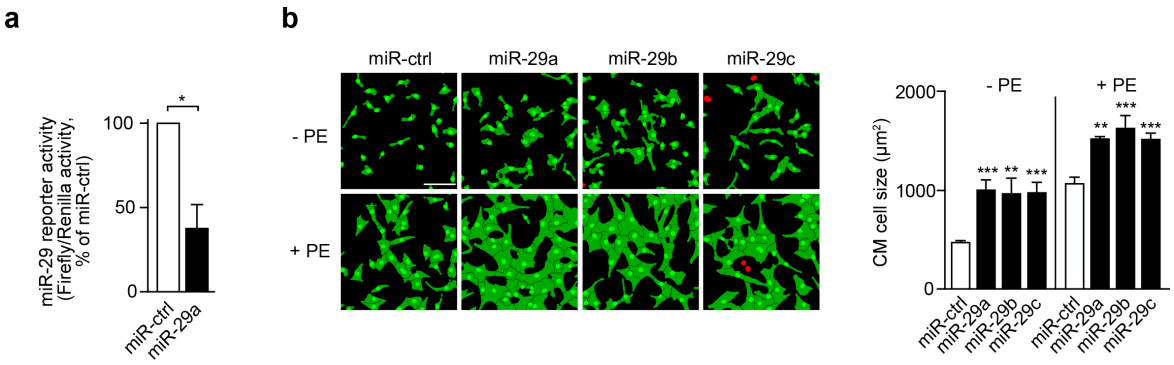

Figure 1.7. Each miR-29 family member promotes hypertrophy of cardiac myocytes *in vitro*

(**a**) Effect of a synthetic mimic of miR-29a on reporter suppression in primary cardiac myocytes. MiR-29a activity was determined by a reporter system where luciferase is under control of a miR-29a binding site, located 3' to the coding sequence of luciferase. Cardiac myocytes from neonatal rat

hearts (NRCMs) were transfected with miR-29a or miR-ctrl (50 nM each). Data are from 4 independent experiments performed in triplicate. P values determined by Student's t-test. (**b**) (Left) Automated cell detection-based imaging to determine cardiac myocyte cell size and purity of the cell preparations. After transfection of synthetic miRNAs or a control molecule, NRCMs were treated with the prohypertrophic α1-adrenoceptor agonist phenylephrine (50 μM for 48 h), fixed and stained with an antibody directed against α-actinin and DAPI. Automated cell scoring was then employed to determine cardiac myocyte dimensions (green) and the presence of contaminating non-myocytes (α-actinin-negative, depicted in red). Scale bar: 100 μm. (Right) Quantitative analysis of the results. Data are from 5-10 independent primary cell isolations. P values were determined by one-way ANOVA followed by Bonferroni's post hoc test. All quantitative data are reported as means ± SEM. *P<0.05, **P<0.01, ***P<0.001. Figure from Sassi, Avramopoulos, et al.[47]

1.3 MicroRNA manipulation strategies and microRNA detection methods

Considering the impact of microRNAs in regulating the expression of genes during development and homeostasis, but also under disease conditions, the need for evolving of microRNA manipulation strategies was evident. Currently, most of the clinical trials use antimiRs and not microRNA mimics. Miravirsen, an LNA-based inhibitor of the liver-specific miR-122 that combats hepatitis C viral infection (HCV), was the first microRNA-related drug used by Santaris/Roche in a Phase II clinical trial with positive results: it showed a dose-dependent antiviral activity[130]. Regulus/Sanofi is currently recruiting for a Phase II clinical trial, where RG-012, a miR-21 inhibitor, will be used in male subjects with Alport syndrome[131], a genetic condition caused by mutations in collagen type IV genes, that leads to hearing loss, eyes abnormalities, and, most importantly, progressive kidney disease. MiRagen Therapeutics Inc. is also recruiting for a Phase II clinical trial, but will use a miR-29 mimic, MRG-201, in order to investigate, if it can prevent or reduce the formation of fibrous scar tissue, in patients with a history of keloids.

1.3.1 Synthetic microRNA inhibitors

Based on beneficial effects upon manipulation of microRNAs in experimental disease models, an entirely new field of therapeutic development has emerged. Antisense oligonucleotides (ASOs) against miRNAs (AMOs or antimiRs) have become the gold standard for miRNA inhibition *in vitro*[132,133] as well as in preclinical[134–136] and clinical trials[130]. Although the vast majority of such synthetic oligonucleotides end up in the kidney and the liver, they have been shown to also target the heart[42,43,47,134,135,137]. A variety of chemical modifications has been applied to antimiRs in order to increase their nuclease resistance, cellular uptake, as well as the affinity to their target miRNA[132,133,138–144].

The most potent - in regard to target affinity - are the 2' ribose modifications, namely the 2'-O-Me, 2'-O-methoxyethyl (2'-MOE), 2'-F, and the locked nucleic acid (LNA) modification, where the sugar is constrained in a C3'-endo conformation through a 2'-O, 4'-C methylene

bridge[132,139,140,145–147]. The highest affinity to RNA is conferred by LNA moieties, with each single LNA monomer increasing the duplex melting temperature (Tm) from +2 to +8^{0}C[145,148–150]. A similar chemistry to LNA, cEt (2',4'-constrained ethyl), displays similar thermal stability and base discrimination ability, but increased nuclease resistance[151].

A remarkable nuclease resistance is granted by substitution of the phosphodiester backbone linkages with phosphorothioates (PS), where one of the non-bridging oxygen is replaced by a sulfur atom within the phosphate group. This, together with the increased binding to plasma proteins enhances the pharmacokinetic properties of an antimiR carrying a PS backbone[141,152,153]. On the other hand, each PS modification decreases the duplex melting temperature by 0.43 ^{0}C[154], and a fully PS modified backbone can become toxic, because of its extensive binding to plasma proteins[152]. Other chemistries used to confer nuclease resistance are the peptide nucleic acid (PNA) and morpholino ribose analogs[142,155–160]. PNA are uncharged peptide-like oligonucleotide analogs[161] that can bind microRNAs more effectively than 2'-O-Me analogs[155]. Although they cannot readily penetrate the cell, linkage to lysine residues or encapsulation in nanoparticles has been proved to enhance their cellular uptake[142,155–157]. Morpholino analogs are mainly used by developmental scientist for injection into embryos of *Zebrafish* or *Xenopus* species[158–160]. The diverse chemical modifications used in synthetic miRNA modulators are depicted in **Figure 1.8**.

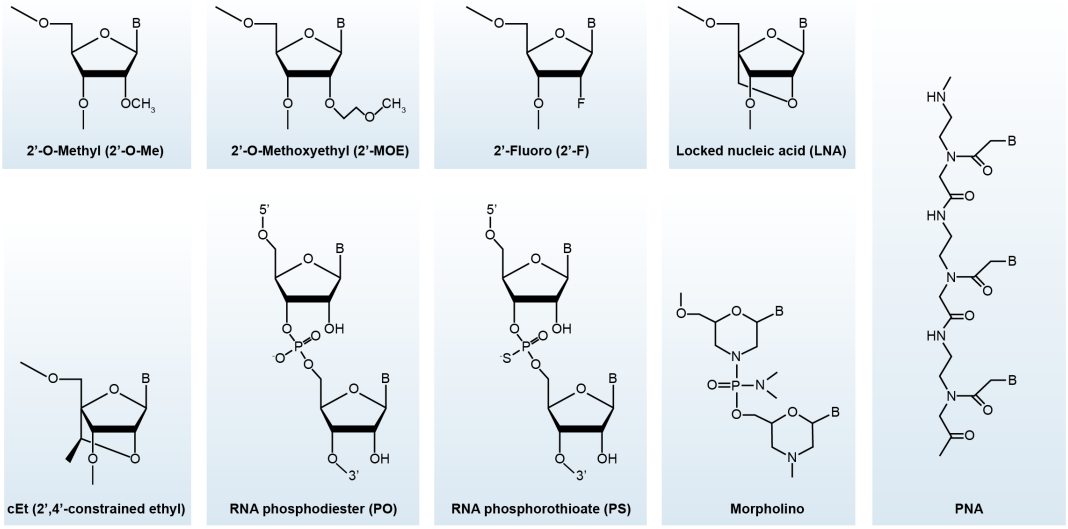

Figure 1.8. Chemical modifications used in synthetic miRNA modulators

Several sugar modifications are used to increase the duplex melting temperature (Tm) of antimiRs. The 2'-O-methyl (2'-O-Me), 2'-O-methoxyethyl (2'-MOE) and 2'-fluoro (2'-F) nucleotides replace the 2'-OH of the sugar, whereas LNA and cEt are bicyclic RNA analogs in which the ribose is locked in a C3'-endo conformation. Phosphorothioate (PS) backbone linkages increase nuclease resistance and enhance the pharmacokinetic properties of antimiRs in comparison to the normal phosphodiester (PO) bonds. Morpholino are uncharged oligomers that replace the sugar by a six-membered morpholine ring and display a slight increase in binding affinity to microRNAs. PNAs are also uncharged oligonucleotide analogs, where the sugar–phosphate backbone has been replaced by a peptide-like backbone. Modified and redrawn after van Rooij, Kauppinen (2014)[162].

The first antimiRs used *in vivo* were 3' cholesterol-conjugated, with 2'-O-Me ribose analogs, and complementary to the full length of the microRNA sequence and additionally modified with terminal PS linkages. These were termed antagomiRs[134] and were used for the first time in the cardiac context by the Condorelli's[43] and Engelhardt's[42] groups. The increased Tm conferred by the LNA moieties allowed the development of truncated antimiRs of 15-16 nucleotides in length[135,163,164]. Another approach to target microRNA families is to use the so-called tiny LNAs, fully LNA-modified 8-meR PS oligonucleotides complementary to the seed region of a microRNA[165,166]. Also chimeric oligonucleotides with two 2'-methoxyethyl (2'-MOE) nucleotides at both ends of the oligonucleotide and the rest being 2'-F analogs using a fully PS modified backbone, also known as 2'-F/MOE oligonucleotides, have been used with high potency in microRNA inhibition[140]. The various designs of antimiRs are depicted in **Figure 1.9**. Studies employing northern blotting and radiolabeled antimiRs showed that 2'-modified nucleic acids lead to a wide distribution of the antimiR, with the highest accumulation being in the kidney and the liver[134,135,137,165,167].

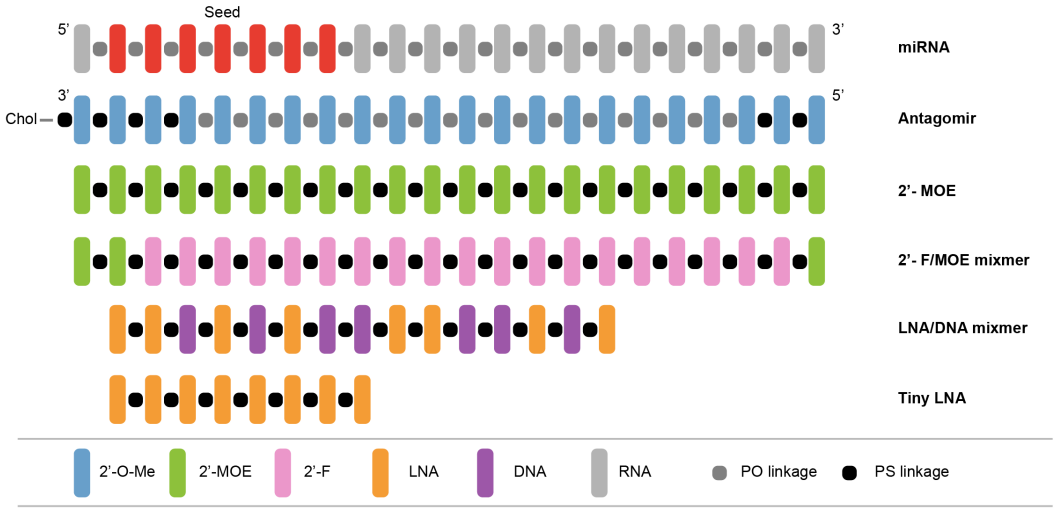

Figure 1.9. Design of chemically modified antimiR oligonucleotides

Antagomirs have a cholesterol molecule in their 3' to increase cellular uptake, 2'-O-Me oligonucleotides complementary to the full microRNA sequence with PS linkages at both ends to increase nuclease resistance. 2'- MOE-, 2'- F/MOE- or LNA-modified antimiRs with a complete PS backbone are comprising other designs. The higher affinity to their cognate microRNAs allow LNA-modified oligonucleotides to be shorter, with 15–16-nucleotide LNA/DNA antimiR being sufficient to target the 5' region of the microRNA. Moreover, 8-mer fully LNA PS modified antimiRs, also known as tiny LNAs, allow the inhibition of an entire microRNA family by targeting the shared seed sequence. Modified and redrawn after van Rooij, Kauppinen (2014)[162].

Because of the accumulation of the synthetic oligonucleotides in the liver, the liver-specific miR-122 was one of the first target molecules. MiR-122 has an important role in cholesterol homeostasis and HCV[41,135,168]. After studies in cell culture, several synthetic inhibitors of miR-122 were tested in mice[134,135,155,167,168]. Intriguingly, an antimiR-22 could decrease the cholesterol levels in African green monkey[135], while in another study inhibition of miR-122 in chimpanzees resulted in reduced viremia in animals infected with HCV[136]. This LNA-modified

miR-122 inhibitor, also known as SPC3649 or Miravirsen, was the first microRNA-based drug to be used in a phase II clinical trial[130]. Patients received Miravirsen at doses of 3, 5, or 7 mg/kg 5 times per week subcutaneously over a 29-day period. The miR-122 inhibitor resulted in dose-dependent anti-HCV effect with some patients having undetectable HCV RNA levels at the end of the study, without any severe adverse effects. The scientists also observed a decrease in cholesterol levels, in agreement with the results observed in non-human primates[135]. An additional modification used to target the liver comprises the N-acetylgalactosamine (or GalNAc) conjugation, with GalNAc being the ligand for the asialoglycoprotein receptor (ASGPR), which is highly expressed in hepatocytes[169]. This conjugation is used in RG-101, another miR-122 inhibitor, similar to Miravirsen, with cEt instead of LNA analogs by Regulus Therapeutics. A phase 1B clinical trial showed well toleration and substantial decrease in the HCV viral titer within 4 weeks[170].

1.3.2 MicroRNA sponges

Ebert et al. developed a competitive inhibitor of microRNAs termed microRNA sponge, which can be expressed as a transcript from strong promoters in mammalian cells[171]. These molecular constructs contain multiple imperfect microRNA target sites in tandem, usually after a fluorescent reporter gene. That way the cells expressing the sponge can be identified and sorted. The multiple microRNA target sites act as a decoy for the cognate miR thereby sequestering it and leading to derepression of its natural targets. A big advantage of the microRNA sponge method in comparison to synthetic antisense oligonucleotides is that it can be delivered to specific tissues and cell types *in vivo* using AAVs or lentiviral vectors[40,124,172,173].

1.3.3 MicroRNA mimicry

Similar to microRNA antagonism, in occasions where the microRNA levels are reduced in a disease, the microRNA needs to be supplemented. This need led to the development of microRNA mimics or microRNA replacement therapy. Although a single-stranded RNA with the same sequence as the mature microRNA should be able to mimic the microRNA, double-stranded synthetic RNAs have been shown to have much greater potency[174]. Similar to antimiRs, nucleotide analogs can be used to improve the stability, permeability and activity of miRNA mimics[174–176]. The undesired strand (passenger strand) is synthesized to be less stable, can be linked to a cholesterol molecule to increase cellular uptake and can be further modified by the addition of a 5'-O-methyl group in order to prevent its loading into the RISC complex[177]. The guide strand must be recognized as a microRNA by the RISC, therefore, the 2'-modifications that can be incorporated here are limited. The 2'-F modification confers resistance against exonucleases, while it does not interfere with RISC loading[178]. One possible design of a synthetic double-stranded microRNA mimic is illustrated in **Figure 1.10**.

Several mimics formulation have been used to treat mouse cancers with intratumoral injections of the complex mimics with liposome nanoparticles[179], polyethyleneimine (PEI)[180], or atelocollagen[181]. More recently, a single intracardial injection of pro-regenerative microRNAs with a lipid formulation after myocardial infarction led to reduced infarct size and improved cardiac function[182].

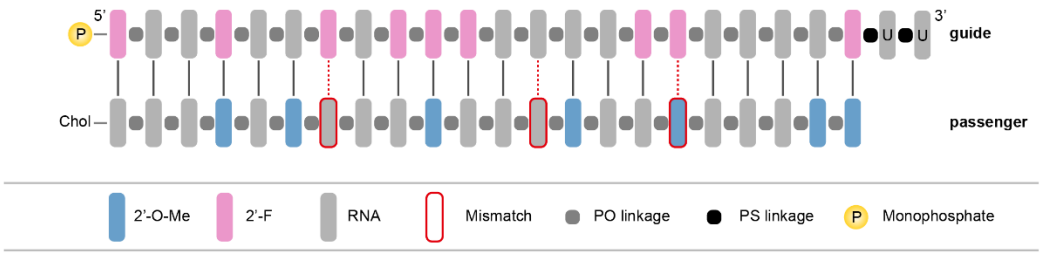

Figure 1.10. Design of a synthetic double-stranded microRNA mimic

The same chemical modifications used for antimiRs to increase stability and cellular uptake can also be used for microRNA mimics. The guide strand has the sequence of the miRNA of interest, while a cholesterol molecule is often attached to the 3' of the passenger strand to enhance cellular uptake. The chemical modifications of the guide strand confer increased stability and promote its loading into the RISC complex. Several mismatches can be introduced in the passenger strand in order to avoid its function as an antimiR, while it is further left unmodified to stimulate its degradation. The 2'-F modification has been shown not to interfere with the loading of the guide strand into the RISC complex. Modified and redrawn after van Rooij, Kauppinen (2014)[162].

Of note, double-stranded miRNA mimics can result in nonspecific -Toll-like receptor-mediated-interferon response[183]. Another consideration when coming to using microRNA mimics is the delivery of the microRNA of interest and therefore the subsequent regulation of a cadre of genes in non-target tissues and cell types where the microRNA is normally not expressed. Therefore, targeted delivery is becoming an important consideration for microRNA replacement therapy.

1.3.4 MicroRNA detection methods

Northern blotting

Since the discovery of the first microRNA[3], northern blotting was used by the vast majority of investigators for the detection of this new class of RNA molecules[4,6,8]. First, gel electrophoresis is performed for size-dependent-separation of the RNA molecules, followed by their transfer to a membrane, cross-linking and hybridization with nucleic acid probes. The radiolabeled probes are then detected by autoradiography. The advantages of this technique are that it is well established and accepted by the RNA field, and that the microRNA is visualized, allowing the determination of its size, as well as its relative quantity. On the other hand, it is a laborious and time consuming method, requiring radioactive material and equipment, although alternative methods, such as digoxigenin-labeled probes, have also been established[184]. Moreover, it is a low-throughput method, semi-quantitative, and requires a lot of starting

material (usually 5-30 µg of RNA are required, even though LNA-based probes have increased the sensitivity of the detection approximately ten-fold[185]). The latter renders the detection of low abundant microRNAs inconceivable.

Real-time PCR

Because of its precision, wide dynamical range, low amount of material needed, relatively low price, and time required, RT-qPCR is the gold standard concerning microRNA quantification. The first step, which is the conversion of RNA to cDNA, or reverse transcription (RT), can be performed either using microRNA-specific (**Figure 1.11a**) or universal primers (**Figure 1.11b**). Although the first method removes more background and gains sensitivity for the detection of a specific microRNA, the second method allows the parallel detection and comparison of many microRNAs at once. In most cases, the universal primer approach comprises the addition of a poly(A) tail by a polyadenylate polymerase (PAP) and oligo-dT primers, that bind to the extended microRNA and mediate the cDNA synthesis. The following step is qPCR, either using SYBR Green or dual-labeled hydrolysis probes (TaqMan).

SYBR Green is a fluorescent dye, which binds to dsDNA. Upon binding, its fluorescence increases approximately 100-fold, allowing the detection of PCR products. The fact that this method does not require microRNA-specific probes in addition, makes it financially more affordable. Nevertheless, because of nonspecific PCR products, a dissociation curve analysis should be performed each time to verify that a single amplicon was produced. For the dissociation, after the qPCR the temperature is gradually increased from a temperature above the Tm of the primers (~65ºC) until 95ºC and fluorescence is constantly monitored, producing a dissociation (or melting) curve. Plotting the negative first derivative of the fluorescence on the y-axis and the temperature on the x-axis, only one peak corresponds to specific amplification.

TaqMan is the most common example of dual-labeled probes. It is an oligonucleotide that can hybridize to the cDNA of the microRNA in a sequence-specific manner and carries a fluorophore at the 5′ and a quencher moiety at the 3′ end of the probe. During PCR, the Taq DNA polymerase cleaves only probes that are hybridized to the target sequence, separating the fluorescence dye from the quencher. This results in increased fluorescence by the reporter that reflects the quantity of the PCR amplicon. This increase occurs only if the target sequence is complementary to the probe, and amplified during PCR, minimizing the nonspecific signal. The latter is the main advantage of the TaqMan method compared to SYBR Green.

If absolute quantification is desired, a synthetic RNA oligonucleotide with the microRNA sequence and known amount of molecule copies can be used in order to create a standard curve. In most cases though, relative quantification is applied, using a so-called “housekeeping gene” like snRNA U6. The optimal “housekeeping gene” should not be regulated between the

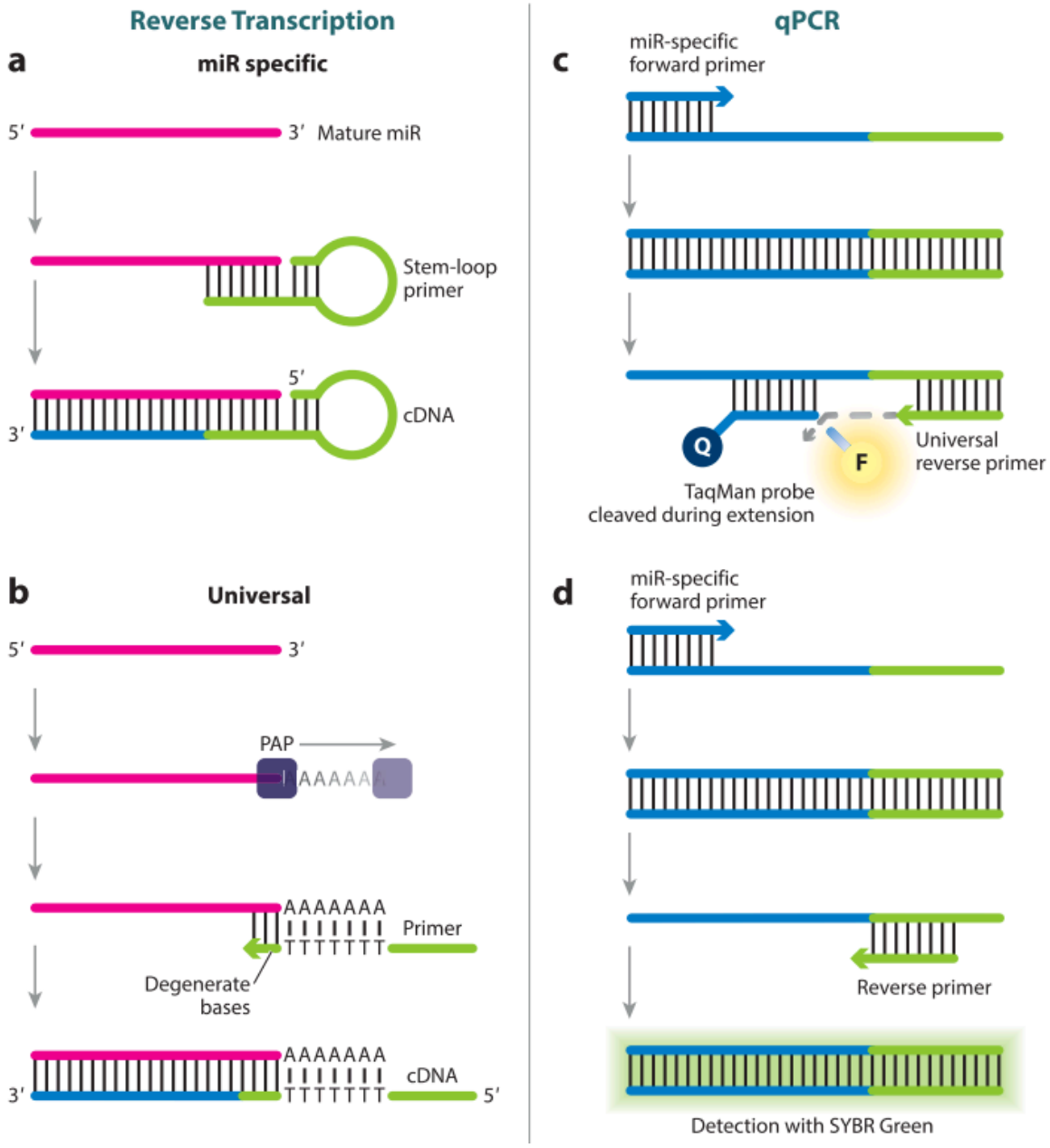

Figure 1.11. Methods for cDNA synthesis and qPCR of microRNAs

The main two methods for cDNA generation for subsequent microRNA quantitation by RT-qPCR include microRNA-specific (**a**) or universal (**b**) primers. MicroRNA-specific primers have a complementary sequence against the microRNA of interest (**a**), whereas universal primers bind to a common sequence that is added to all microRNAs by a polymerase (**b**). Two different fluorescence-based methods are used to detect microRNAs during qPCR: A TaqMan probe hybridizes to the target DNA sequence, keeping the fluorophore and the quencher moiety in close proximity. This results in no fluorescence. As soon as the Taq polymerase starts amplifying the cDNA it encounters the hybridized TaqMan probe and cleaves it using its 5'-3' exonuclease activity resulting in separation of the fluorophore and the quencher moiety, generating fluorescence (**c**). SYBR Green is a dye that nonspecifically binds double-stranded DNA, resulting in more fluorescence, the more dsDNA is produced during qPCR (**d**). PAP: polyadenylate polymerase, qPCR: quantitative polymerase chain reaction, RT-qPCR: reverse transcription quantitative polymerase chain reaction. Adapted from Hunt et al. (2015)[186].

different groups, should be similar in size as the microRNA studied, and the primers' efficiencies for it and the microRNA in question should be close to 100%. A scientific report

summarizes all the critical points that should be taken into account in order to perform a high quality RT-qPCR[187].

Microarray

In a microarray, appropriate designed capture probes are used to anneal, ideally with high specificity and sensitivity, with their target microRNAs, which have been previously fluorescently labeled. The fluorescence signal from each probe is then recorded and quantified. Because of the length of the miRNAs (~22 nt), the feasibility for many alternative probe designs is limited. Lower Tm generate weaker signals, whilst higher Tm values result in poor specificity[188]. In order to improve the characteristics of the miR : probe duplex, that is the affinity, specificity, and stability, 2'-O-methyl, as well as LNA have been used[145,189]. Although modifications of the probe bases can be used to fine-tune the Tm of the miR : probe duplex, the microarrays should not be used to draw quantitative conclusions, but rather in order to detect the presence of a microRNA, or to compare a microRNA between two conditions, for example in healthy and patients with heart failure. While one can screen hundreds of microRNAs at once, novel microRNAs cannot be detected using this method.

Small RNA sequencing

Isolated total RNA is usually enriched for the small RNAs and massively parallel high-throughput sequencing is performed. This method is quantitative and estimates the absolute abundance of thousands of microRNAs simultaneously. Besides, microRNA sequencing is able to identify novel microRNAs, something not possible with other hybridization methods, like microarrays. The potential new microRNA must annotate perfectly to the genome of interest[190], be able to create a microRNA-like hairpin structure[191], and be approximately 22 nt long. Its sensitivity is also superior in comparison to a microarray, since microRNA sequencing can detect even a few microRNAs per cell. Its most significant limitations are that it requires special infrastructure and bioinformatic expertise in order to analyze the results. The time required to generate the results (1-2 weeks), is also a drawback compared to alternative quantitative techniques at the current time point.

Fluorescent *in situ* hybridization (FISH)

This method requires that the cells are first fixed in order to preserve the subcellular morphology and uses labeled probes that have high affinity to the target microRNA. Although the small length of the microRNAs was initially a problem for their detection by *in situ* hybridization, the introduction of LNA bases in the probes increased their specificity and allowed the visualization of microRNAs from whole-mount embryos[192]. Whole-mount FISH is efficient until embryonic day 11.5, thicker skin size inhibits the probe penetration, so that tissue sections are required in order to facilitate the probe uptake[193]. Albeit FISH can be performed

for formalin-fixed paraffin-embedded (FFPE) samples, cryosections are usually preferred[194–196]. A novel flow-FISH combined ISH and flow cytometry for high-throughput detection of microRNAs and target mRNAs simultaneously at the single-cell level[197]. Even though FISH methods have been improved drastically in the last decade, most protocols still need optimization from the user and are technically challenging and laborious. A thorough analysis of all the critical parameters for a successful microRNA FISH has been performed by Urbanek et al.[198].

MicroRNA biosensors

MicroRNA biosensors employ molecular probes together with sensitive converters (or transducers). Hybridization of a microRNA to its probe is transduced to a signal. Based on the transduction mechanism used to generate the signal, electrochemical[199], electromechanical[200], and optical[201] biosensors have been reported. All of them have achieved femtomolar sensitivity and have the advantage to avoid the artifacts produced by sample amplification, used by other detection methods, such as qPCR. The above mentioned techniques require an immobilized molecular detection probe on a surface with transducer characteristics[202].

1.3.5 MicroRNA inhibition assessment

The most common readout for miRNA activity is the quantification of the expression level of the miRNA or its target genes. Targets of microRNAs are not trivial to be identified and even then they might be differentially or not at all regulated in different cell types after antimiR application. Furthermore, the effect of microRNAs on each of their targets is often mild, on average only 35% at the mRNA level[203,204], and less than two-fold at the protein level[205,206]. Hybridization-based assays, such as northern blotting and ISH are between the most popular techniques for determining microRNA levels. However, there are a number of caveats, when these methods are used to assess antimiR-mediated microRNA inhibition.

First, the chemical modifications of the antimiR result in different modes of action. Whereas high affinity antimiRs, such as LNA/DNA, LNA/2'-O-Me and 2'-F/MOE result in microRNA sequestration[135,136,140,165,167,207], lower affinity chemistries, such as 2'-O-Me, 2'-MOE and cholesterol-conjugated 2'-O-Me modified antagomiRs, lead to microRNA degradation[134,137,140,168,207]. Although miR : antimiR duplexes have been reported as a slower migrating band in northern blotting[135,136,165,167,207], the antimiR might not be able to be displaced by the probe for the microRNA detection, even under denaturing polyacrylamide gel electrophoresis (PAGE) conditions[140]. Moreover, if antimiRs are used, part of the miR : antimiR duplexes might be present in the supernatant of the isopropanol precipitation step when using the gold standard guanidinium thiocyanate-phenol-chloroform RNA extraction protocol[208], leading to an RNA extract that does not depict the physiological levels of the miRNA of

interest[140,155,209]. Besides that, the part of the antimiR that is in intracellular vesicles, and otherwise not accessible to its cognate microRNA, can artificially bind to it during cell lysis and RNA isolation and result in a misleading interpretation of the results acquired for example by qPCR[210].

Besides the efficacy of an antimiR, its tissue distribution has been investigated. Fluorophore- as well as radioactive isotope-labeled antimiRs have been used to address this question[42,165]. In both cases, however, the intracellular presence of the antimiR and its biological functionality could not be verified.

To address both the microRNA activity (repression), as well as the distribution of the antimiR, a microRNA activity sensor can be employed by inserting one or more perfect or imperfect microRNA binding sites in the 3' of a reporter gene, such as luciferase or green fluorescent protein (GFP)[143].

1.3.6 MicroRNA activity sensors

MiRNA activity sensors, in which a miRNA binding site is cloned into the 3'-UTR of a reporter gene, are widely used to assess antimiR potency *in vitro*[135,139,141,167,211–213]. A typical example of the design of such a sensor is shown in **Figure 1.12**. The reporter gene can be either LacZ[214], a fluorescent protein such as GFP[215], or a luciferase[216,217]. Except for the standard "OFF-system", when the microRNA leads to suppression of the sensor and no signal, there are also "ON-system" reports, where the microRNA activity leads to increased signal. In these cases, the microRNA binding sites are placed in the 3' UTR of a repressor gene, followed by a reporter cassette, that is under the control of this repressor[218,219].

The *E.coli* lacZ gene encodes beta-galactosidase, which catalyzes the cleavage of lactose to glucose and galactose. The activity of beta-galactosidase can be visualized, as incubation with its substrate X-gal results in generation of a blue dye.[220] The luciferases are oxidative enzymes that after reaction with a substrate, produce bioluminescence. The term stems from the Latin word *lucifer*, meaning the "light-bringer". Firefly luciferase, or Fluc, is one of the best studied luminescent proteins, and the genes used in most reports stem from the firefly *Photinus pyralis*[221]. It catalyzes the oxidation of luciferin in the presence of oxygen and ATP-Mg^{2+} and produces oxyluciferin, AMP, PPi, CO_2, and light at 562 nm. Renilla luciferase, or Rluc, another very frequently used luciferase, was initially isolated from *Renilla reniformis*[222]. Rluc catalyzes the oxidative decarboxylation of coelenterazine in the presence of oxygen to produce coelenteramide, CO_2, and light at 480 nm. GFP was isolated from the jellyfish *Aequorea victoria* as a byproduct of aequorin, a luminescent substance, owing to its bright green fluorescence[223].

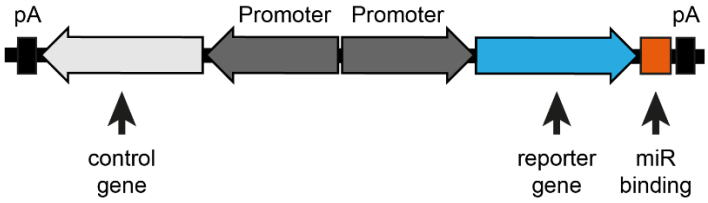

Figure 1.12. Design of microRNA activity sensors

Two genes are transcribed under two separate ubiquitous promoters. One serves as an internal reference (control gene), while the second gene serves as the reporter gene, with the microRNA binding site(s) in its 3' regulating its expression depending on the microRNA activity. Most commonly luciferase or fluorescent genes are used for such approaches. pA: polyA signal.

Despite the fact, that several studies have used microRNA activity sensors *in vivo* in order to monitor microRNA biogenesis or expression patterns[214,215,224,225], little has been undertaken in order to measure antimiR-mediated microRNA activity inhibition. Obad et al.[165] transplanted cells expressing a miR-21 luciferase reporter in a mouse orthotopic breast tumor model and showed an increased luciferase activity upon antimiR-21 administration. However, this approach has several disadvantages, since antimiR efficacy and distribution could only be assessed in a small cell population of the mice. Most importantly, the transplantation of cells would be less feasible for organs such as the heart or the brain. A sensitive reporter for microRNA *in vivo* is therefore highly needed.

1.4 Scientific questions

The aims of this thesis are to investigate the role of miR-29 in cardiac remodeling and to develop a molecular reporting system to determine the activity of miRNAs *in vivo*.

MicroRNA-29, attracted our interest, since preliminary evidence from our laboratory indicated a profibrotic activity in the myocardium, something opposing to the canonical interpretation of its function (with potential consequences for therapy development). This is of importance, since a Phase II clinical trial is currently recruiting subjects, in order to use a miR-29 mimic, MRG-201, for prevention or reduction of the formation of fibrous scar tissue, in patients with a history of keloids. This thesis intends to elucidate the role of miR-29 in the development of cardiac hypertrophy and fibrosis, and to identify the cell type within the myocardium, in which miR-29 exerts its function, as well as to shed light on potential underlying molecular signaling pathways. The results of this study, should give rise to new perspectives for microRNA-related therapy of cardiac hypertrophy and fibrosis.

Regarding the microRNA-activity sensor, a fluorescence-based molecular reporter would be developed, in order to detect the microRNA activity quantitatively, and at the single cell level. A reporter of that kind has been thoroughly investigated in cases of highly expressed microRNAs in order to determine their tissue- or cell type specificity. In contrast, the use of such microRNA activity sensors to determine the efficacy of microRNA inhibition by antimiRs has been poorly studied, mainly due to the reason, that the commonly studied microRNAs are far too high expressed for their inhibition to be assessed by a microRNA activity sensor *in vivo*. This thesis aims to identify a microRNA, whose activity will be within a specific range, allowing for sensitive antimiR-mediated microRNA inhibition detection. A microRNA activity sensor will be tested for its potency to detect antimiR-mediated microRNA inhibition both *in vitro* and *in vivo*. That would permit the determination of the efficacy and distribution of synthetic microRNA inhibitors, which are candidates for use in clinical trials.

2 Materials

2.1 Chemicals

2-mercaptoethanol	AppliChem (Darmstadt, Germany)
2-propanol	Roth (Karlsruhe, Germany)
2,3-butanenione monoxime (BDM)	Sigma Aldrich (Taufkirchen, Germany)
4-(2-hydroxyethyl)-1-piperazineethanesulfonic acid (HEPES)	Sigma Aldrich (Taufkirchen, Germany)
Acetic acid glacial	Roth (Karlsruhe, Germany)
Agar	AppliChem (Darmstadt, Germany)
Agarose standard	Roth (Karlsruhe, Germany)
Ammonium acetate	Sigma Aldrich (Taufkirchen, Germany)
Ammonium persulfate (APS)	Sigma Aldrich (Taufkirchen, Germany)
Ampicillin	Roth (Karlsruhe, Germany)
Bovine serum albumin (BSA) fraction V	AppliChem (Darmstadt, Germany)
Bromodeoxyuridine (BrdU)	Sigma Aldrich (Taufkirchen, Germany)
Bromophenol blue	Roth (Karlsruhe, Germany)
Chloramphenicol	Roth (Karlsruhe, Germany)
Chloroform (Trichloromethane, $CHCl_3$)	Roth (Karlsruhe, Germany)
Citric acid	Roth (Karlsruhe, Germany)
Dimethyl sulfoxide (DMSO)	AppliChem (Darmstadt, Germany)
Dithiothreitol (DTT)	Roth (Karlsruhe, Germany)
Ethanol	Roth (Karlsruhe, Germany)
Ethidium bromide	Roth (Karlsruhe, Germany)
Ethylenediaminetetraacetic acid (EDTA)	Roth (Karlsruhe, Germany)
Hydrochloric acid 37% (HCl)	Roth (Karlsruhe, Germany)
Hydrogen peroxide 30% (H_2O_2)	Roth (Karlsruhe, Germany)
Glycerol	AppliChem (Darmstadt, Germany)
Kanamycin sulfate	Roth (Karlsruhe, Germany)
Magnesium chloride ($MgCl_2$)	Sigma Aldrich (Taufkirchen, Germany)
Magnesium sulfate ($MgSO_4$)	Sigma Aldrich (Taufkirchen, Germany)
Magnesium sulfate heptahydrate ($MgSO4.7H_2O$)	Merck (Darmstadt), Germany
Methanol	Roth (Karlsruhe, Germany)
Paraformaldehyde (PFA)	Sigma Aldrich (Taufkirchen, Germany)
Penicillin / Streptomycin	Gibco (Karlsruhe, Germany)
Phenol/Chloroform/Isoamyl alcohol	Roth (Karlsruhe, Germany)
Phenol Red	Sigma Aldrich (Taufkirchen, Germany)
Phenylephrine (PE)	Sigma Aldrich (Taufkirchen, Germany)
Potassium acetate	Roth (Karlsruhe, Germany)
Potassium bicarbonate ($KHCO_3$)	Sigma Aldrich (Taufkirchen, Germany)

Potassium ferricyanide ($K_3[Fe(CN)_6]$)	Roth (Karlsruhe, Germany)
Potassium ferrocyanide ($K_4[Fe(CN)_6]$)	Roth (Karlsruhe, Germany)
Saccharose	Roth (Karlsruhe, Germany)
SOB medium powder	Roth (Karlsruhe, Germany)
Sodium acetate ($NaCH_3COO$)	Merck (Darmstadt, Germany)
Sodium chloride (NaCl)	Sigma Aldrich (Taufkirchen, Germany)
Sodium dihydrogen phosphate dihydrate ($NaH_2PO_4.2H_2O$)	Roth (Karlsruhe, Germany)
Sodium dodecyl sulfate (SDS)	Roth (Karlsruhe, Germany)
Sodium hydrogen phosphate dibasic (Na_2HPO_4)	Roth (Karlsruhe, Germany)
Sodium hydroxide (NaOH)	Roth (Karlsruhe, Germany)
Sodium hydroxide (NaOH)	Roth (Karlsruhe, Germany)
Sodium orthovanadate (Na_3VO_4)	Sigma Aldrich (Taufkirchen, Germany)
Taurine	Sigma Aldrich (Taufkirchen, Germany)
Tri-sodium-citrate (dihydrate)	Roth (Karlsruhe, Germany)
Tris base	Roth (Karlsruhe, Germany)
Triton-X 100	Sigma Aldrich (Taufkirchen, Germany)
Tryptone-peptone	AppliChem (Darmstadt, Germany)
Tween 20	Roth (Karlsruhe, Germany)
Yeast extract	AppliChem (Darmstadt, Germany)

2.2 Reagents and solutions

11R-VIVIT	Merck (Darmstadt, Germany)
4′,6-diamidino-2-phenylindole (DAPI)	Sigma Aldrich (Taufkirchen, Germany)
Acrylamide 30%	Bio-Rad (Munich, Germany)
Aqua ad iniectabilia (Apo water)	Braun (Melsungen, Germany)
Bradford dye reagent (5x)	Bio-Rad (Munich, Germany)
Cryomatrix (Shandon)	Thermo Scientific (Surrey, United Kingdom)
Deoxy-thymine nucleotides (oligo dTs)	Roth (Karlsruhe, Germany)
Deoxynucleotide triphosphates (dNTPs)	Thermo Fisher Scientific (Surrey, United Kingdom)
Direct red 80	Sigma Aldrich (Taufkirchen, Germany)
DNA loading (GelPilot) dye 5x	Qiagen (Hilden, Germany)
DNase/RNase-free water	Gibco (Karlsruhe, Germany)
Dulbecco's modified eagle medium (DMEM)	Gibco (Karlsruhe, Germany)
Eosin Y solution aqueous (0.5% w/v)	Sigma Aldrich (Taufkirchen, Germany)
FastGreen FCF	Sigma Aldrich (Taufkirchen, Germany)
Fetal bovine serum (FBS)	Sigma Aldrich (Taufkirchen, Germany)
Fetal calf serum	Sigma Aldrich (Taufkirchen, Germany)
Glycogen, RNA grade	Thermo Fisher Scientific (Darmstadt, Germany)
Goat serum	Thermo Scientific (Surrey, United Kingdom)

Hematoxylin 2	Thermo Scientific (Surrey, United Kingdom)
Isoflurane	Abbott (Wiesbaden, Germany)
IWR-1	Sigma Aldrich (Taufkirchen, Germany)
Laminin	BD Biosciences (Heidelberg, Germany)
Lipofectamine 2000	Thermo Scientific (Surrey, United Kingdom)
Minimum Essential Eagle (MEM)	Gibco (Karlsruhe, Germany)
Mounting medium for fluorescence	Vector Laboratories (Burlingame, USA)
Murine RNase inhibitor	Thermo Scientific (Surrey, United Kingdom)
Nonident P40 (MP-40)	AppliChem (Darmstadt, Germany)
Opti-MEM	Gibco (Karlsruhe, Germany)
OptiPrep	Sigma Aldrich (Taufkirchen, Germany)
peqGOLD Trifast	PeqLAB (Erlangen, Germany)
Phosphate buffered saline (PBS)	Gibco (Karlsruhe, Germany)
Poly-D-Lysine hydrobromide	Sigma Aldrich (Taufkirchen, Germany)
Polyethyleneimine (PEI MAX)	Polysciences Inc. (Warrington, PA, USA)
Prestained protein ladder	Fermentas (St. Leon-Rot, Germany)
PVDF membrane	Millipore (Billerica, USA)
RNase Zap	Sigma Aldrich (Taufkirchen, Germany)
SOC outgrowth medium	New England Biolabs (Ipswich, MA, USA)
SYTOX Green	Thermo Fisher Scientific (Darmstadt, Germany)
Trypan blue	AppliChem (Darmstadt, Germany)
Vitamin B12	Sigma Aldrich (Taufkirchen, Germany)
WGA-647	Thermo Fisher Scientific (Darmstadt, Germany)
WNT3a	Cell Guidance Systems Ltd (Cambridge, United Kingdom)

2.3 Buffers and media

Adeno-associated virus (AAV) lysis Buffer

6.06 g	Tris-base (50 mM)
8.77 g	NaCl (150 mM)
1.02 g	$MgCl_2.6H_20$ (5 mM)
900 ml	Gibco water
Adjust pH to 8.5	MEM
ad. 1l	ddH_2O

AMCF/ NRCF preplating medium

94 ml	NRCM incomplete medium
5 ml	FBS
1 ml	Penicillin/Streptomycin

AMCM preplating medium

1 ml	Penicillin/Streptomycin
5 ml	FBS
2 ml	BDM (500 mM)
1 ml	L-Glutamine (200 mM)
91 ml	MEM

Ampicillin stock solution 1000X (100 mg/ml))

5 g	Ampicillin
ad. 50 ml	ddH_2O

BrdU

230 mg	BrdU
74.8 ml	ddH_2O
Sterile filter and aliquot a 2 ml	
Store at -20^0C	

Calcium-free HBSS (Hank's Buffered Salt Solution)

0.4 g	KCl
0.06 g	KH_2PO_4
0.19 g	$MgSO_4.7H_2O$
0.35 g	$NaHCO_3$
8 g	NaCl
0.1 g	$Na_2HPO_4.7H_2O$
ad. 1l	ddH_2O

CBFHH (Ca^{2+} and HCO^{3-} free Hank's with Hepes) medium

137 mM	NaCl
5.36 mM	KCl
0.81 mM	$MgSO_4.7H_2O$
5.55 mM	Dextrose
0.44 mM	KH_2PO_4
0.34 mM	$Na_2HPO_4.7H_2O$
Adjust pH to 7.3 with NaOH	
Sterile filter	

Collagenase/Pancreatin solution for NRCM preparation

120 mg	Collagenase
80 mg	Pancreatin
ad. 200 ml	CBFHH warm
Sterile filter	

Digestion Buffer

107 mg	Collagenase Type II
15 µl	$CaCl_2$ (100 mM)
50 ml	Perfusion Buffer

DNA loading buffer

0,025 g	Xylene Cyanol
1.4 ml	EDTA (0.5 M)
3.6 ml	Glycerol
7.0 ml	H_2O

DNA lysis buffer (for genotyping)

12.1 g	Tris
1.87 g	EDTA
11.7 g	NaCl
0.2 g	SDS
ad. 1l	ddH_2O

Eosin solution, 0.1%

20 ml	Eosin Y Solution aqueous (0.5% w/v)
80 ml	ddH_2O
1 drop	Acetic Acid glacial

Erythrocyte lysis buffer

1 ml	Tris-HCl (0.1 M)
9 ml	NH_4Cl (155 mM)

FACS buffer, 0.1% BSA

500 mg	BSA
ad. 500 ml	DPBS

FastGreen Solution, 0.1%

500 mg	FastGreen FCF
ad. 500 ml	ddH_2O

HEK293T / HEK293/ 3T3/ A549 culture medium

450 ml	DMEM (+4.5g/l D-Glucose, L-Glutamine, Pyruvate)
50 ml	FBS
5 ml	Penicillin/Streptomycin

Iodixanol gradients

60% Iodixanol:	50 ml OptiPrep + 62.5 µl Phenol Red (0.5%)
40% Iodixanol:	30 ml OptiPrep + 15 ml PBS-MK
25% Iodixanol:	20 ml OptiPrep + 28 ml PBS-MK +120 µl Phenol Red (0.5%)
15% Iodixanol:	12 ml OptiPrep + 36 ml PBS-MKN

Kanamycin stock solution 300X (10 mg/ml))

500 mg	Kanamycin
ad. 50 ml	ddH_2O

LB Agar

10 g	Peptone
5 g	Yeast extract
5 g	NaCl
15 g	Agar
1 ml	NaOH (1 M)
ad. 1l	ddH_2O

LB Medium

10 g	Peptone
5 g	Yeast extract
5 g	NaCl
1 ml	NaOH (1 M)
ad. 1l	ddH_2O

NRCM incomplete medium

10.7 g	MEM
0.35 g	$NaHCO_3$
1 ml	Vitamin B12 67% (w/v)
ad. 1l	ddH_2O
Adjust to pH 7.3 and sterile filter	

P1 Buffer

9 ml	Perfusion Buffer
1 ml	FCS
12.5 µl	$CaCl_2$ (10 mM)

P2 Buffer

47.5 ml	Perfusion Buffer
2.5 ml	FCS
62.5 µl	$CaCl_2$ (10 mM)

PBS (10X)

80 g	NaCl
2 g	KCl
11.5 g	$Na_2HPO_4.7H_2O$
2 g	KH_2PO_4
ad. 1l	ddH_2O

PBS-MK solution

101.7 mg	$MgCl_2.6H_2O$ (1 mM)
93.2 mg	KCl (2.5 mM)
ad. 500 ml	DPBS, pH 7.4
Sterile filter	

PBS-MKN solution

101.7 mg	$MgCl_2.6H_2O$ (1 mM)
93.2 mg	KCl (2.5 mM)
29.22 g	NaCl (1 M)
ad. 500 ml	DPBS, pH 7.4
Sterile filter	

PBST

100 ml	PBS (10X)
1.0 ml	Tween 20
ad. 1l	ddH_2O

PEI solution

50 mg	PEI MAX
ad. 45 ml	pharmaceutical water
Adjust pH to 1.9	
Stir 2h at RT (PEI should be completely dissolved)	
Carefully bring pH to 7.1 (avoid too high pH as it will lead to PEI precipitation)	
ad. 50 ml	pharmaceutical water
Sterile filter, aliquot and store at -20^{0}C	

Perfusion Buffer (1X)

6.6 g	NaCl
0.35 g	KCl
0.082 g	KH_2PO_4
0.085 g	Na_2HPO_4
0.3 g	$MgSO_4.7H_2O$
0.012 g	Phenol Red
1.01 g	$NaHCO_3$
1.01 g	$KHCO_3$
10 ml	HEPES Buffer (1 M)
3.75 g	Taurine
ad. 1l	ddH_2O
Sterile filter the solution	

Protein lysis buffer

50 mM	Tris (1 M pH 6.7)
2%	SDS
1 mM	Na_3VO_4
1 tablet per 10 ml	Complete mini protease inhibitor

S.O.C. medium

2%	Tryptone
0.5%	Yeast extract
10 mM	NaCl
2.5 mM	KCl
10 mM	$MgCl_2$
10 mM	$MgSO_4$
20 mM	Glucose

Sirius Red Solution, 0.01%

50 mg	Direct Red 80
ad. 15 ml	ddH_2O
filter and then add	
485 ml	Picric acid-saturated solution 1.3%

TAE Buffer (50X)

242 g	Tris
57.1 ml	Acetic Acid
37.2 g	$Na_2EDTA.2H_2O$
ad. 1l	ddH_2O

Tris-EDTA (TE) buffer

10 mM	Tris
1 mM	EDTA

2.4 Enzymes

AccuPrime GC-rich DNA polymerase	Invitrogen (Karlsruhe, Germany)
AccuPrime Pfx DNA polymerase	Invitrogen (Karlsruhe, Germany)
Antarctic phosphatase	New England Biolabs (Ipswich, MA, USA)
Benzonase	Merck (Darmstadt, Germany)
Collagenase type 2	Worthington Biochemical Corporation (Lakewood, USA)
DNase	Sigma Aldrich (Taufkirchen, Germany)
Gateway BP clonase II enzyme mix	Invitrogen (Karlsruhe, Germany)
Gateway LR clonase II enzyme mix	Invitrogen (Karlsruhe, Germany)
GoTaq green master mix	Promega (Madison, USA)
Murine RNase inhibitor	New England Biolabs (Ipswich, MA, USA)
Pancreatin	Sigma Aldrich (Taufkirchen, Germany)
Proteinase K	Fermentas (St. Leon-Rot, Germany)
Restriction endonucleases	New England Biolabs (Ipswich, MA, USA)
Superscript II reverse transcriptase	Invitrogen (Karlsruhe, Germany)
T4 DNA Ligase	New England Biolabs (Ipswich, MA, USA)
Taq DNA polymerase	Fermentas (St. Leon-Rot, Germany)
Taq DNA polymerase	Genscript (Piscataway, NJ, USA)
Trypsin-EDTA (0.25%)	Gibco (Karlsruhe, Germany)

2.5 Antibodies

Antigen/ Conjugate	Source	Dilution	Application	Manufacturer/ Catalogue No.
α-actinin	mouse, EA53, monoclonal	1:1000	IF	Sigma Aldrich/ A7811
vimentin	chicken, polyclonal	1:1000	IF	Abcam/ ab24525
Ki-67	rabbit, SP6, monoclonal	1:250	IF	Abcam/ ab16667
CD45/FITC	rat, 30-F11, monoclonal	1:50	FACS	Biolegend/ 103107
CD105/PE	rat, MJ7/18, monoclonal	1:50	FACS	eBioscience/ 12-1051-81
CD140a/PE-Cyanine7	rat, APA5, monoclonal	1:100	FACS	eBioscience/ 25-1401-80
CD16/CD32 (Fc block)	rat, 2.4G2 (RUO), monoclonal	1:50	FACS	BD Pharmingen/ 553142

2.6 Cell lines and primary cells

Abbreviation	Cell Type	Source
NRCM	neonatal rat cardiac myocytes	isolation described in methods
NRCF	neonatal rat cardiac fibroblasts	isolation described in methods
AMCM	adult mouse cardiac myocytes	isolation described in methods
AMCF	adult mouse cardiac fibroblasts	isolation described in methods
CD45+	cardiac leukocytes	isolation described in methods
CD105+	cardiac endothelial cells	isolation described in methods
HEK293	human embryonic kidney cell line	ATCC (Manassas, VA, USA)
HEK293T	HEK293 cells transformed with the SV40 large T antigen	ATCC (Manassas, VA, USA)
NIH/3T3	fibroblast line originally obtained from Swiss albino mouse embryo tissue	Sigma Aldrich (Taufkirchen, Germany)
A549	cell line of adenocarcinomic human alveolar basal epithelial cells	Sigma Aldrich (Taufkirchen, Germany)

2.7 Bacterial strains

Strain	Genotype	Manufacturer
DH10B	F⁻*mcr*A Δ(*mrr-hsd*RMS-*mcr*BC) Φ80*lac*ZΔM15 Δ*lac*X74 *rec*A1 *end*A1 *ara*D139Δ(*ara*, *leu*)7697 *gal*U *gal*K λ⁻*rps*L *nup*G	Invitrogen (Karlsruhe, Germany)
Stbl2	F− endA1 glnV44 thi1 recA1 gyrA96 relA1 Δ(lac-proAB) mcrA Δ(mcrBC-hsdRMS-mrr) λ−	Invitrogen (Karlsruhe, Germany)
SURE	e14– (McrA–) Δ(mcrCB-hsdSMR-mrr)171 endA1 supE44 thi-1 gyrA96 relA1 lac recB recJ sbcC umuC::Tn5 (Kanr) uvrC [F' proAB lacIqZΔM15 Tn10 (Tetr)]	Stratagene (San Diego, CA, USA)

2.8 Oligonucleotides

Cloning oligonucleotides

For the miR-29 sponges following oligonucleotides were ordered from Sigma Aldrich (Taufkirchen, Germany):

Name	Sequence	Comments
dsRed F	GGGG AAGCTT GCCACCATGGATAGCACTG	Introducing HindIII sites
dsRed R	GGGG AAGCTT CTACTGGAACAGGTGGTGGC	
dsRed R (KpnI)	AAAAAA GGTACC CTACTGGAACAGGTGGTGGC	For excising the b-globin intron
Nattel (top)	GGGG **ACAAGTTTGTACAAAAAAGCAGGCT** AACACTGATTTCTGTGGTGCTA AACACTGATTTCTGTGGTGCTA AACACTGATTTCTGTGGTGCTA **ACCCAGCTTTCTTGTACAAAGTGGT**	3xmiR-29b sponge (in **bold** the attB sites) [124]
Nattel (bottom)	**ACCACTTTGTACAAGAAAGCTGGGT** TAGCACCACAGAAATCAGTGTT TAGCACCACAGAAATCAGTGTT TAGCACCACAGAAATCAGTGTT **AGCCTGCTTTTTTGTACAAACTTGT** CCCC	
Nattel + spacer (top)	GGGG **ACAAGTTTGTACAAAAAAGCAGGCT** AACACTGATTTCTGTGGTGCTA ACTAGT AACACTGATTTCTGTGGTGCTA GAATAT AACACTGATTTCTGTGGTGCTA TCTAGA **ACCCAGCTTTCTTGTACAAAGTGGT**	3xmiR-29 sponge with 6 nt spacers (in **bold** the attB sites, underlined the spacers) [124]
Nattel + spacer (bottom)	**ACCACTTTGTACAAGAAAGCTGGGT** TAGCACCACAGAAATCAGTGTT TCTAGA TAGCACCACAGAAATCAGTGTT ATATTC TAGCACCACAGAAATCAGTGTT ACTAGT **AGCCTGCTTTTTTGTACAAACTTGT** CCCC	

Concerning the longer miR-29 sponges, following sequences were synthesized from GeneArt, Life Technologies (Carlsbad, CA, USA):

Name	Sequence	Comments
5 x miR-29spg + spacer	GGGG **ACAAGTTTGTACAAAAAAGCAGGCT** TAACCGATTTTCTTGGTGCTA ACTAGT TAACCGATTTTCTTGGTGCTA GAATAT TAACCGATTTTCTTGGTGCTA TCTAGA TAACCGATTTTCTTGGTGCTA CAGTAA TAACCGATTTTCTTGGTGCTA **ACCCAGCTTTCTTGTACAAAGTGGT**	5xmiR-29 sponge (in **bold** the attB sites)
5 x miR-29pf + spacer	GGGG **ACAAGTTTGTACAAAAAAGCAGGCT** TAACCGATTTCAAATGGTGCTA ACTAGT TAACCGATTTCAAATGGTGCTA GAATAT TAACCGATTTCAAATGGTGCTA TCTAGA TAACCGATTTCAAATGGTGCTA CAGTAA TAACCGATTTCAAATGGTGCTA **ACCCAGCTTTCTTGTACAAAGTGGT**	5xmiR-29 perfect binding sites with 6 nt spacers (in **bold** the attB sites, underlined the spacers)
12 x miR-29spg	GGGG **ACAAGTTTGTACAAAAAAGCAGGCT** TAACCGATTTTCTTGGTGCTA TAACCGATTTTCTTGGTGCTA TAACCGATTTTCTTGGTGCTA TAACCGATTTTCTTGGTGCTA TAACCGATTTTCTTGGTGCTA TAACCGATTTTCTTGGTGCTA TAACCGATTTTCTTGGTGCTA TAACCGATTTTCTTGGTGCTA TAACCGATTTTCTTGGTGCTA TAACCGATTTTCTTGGTGCTA TAACCGATTTTCTTGGTGCTA TAACCGATTTTCTTGGTGCTA **ACCCAGCTTTCTTGTACAAAGTGGT**	12xmiR-29 sponge (in **bold** the attB sites, underlined the spacers)
12 x miR-29spg + spacer	GGGG **ACAAGTTTGTACAAAAAAGCAGGCT** TAACCGATTTTCTTGGTGCTA ACTAGT TAACCGATTTTCTTGGTGCTA GAATAT TAACCGATTTTCTTGGTGCTA TCTAGA TAACCGATTTTCTTGGTGCTA CAGTAA TAACCGATTTTCTTGGTGCTA GTCAAT TAACCGATTTTCTTGGTGCTA TACGTA TAACCGATTTTCTTGGTGCTA TTAGCA TAACCGATTTTCTTGGTGCTA ATCAAT TAACCGATTTTCTTGGTGCTA AGATAT TAACCGATTTTCTTGGTGCTA CATATC TAACCGATTTTCTTGGTGCTA GTAATC TAACCGATTTTCTTGGTGCTA **ACCCAGCTTTCTTGTACAAAGTGGT**	12xmiR-29 sponge with 6 nt spacers (in **bold** the attB sites, underlined the spacers)

To test for the successful dsRed incorporation in the dsAAV-GwDest-6 vector, following sequencing primers were used:

Name	Sequence	Comments
dsRed sequencing F	CGTGTACGGTGGGAGGTCTA	In CMV F
dsRed sequencing R	ACGACCAACTTCTGCAGCTT	In b-globin intron R

Mutagenesis primers

Gsk3β WT	AAAAGAATGTTCCCCCACCATCACC, AAAAGAATTCGGCAAGACCTCAACGTGACTTA	
Gsk3β MUT	G**G**TTATGGGCCATTACTTGAC, **G**C**G**AAGGTTCATTTTAGAGTATATAAGG	in **bold** the introduced mutations
Ctnnbip1 F	AAAAAAACCGGTGGTAGCAAACCACCGTCTTC	
Ctnnbip1 R	AAAAAAGAATTCCCAAACCCTGTTTTCTGCTT	
Ctnnbip1 MUT F	TTCCCCGGAAGCTCTCCGAGCTCT**C**G**C**G**G**TTT ATTTAGGTCATTTTTAGGAATG	in **bold** the introduced mutations
Hbp1 WT	AAAAAAACCGGTGGTGAGGATTGCTTTCTCCA, AAAAAAGAATTCACATGAGGGTATGTGGCTGAGG	
Hbp1 MUT1 F	TAGGCTTGAAAATTGATATCCTGT**C**G**C**G**G**TAAAG TACAGTAGAAAGATGTGTATAC	in **bold** the introduced mutations
Hbp1 MUT2 R	AAAAAAGAATTCACATGAGGGTATGTGGCTGAGGA GACAGGAACGCGGTCAAACACAATGGTGTCGACT GGTAACA**C**C**G**C**G**ATTACAATGACTGTCCCAATGC	in **bold** the introduced mutations
Glis2 F	AAAAAAACCGGTCCCGACGAACAGAAACTC, AAAAAACAATTGACTCTAAGGCCAGCAGTC	
Glis2 MUT3 F	TCTAGTTGAACCCTTTTCTT**C**G**C**G**G**TGCCTCTC TTGCCCATGAGCT	in **bold** the introduced mutations
Glis2 MUT4 R	AAAAAACAATTGACTCTAAGGCCAGCAGTCAGG TAGGTTAGGGAAGGGTGACCCTTCTGAAACAGA AAGGCAGTCTGAGAAAAAGACTAGACAGAACTG CTCAGAGGAACCACAGAGCCAAGGACCCACTA**C** C**G**C**G**TCAGCAGCTCTCTTGTTCTA	in **bold** the introduced mutations

Glis2 MUT1,2 DNA fragment synthesized by Invitrogen (Karlsruhe, Germany):

ACCGGTCCCGACGAACAGAAACTCTTCTGCGAAATAGCAATAATATCCTACTGCCCCAG
GGCCAAGCTGCAGCCCCAGACAAGCTGGGTGGCAAGGTGGCAAGGAT**C**G**C**G**G**TAGAA
GGTCTGTGCTGGCCTCCTGGCTCCAAAGTGAGGACTTGGCTTGGACCTGCTGTCCAAG
AAGAGCCATTCTCTTG**C**G**C**G**G**TAAGGCCTCAATCACTTCCATTTCCCTAGTCTGTAGTCT
GGGTGAGGCCTTTGCCTGTCCTCCCAGGACGCTCAGTCCTGCCTCTTGCTCTGGTGCG
TTCCTCTCTATGGCCACCCTGGCTGGGCAGGGTTCCAGTCCTCCCTGCCTTACCTACTT
GTCAGCTAGGAGCCCCCAGTGATCATAGATAGGCCCACACTTGGGAATTC

* Underlined are the restriction sites for AgeI and EcoRI, respectively; in **bold** the mutated bases.

Genotyping primers

miR-29ab1 WT	CTTAATTCTTACCTGTGGCTCCAACG, GAACTATTGCACGGACTTCACCTTCC
miR-29ab1 KO	AAATGGTTCAAACGCTCCAC, CAGAAAGCGAAGGAGCAAAG
miR-29b2c WT	GCTGCCAAGGTTAGAGATCA, GAGGAGGGTCAGAGTCCACA
miR-29b2c KO	ACAGCCAGGAGCCATAAAAA, GAGGAGGGTCAGAGTCCACA
miR-29b2c$^{fl/fl}$	GCTGCCAAGGTTAGAGATCA, GAGGAGGGTCAGAGTCCACA

Real time primers

Nppa mouse	GCTTCCAGGCCATATTGGAG, GGGGGCATGACCTCATCTT
Myh6 mouse	GCCCAGTACCTCCGAAAGTC, GCCTTAACATACTCCTCCTTGTC
Myh7 mouse	ACTGTCAACACTAAGAGGGTCA, TTGGATGATTTGATCTTCCAGGG
Gsk3β mouse	CAAGCAGACACTCCCTGTGA, AATGTCTCGATGGCAGATCC
Rcan1 mouse	GCTTGACTGAGAGAGCGAGTC, CCACACAAGCAATCAGGGAGC
Gapdh mouse	GTGAAGGTCGGTGTGAACG, TCGTTGATGGCAACAATCTC

Col1a1 mouse	CTGGCAAGAAGGGAGATGA, CACCATCCAAACCACTGAAA
Col1a2 mouse	AGGTCTTCCTGGAGCTGATG, ACCCACAGGGCCTTCTTTAC
Col3a1 mouse	ACAGCAAATTCACTTACACAGTTC, CTCATTGCCTTGCGTGTTT

2.9 Kits

Agilent RNA 6000 pico kit	Agilent Technologies (Böblingen, Germany)
BCA protein assay kit	Thermo Scientific (Surrey, United Kingdom)
Endofree plasmid maxi kit	Qiagen (Hilden, Germany)
Luciferase assay system (one- & dual-Glo)	Promega (Madison, USA)
PureLink HiPure plasmid filter gigaprep kit	Thermo Fisher Scientific (Darmstadt, Germany)
PureLink HiPure plasmid filter maxiprep kit	Thermo Fisher Scientific (Darmstadt, Germany)
PureLink HiPure plasmid filter midiprep kit	Thermo Fisher Scientific (Darmstadt, Germany)
Q5 Site-directed mutagenesis kit	New England Biolabs (Ipswich, MA, USA)
QIAprep spin miniprep kit	Qiagen (Hilden, Germany)
QIAquick gel extraction kit	Qiagen (Hilden, Germany)
QIAquick PCR purification kit	Qiagen (Hilden, Germany)

2.10 Instruments

AE31 inverted phase contrast microscope	Motic (Wetzlar, Germany)
Agilent 2100 bioanalyzer	Agilent Technologies (Böblingen, Germany)
Barnstead NanoPure water purification system	Thermo Fisher Scientific (Darmstadt, Germany)
Centrifuge 5417R	Eppendorf (Hamburg, Germany)
Centrifuge 5702R	Eppendorf (Hamburg, Germany)
Centrifuge 5804R	Eppendorf (Hamburg, Germany)
Countess automated cell counter	Thermo Fisher Scientific (Darmstadt, Germany)
Electrophoresis power supply –EPS 301	GE Healthcare (Munich, Germany)
Fluorescence microscope Observer.Z1 Axio	Zeiss (Oberkochen, Germany)
Gel electrophoresis chamber	Peqlab (Erlangen, Germany)
GS-6KR kneewell refrigerated centrifuge	Beckman Coulter (Brea, CA, USA)
Infinite M200 plate reader	Tecan (Männedorf, Switzerland)
Leica SP5 confocal microscope	Leica (Wetzlar, Germany)
Mastercycler pro PCR system, 96-well	Eppendorf (Hamburg, Germany)
MicroPublisher 5.0 RTV CCD camera	QImaging (Surrey, Canada)
MicroPulser electroporator	Bio-Rad (Hercules, CA, USA)

MiniSpin plus microcentrifuge	Eppendorf (Hamburg, Germany)
Mixers thermomixer comfort	Eppendorf (Hamburg, Germany)
MR Hei-Standard magnetic stirrer	Heidolph Instruments (Schwabach, Germany)
Nanodrop ND-1000	Thermo Scientific (Surrey, England)
Optima L-80 XP type 75 Ti rotor	Beckman Coulter (Brea, CA, USA)
Optima L-80 XP ultracentrifuge	Beckman Coulter (Brea, CA, USA)
PHERA Star FS microplate reader	BMG Technologies (Ortenberg, Germany)
QuantStudio 5 Real-Time PCR system, 384-well	Thermo Fisher Scientific (Darmstadt, Germany)
Qubit 4 fluorometer	Thermo Fisher Scientific (Darmstadt, Germany)
Retiga-4000DC CCD camera	QImaging (Surrey, Canada)
S3 cell sorter	Bio-Rad (Hercules, CA, USA)
StepOnePlus Real-Time PCR system, 96-well	Applied Biosystem (Foster City, USA)
T 10 basic ULTRA-TURRAX	IKA Works (Wilmington, NC, USA)
Vortex-Genie 2	Scientific Industries (Bohemia, NY, USA)

2.11 Software

Adobe Acrobat X, version 10.1.16	Adobe Systems Incorporated (San Jose, CA, USA)
Adobe Illustrator CS6, version 16.0.4	Adobe Systems Incorporated (San Jose, CA, USA)
Adobe Photoshop CS6, version 13.0.6	Adobe Systems Incorporated (San Jose, CA, USA)
FlowJo for Mac, version 10.3	FlowJo LLC (Ashland, OR, USA)
i-control 1.6	Tecan (Männedorf, Switzerland)
MacVector, version 13.5.5	MacVector Inc. (Apex, NC, USA)
MARS data analysis software	BMG Technologies (Ortenberg, Germany)
MetaMorph Offline, version 7.10.1	Molecular Devices (San Jose, CA, USA)
MetaMorph Premier imaging system, version 7.10.1	Molecular Devices (San Jose, CA, USA)
Microsoft Office for Mac, version 16.12	Microsoft (Redmond, WA, USA)
Prism 6 for Mac OS X, version 6.0c	GraphPad Software (La Jolla, CA, USA)
StepOne software v2.1	Applied Biosystems (Foster City, CA, USA)

2.12 Mouse lines

Mouse line	**Nomenclature**	**Reference**
C57BL/6N (common inbred strain)	*C57BL/6N*	Charles River (Wilmington, MA, USA)
miR-29ab1 knockout	*miR-29ab1*$^{-/-}$	Acquired from Bart de Strooper Laboratory (Leuven, Belgium) [226]

miR-29b2c knockout	*miR-29b2c*$^{-/-}$	Acquired from Bart De Strooper Laboratory (Leuven, Belgium)
miR-29b2c conditional knockout	*miR-29b2c*$^{fl/fl}$	Acquired from Bart De Strooper Laboratory (Leuven, Belgium)

2.13 Others

Cell Factory (Nunc), 10-Tray	Thermo Fisher Scientific (Darmstadt, Germany)
Pap Pen	Vector Laboratories (Peterborough, United Kingdom)
TripleFlask (Nunc)	VWR (Darmstadt, Germany)
VECTASHIELD mounting medium for fluorescence H-1000	Vector Laboratories (Burlingame, USA)

3 Methods

3.1 Molecular biology methods

3.1.1 Polymerase chain reaction (PCR)

For standard DNA amplification the following 3-step PCR protocol was performed using the AccuPrime *Pfx* DNA polymerase:

10X AccuPrime *Pfx* reaction mix	5 µl
Primer mix (10 µM each)	1.5 µl
AccuPrime *Pfx* DNA polymerase	1 µl
Template DNA	100 ng
DMSO (optional)	2.5 µl
ddH_2O	ad. 50 µl

Step	3-step PCR		2-step-PCR		No. of steps
	Temp.	Time	Temp.	Time	
Initial denaturation	95^0C	2 min	95^0C	2 min	1
Denaturation	95^0C	15 s	95^0C	15 s	35
Annealing	55-64^0C	30 s	-	-	
Extension	68^0C	1 min/kb	68^0C	1 min/kb	
Final extension	68^0C	10 min	68^0C	10 min	1
Hold	4^0C	∞	4^0C	∞	-

The 2-step PCR protocol was preferred for long primers with high T_m. Usually the annealing temperature was set 5^0C lower than the T_m of the primers, for special cases a temperature gradient was selected for the annealing step. For amplification of GC-rich regions, the AccuPrime GC-rich DNA polymerase was used:

5X Buffer A(for genomic DNA) or B (for cDNA or plasmid DNA)	5 µl
Primer mix (10 µM each)	1 µl
AccuPrime GC-rich DNA polymerase	0.5 µl
Template DNA	100 ng
ddH_2O	ad. 25 µl

Step	3-step GC-rich PCR		No. of steps
	Temp.	Time	
Initial denaturation	95^{0}C	3 min	1
Denaturation	95^{0}C	30 s	30
Annealing	55-65^{0}C	30 s	
Extension	72^{0}C	1 min/kb	
Final extension	72^{0}C	10 min	1
Hold	4^{0}C	∞	-

3.1.2 PCR purification

Only when one specific PCR product was produced, the QIAquick PCR purification kit was used to isolated the amplified DNA. 5 volumes of PB buffer were added to 1 volume of PCR product and mixed. If the color of the mixture was not yellow but orange or violet, 10 µl of 3 M sodium acetate, pH 5.0, were added, so that the color turned into yellow. A QIAquick spin column was placed into a provided 2 ml collection tube. To bind DNA, the sample was applied to the QIAquick spin column and centrifuged for 60 seconds in a tabletop microcentrifuge at room temperature and 13000 rpm. The flow-through was discarded and the column was washed with 0.75 ml PE buffer and centrifuged for another minute. The flow-through was discarded and the empty column was again placed on the collection tube and centrifuged for an additional 1 min to remove residual washing buffer. The column was then transferred to a clean 1.5 ml microcentrifuge tube. To elute DNA, 20 µl of DNase/RNase-free H_2O were added to the center of the membrane, the column was let to equilibrate for 60 seconds and then centrifuged for 1 min.

3.1.3 Agarose gel electrophoresis

In most of the case 0.7-1% agarose gels were prepared by adding the proper amount of agarose powder in TAE buffer. For separation of small-sized bands 1.5-2% agarose gels were preferred. For a small gel 80 ml and for a big gel 120 ml of solution were prepared, inserted in a microwave and boiled at 80 Watt for approximately 3 mins, until the agarose was completely dissolved. The solution was then cooled down to below 60^0C, ethidium bromide was added at a final concentration of 0.5 µg/ ml and the solution was poured in the respective tray and the desired combs were inserted in the solution at the predefined positions. After 30 minutes loading buffer was added to the DNA samples at a final concentration of 1X and the samples were pipetted into the gel. 100 bp and 1kbp ladders were also pipetted as size controls. 140 V were applied to the gel and the DNA was let to migrate for the desired time. The ethidium bromide-DNA complex was excited by UV light and emitted orange light for visualizing the DNA bands using a UV transilluminator.

3.1.4 Gel extraction

The DNA bands were exposed to low intensity UV light in order to prevent mutagenesis and a thin gel piece including the desired DNA band was excised using a sterile scalpel and weighed. For extracting the DNA the QIAquick gel extraction kit was used. 3 volumes of QG buffer were added to 1 volume of gel (100 mg ~ 100 µl) and incubated at 50^0C for roughly 10mins shaking at 500 rpm, until the gel was completely dissolved. The mixture color was checked to be yellow, 1 gel volume of isopropanol was added, mixed and then applied to a QIAquick column that was placed in a 2 ml collection tube and centrifuged for 1 min at 13000 rpm and at RT using a tabletop microcentrifuge. The flow-through was discarded, the column was placed back in the 2 ml collection tube and 0.5 ml QG buffer was applied to the column and centrifuged for another 1 min to remove agarose traces. The flow through was again discarded, 0.75 ml PE buffer was applied to the column, let to stand for 2-5 mins and then centrifuged for 1 min. The flow-through was discarded and the column was centrifuged again for 1 min to remove any residual PE buffer. To elute DNA, the column was then transferred to a clean 1.5 ml microcentrifuge tube, 20 µl of DNase/RNase-free H_2O were added to the center of the membrane, let to equilibrate the column for 60 seconds and then centrifuged for 1 min.

3.1.5 Oligonucleotide annealing

To clone a complementary sequence of a microRNA of interest into a plasmid, the desired sequence (top strand), as well as the bottom strand were ordered from Sigma Aldrich with the desired restriction endonuclease recognition sites' overhangs at their two ends. The oligonucleotides were first dissolved to a concentration of 100 µM and the annealing was performed using a PCR cycler under the following conditions:

10X annealing buffer (T4 DNA ligase buffer)	5 µl
Top strand (100 µM)	5 µl
Bottom strand (100 µM)	5 µl
ddH_2O	ad. 50 µl

The mixture was heated to 95^0C for 3 mins, and then cooled down to 25^0C with a 2% ramp. The reaction was kept at 4 degrees until the next step. For ligation into the vector of interest, 1 µl of the annealed oligonucleotide was diluted with 99 µl of ddH_2O and 1 µl of the dilution (100 fmol) were then used for the ligation for simplicity reasons (most of the used oligonucleotides were of similar size (~30 bp) and thus of similar molecular weight).

3.1.6 Endonuclease restriction digestion

Restriction digestion was performed for either integrity testing reasons or for cloning. In both cases, the enzymes were acquired from New England Biolabs (Ipswich, MA, USA) and 5 Units per µg DNA were incubated under the recommended -for each enzyme specific- conditions of buffers and temperature for 1 hour.

3.1.7 Antarctic phosphatase treatment of digested DNA

After digesting a plasmid with only one restriction enzyme or with enzymes that create blunt ends, dephosphorylation of the vector was performed prior to ligation to prevent vector self-ligation. 5 Units of Antarctic phosphatase from New England Biolabs (Ipswich, MA, USA) as well as Antarctic phosphatase reaction buffer 1X concentration were directly added to the digestion reaction, incubated at 37^0C for 30 min, followed by enzyme inactivation at 80^0C for 2 minutes. If the restriction enzyme could not be inactivated by heat-inactivated, DNA purification was performed prior to ligation.

3.1.8 DNA ligation

For ligating two DNA fragments that were previously digested with the same enzymes, the T4 DNA ligase from New England Biolabs (Ipswich, MA, USA) was used. This enzyme catalyzes the formation of a phosphodiester bond between a 5' phosphate and a 3' hydroxyl termini of two digested DNA fragments. The following equation was used to calculate the amount of insert to be used for the ligation:

$$\text{insert}\ (ng) = 5 * \frac{\text{insert length}\ (bp) * \text{vector mass}\ (ng)}{\text{vector length}\ (bp)} \quad (1)$$

10X T4 DNA ligase buffer	1 µl
Vector DNA	10 - 50 ng
Insert DNA	calculated in (1)
T4 DNA ligase	1 µl
ddH_2O	ad. 10 µl

For cohesive (sticky) ends, the reaction was incubated at RT for 10 minutes or at 16^0C overnight. For blunt ends or single band overhangs, the ligation was carried out at RT for 2 hours or at 16^0C overnight. The ligation was then either directly transformed in bacteria or a precipitation step was involved in between in order to increase the transformation efficiency.

3.1.9 DNA precipitation with glycogen

To increase the DNA recovery after a ligation and thereby increase the electroporation efficiency of the bacteria, 2 µl of glycogen, RNA grade (Thermo Fisher Scientific, Darmstadt, Germany), were added to the 10 µl of the ligation solution, followed by addition of 0.5 volumes (6 µl) of 7.5 M $NH_4CH_3CO_2$ and then 2.5 volumes 100% ethanol (45 µl). After mixing the solution by pipetting, it was centrifuged at 14000 rpm and 4^0C for 20 minutes using a 5417R centrifuge (Eppendorf, Hamburg, Germany). Afterwards, the supernatant was discarded and the visible pellet was washed twice with 100 µl 70% ethanol for 10 minutes at 14000 rpm and 4^0C. After air-drying the pellet for approximately 10 minutes, it was resuspended in 10 µl DNase/RNase free H_2O.

3.1.10 Gateway cloning - BP and LR reactions

The Gateway cloning technology was used to produce the miR-29 sponge AAV constructs. The DNA fragment of interest (multiple miR-29 binding sites) was synthesized by GeneArt, Life Technologies (Carlsbad, CA, USA), flanked by *attB* sites. In a first step, a BP reaction was carried out between the *attB* sites of the synthesized DNA and the *attP* sites of the pDONR-221 donor vector to create the entry clone containing the desired DNA sequence. After the recombination, the desired DNA sequence in the entry clone was flanked by *attL* sites. To increase the efficiency of the recombination, a part of the synthesized plasmid containing the *attB* sites and the desired sequence was first digested out of the plasmid, purified, and the BP reaction was carried out between this purified DNA and the pDONR-221 plasmid. The BP reaction protocol was:

50 fmol (1 - 7 µl)	linearized *attB* expression clone
1 µl	pDONR-221 vector (150 ng/µl)
ad. 8µl	TE Buffer, pH 8.0

To convert *fmol* of DNA to *ng*, the following formula was used:

$$(ng) = (\text{fmol})(\text{N}) * (\frac{660\ fg}{fmol})(\frac{1\ ng}{10^6\ fg})$$

where N is the size of the DNA in *bp*.

After mixing the *attB* and *attP* containing DNA fragments as described above, the Gateway BP Clonase II enzyme mix was removed from the -20^{0}C, thawed on ice for 2 min and vortexed briefly (2 s each time) twice. 2 µl were then added to the DNA-containing solution, which was mixed well by brief vortexing and the reaction was incubated at 25^{0}C for 1 h. The reaction was then stopped by a 10 min incubation step at 37^{0}C with proteinase K. 1 - 3 µl were used to transform *DH10B* electrocompetent cells. After Kanamycin-based selection of a proper entry clone containing the desired DNA flanked by *attL* sites, this was recombined with an AAV destination vector containing *attR* sites using an LR reaction:

150 ng (1 - 7 µl)	entry clone
1 µl	AAV destination vector (150 ng/µl)
ad. 8µl	TE Buffer, pH 8.0

The Gateway LR Clonase II enzyme mix was removed from the -20^{0}C and thawed on ice for 2 min and vortexed briefly (2 s each time) twice. 2 µl were then added to the DNA-containing solution, which was mixed well by brief vortexing and the reaction was incubated at 25^{0}C for 1 h. The reaction was then stopped by a 10 min incubation step at 37^{0}C with proteinase K. 1 - 3 µl were used to transform *DH10B* electrocompetent cells, followed by Ampicillin selection. Positive clones were used to expand the DNA and produce AAV.

3.1.11 Mutagenesis of plasmid DNA

To test whether miR-29 directly targets *Gsk3β*, *Ctnnbpi1*, *Hbp1* and *Glis2*, mutated - for the miR-29 binding sites - versions of reporter plasmids carrying part of the 3'UTRs of the mentioned genes were generated. As templates, the DF-GSK3β, DF-CTNNBIP1, DF-HBP1 and DF-GLIS2 plasmids were used. The DF-GSK3β plasmid was generated by amplifying 460 bp of the mouse *Gsk3β* 3'UTR with primers introducing AgeI and EcoRI sites at the 5'- and 3'-

ends of the amplicon, respectively, and ligating it in a double fluorescent construct. For generating the mutated versions of the three other potential miR-29 targets, the DF-CTNNBIP1, DF-HBP1 and DF-GLIS2 plasmids, cloned by Laurenz Grüter, were used as templates. For mutating the miR-29 binding site in the DF-GSK3β plasmid, the Q5 site-directed mutagenesis kit from New England Biolabs (Ipswich, MA, USA) was used. The primers were designed with 5' ends annealing back-to-back, as instructed by the manufacturer. Following mix was pipetted together:

Step 1: Exponential Amplification

	25 µl RXN	**Final Concentration**
Q5 Hot start high-fidelity 2X master mix	12.5 µl	1X
10 µM forward Primer	1.25 µl	0.5 µM
10 µM reverse Primer	1.25 µl	0.5 µM
Template DNA (1 - 25 ng/µl)	1 µl	1 - 25 ng
Nuclease-free water	9 µl	

Cycling conditions:

Step	**Temp.**	**Time**	**No. of steps**
Initial denaturation	98^0C	30 s	1
Denaturation	98^0C	10 s	25
Annealing	62^0C	20 s	
Extension	72^0C	3 min (20 - 30 s /kb)	
Final extension	72^0C	2 min	1
Hold	4^0C	∞	-

Step 2: KLD Reaction

	Volume	**Final Concentration**
PCR Product	1 µl	
2X KLD Reaction Buffer	5 µl	1X

10X KLD Enzyme Mix	1 µl	1X
Nuclease-free water	3 µl	

The reaction was incubated 5 min at RT, and then 5 µl were electroporated in *DH10B* cells. After the plasmid DNA isolation, Sanger sequencing confirmed the desired mutations, but a part of the backbone of the plasmid was missing, as assessed by a control digestion. To generate the final plasmid carrying the mutated binding site for miR-29, the successfully mutated part of the *Gsk3β* 3' UTR was digested with AgeI-HF and EcoRI-HF (New England Biolabs, Ipswich, MA, USA) and ligated with the backbone of the WT DF-GSK3β plasmid.

Due to the fact that using the Q5 Site-Directed Mutagenesis kit led to partial loss of the vector backbone, plus the complexity of the 3'UTRs of *Hbp1* and *Glis2*, that bear 2 and 4 binding sites for miR-29, respectively, we decided to adapt an alternative strategy, that is depicted in **Figure 3.1**. For mutating each binding site for miR-29, we designed a longer - than usual - primer containing the desired sequence flanked by approximately 20 nucleotides in each side to increase the binding affinity to the template and performed a first PCR using this plus a second primer, that was at the closest end (5'- or 3'-) of the cloned 3' UTR, bearing a restriction site at its end. The DNA of this amplicon containing the desired mutation was isolated and used as a reverse primer, with the second primer being designed at the other end of the cloned 3'UTR, containing another restriction site at its end, in order to perform a second PCR. After the second PCR the wildtype double fluorescent vector and the second amplicon were digested with AgeI-HF and EcorI-HF and ligated with each other.

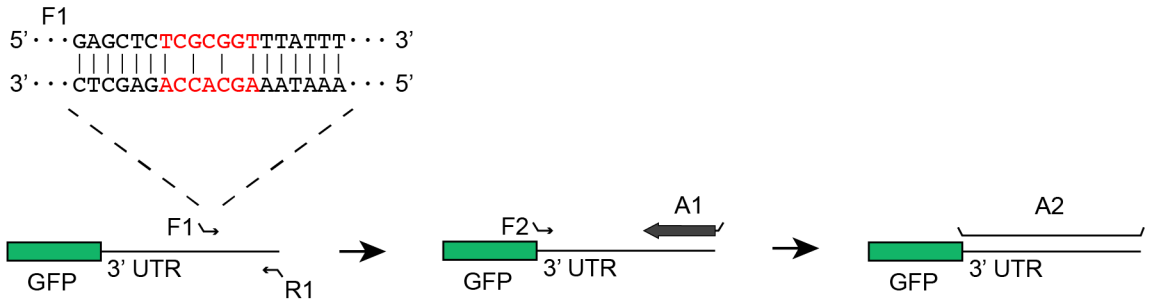

Figure 3.1 Schematic representation of the mutagenesis strategy

The mutagenesis of the DF-CTNNBIP1 reporter is presented here as a representative example of the strategy. A first PCR was performed using primers F1 and R1 and the DF-CTNNBIP1 reporter as a template. The primer F1 consists of the desired sequence, containing 3 mutations within the binding site of the miR-29 seed region, flanked by approximately 20 complementary - to the reporter plasmid - bases. The R1 primer bears a restriction site in its 5' for EcoRI. This reaction resulted in an amplicon (A1), that could then be used as a reverse primer for a second PCR. F2 served as the forward primer in this case. The second PCR led to the desired product (A2), bearing restriction sites at both ends (AgeI at the 5'- and EcoRI at the 3'-end). A2 could then be digested and ligated in the DF-CTNNBIP1 reporter to generate its mutated version. In red the nucleotides corresponding to the miR-29 seed sequence.

For cloning the DF-CTNNBIP1-MUT construct, the DF-CTNNBIP1 wildtype plasmid was used as a template, and the first PCR was performed using *Ctnnbip1* MUT F and *Ctnnbip1* R primers, generating a 203 bp amplicon. This was then used as reverse primer, and with the *Ctnnbip1* F primer a second PCR was performed, using again the DF-CTNNBIP1 wildtype plasmid as the template, resulting in a 443 bp product, containing the desired mutation and having recognition sites for AgeI and EcorI at its 5'- and 3'-ends, respectively. This was then ligated into the DF-CTNNBIP1 construct to produce the DF-CTNNBIP1-MUT.

To clone the DF-HBP1-MUT, bearing 2 mutations for miR-29, the same strategy was used. Using *Hbp1* MUT1 F and *Hbp1* MUT2 R primers, and DF-HBP1 as a template, a 515 bp long amplicon was created. In a second step, this DNA fragment was used as a long reverse primer with the *Hbp1* F primer and the same plasmid as a template. This second PCR resulted in a 625 bp long amplicon with recognition sites for AgeI and EcorI at its 5'- and 3'-ends, respectively, allowing to ligate it in the DF-HBP1, in order to retrieve the DF-HBP1-MUT reporter.

To generate the DF-GLIS2-MUT plasmid, containing 4 miR-29 binding sites the mutations 3 and 4 were first introduced using the same method as before, *Glis2* MUT3 F and *Glis2* MUT4 R primers, and DF-GLIS2 as a template. This resulted in a 345 bp long amplicon, which was used as a reverse primer, bearing an MfeI recognition site at its 5', together with the *Glis2* F primer. The resulted amplicon was cloned in the wildtype double fluorescent reporter to generate the DF-GLIS2-MUT3,4. MfeI was chosen in this case, because it produces the same overhangs as EcoRI. Since *Glis2* 3' UTR contains an EcoRI recognition site, the amplicon could be digested with MfeI and then ligated with the vector, that was digested with EcoRI. In order to introduce mutations 1 and 2, a DNA fragment was synthesized by Invitrogen (Karlsruhe, Germany), bearing the sequence from the 5'-end of the *Glis2* 3' UTR until the endogenous EcoRI recognition site, including mutations 1 and 2. This fragment was digested with AgeI-HF and EcoRI-HF and inserted in the DF-GLIS2-MUT3,4 vector to generate the DF-GLIS2-MUT1,2,3,4, or DF-GLIS2-MUT reporter.

3.1.12 Transformation of bacteria

Depending on the application, a different bacterial strain was used. For common applications the *E. coli* DH10B strain was used, whereas for ligations concerning unstable or sensitive - for recombination – vectors, SURE cells where the choice of preference. A 50 µl aliquot of electrocompetent cells were thawed on ice for 20 - 30 minutes, 2 µl of the ligation was added to the cells and mixed gently by pipetting. The solution was then transferred to a Gene Pulser 0.1 cm cuvette and a short 1.8 kV pulse was applied using the Bio-Rad MicroPulser (Hercules, CA, USA). The electroporated cells were mixed with 200 µl S.O.C. medium, transferred to a 1.5 ml microcentrifuge tube and incubated at 37^0C for 60 minutes shaking at 500 rpm in a

thermomixer (Eppendorf, Hamburg, Germany). 200 µl of the suspension were then plated on LB agar plates containing the proper antibiotic in a serial-dilution manner, so that single cell colony picking would be possible the next day. The plates were then incubated at 37^0C overnight.

3.1.13 Mini culture and DNA purification

For identification of the correct clone, 3 - 6 colonies were picked from the LB agar plates in 5 - 10 ml LB medium containing the proper antibiotic and incubated overnight at 37^0C and 180 rpm. In case the cloned construct was susceptible to recombination, the colonies were first picked in 50 µl LB medium and incubated for 1 h at 37^0C at 500 rpm in a thermomixer and only 20 µl of this pre-culture were then transferred to 5 - 10 ml LB medium and incubated overnight as described above. Once the miniprep was performed and the correct clone was identified, 20 µl of the pre-culture - that was in the meanwhile kept at 4 degrees - were transferred to the proper volume of LB medium for bigger scale plasmid production. After the overnight incubation of the mini culture, 100 µl were transferred to a 1.5 ml microcentrifuge tube and kept as a backup in the fridge, while the rest of the mini culture was centrifuged down at 13000 rpm for 5 min. The DNA was isolated using the QIAprep spin miniprep kit. The supernatant was discarded and the bacterial pellet was resuspended in 250 µl buffer P1 and transferred to a 1.5 ml microcentrifuge tube. To lyse the cells, 250 µl buffer P2 was added, the tube was inverted to gently mix the solution and incubated 5 min at RT. After addition of the P2 buffer the solution turned blue, to help optimal buffer mixing. After the 5 min incubation, 350 µl buffer N3 were added to neutralize the solution, which turned colorless. After mixing in order to get a homogeneous solution, the tube was centrifuged for 10 min at 13000 rpm, that led to a formation of a compact white pellet. 800 µl of the supernatant were transferred to a QIAprep 2.0 spin column by pipetting, and centrifuged in a tabletop microcentrifuge for 60 s. The flow-through was discarded, the column was washed with 500 µl of PB buffer, followed by 60 s centrifugation and discarding the flow-through. 750 µl of PE buffer were added to the column, let to stand for 2 - 5 min and then centrifuged for 60 s at 13000 rpm. The flow-through was discarded and the column was again centrifuged for 60 s to get rid of any PE buffer residues. The column was finally transferred to a clean 1.5 ml microcentrifuge tube, 20 µl of DNase/RNase free H_2O were added to the center of the column, let stand for 1 min and the DNA was eluted by centrifuging for 60 s.

3.1.14 Midi – Maxi – Giga culture and DNA purification

In order to produce plasmid DNA in larger scales, midi, maxi or even giga cultures were prepared. 20 µl from the mini culture or the pre-culture were transferred to 200 or 800 ml of LB medium for midi or maxi culture, or to 1600 ml of TB medium for giga culture and incubate at

37^{0}C and 180 rpm overnight. The Invitrogen (Karlsruhe, Germany) PureLink kits were used to isolate the plasmid DNA according to the manufacturer' s instructions. For eluting the DNA, 0.2, 1 and 4 ml of DNase/RNase free H_2O were used and about 0.2, 1 and 5 mg of plasmid DNA were isolated from midi, maxi and giga cultures, respectively.

3.1.15 Sequencing of PCR products or plasmid DNA

Sanger sequencing was performed from Eurofins Genomics (Ebersberg, Germany). For this, 15 µl of 50 - 100 ng/ µl of plasmid DNA, 15 µl of 5 ng/ µl for 300 - 1000 bp or 15 µl of 10 ng/ µl for 1000 - 3000 bp of purified PCR products were prepared and sent for sequencing. The next day the results could be downloaded and blasted against the desired sequence using MacVector (MacVector Inc., Apex, NC, USA).

3.2 Cell culture methods

3.2.1 Cultivation of HEK293, 3T3-NIH, A549

HEK293, 3T3-NIH and A549 cell lines were maintained in DMEM medium, containing 10% FBS, 1% Penicillin (10000 U/ ml)/ Streptomycin (10000 µg/ ml) in an incubator at 37^{0}C and 5% CO_2. The cells were kept on Nunc culture dishes (Thermo Fisher Scientific, Darmstadt, Germany) and passaged every 2-3 days when split 1:10.

For splitting, the cells were washed once with DPBS and then trypsin was added to cover the cells and incubated for 2 - 5 min in the incubator, until the cells detached. The trypsin was then inactivated by addition of double the volume of culture medium, a single-cell suspension was generated by pipetting, and the desired amount of cells were replated and filled up with culture medium. In trypsin-sensitive cases, the trypsin was removed by centrifugation. In these cases, after inactivation of the trypsin, the cell were centrifuged down at 1500 rpm for 5 min in a 5702R centrifuge (Eppendorf, Hamburg, Germany), the supernatant was aspirated and the cell pellet was resuspended the desired amount of fresh culture medium.

3.2.2 Isolation of neonatal rat cardiac myocytes (NRCM) and cardiac fibroblasts (NRCF)

A minimum of 10 Sprague-Dawley newborn rats (0 - 1 day old) were euthanatized by decapitation. The amounts mentioned in this protocol are for a minimum of 25 pups, for less pups the half amounts should be prepared. For each rat, the chest was opened, the heart was removed with forceps and transferred in a 50 ml falcon containing CBFHH on ice. Once all the hearts had been removed, the atria were cut off on a 10 cm dish containing CBFHH on ice, the ventricles were transferred to a 6 cm dish containing CBFHH on ice and were further cut down into small pieces (3-5/heart). 30 ml of the collagenase/ pancreatin solution were then

added with a 25 ml pipette to the crushed hearts and then transferred to the cell stirrer. Then, serial digestions were performed as indicated:

First	20 min; discard, as most cells are erythrocytes
Second	20 min
Third	25 min
Fourth	25 min
Fifth	15 min
Sixth	10 min

After each digestion, the cell suspension was placed immediately in 4 ml FBS and centrifuged for 5 min at 900 rpm using a 5702R Eppendorf centrifuge (Hamburg, Germany). The pellet was then resuspended in 8 ml FBS and kept in the incubator at 37 degrees. After all digestions, the cell suspensions in FBS were pooled and centrifuged for 5 min at 900 rpm. The pellet was then centrifuged in preplating medium. The suspension was passed through a 40 µm filter and preplated for 75 min on 10 cm dishes in the incubator (37^0C, 1% CO_2). For 10 pups 1 dish and 10 ml medium were used. After 75 min the fibroblast population (NRCF) were attached to the dishes, whereas the NRCM were still in the medium. The medium was collected into a 50 ml falcon and the cells were counted using a countess automated cell counter (Thermo Fisher Scientific, Darmstadt, Germany).

3.2.3 Isolation of adult mouse cardiac myocytes

All the buffers were prepared freshly. The mouse was injected intraperitoneally with 50 µl heparin solution (25000 IU/ 5 ml, Ratiopharm, Ulm, Germany) plus 150 µl isotonic NaCl solution. 5 min later the mouse was euthanatized by cervical dislocation, the chest was cleaned with 70% ethanol, opened, and the heart was removed and placed on a 6 cm dish with perfusion buffer for cleaning. After removing fat, the dish with the heart was moved under a stereo magnifier and the aorta was attached to a cannula. Then the perfusion buffer in the syringe was pulled through the heart to remove any blood residues. Once the cannula was attached to the perfusion system with care to avoid bubbles, the perfusion buffer was turned on for 3 min at a flow rate of 4x10 (4 ml/ min). Next, the digestion buffer was turned on for 6 - 10 min at the same flow rate, with the exact duration depending on the heart appearance. When the heart became flaccid and pale, it was transferred to a 6 cm dish containing digestion buffer and the atria and fat were removed. The ventricle was then transferred in a small beaker with 2.5 ml digestion buffer, cut in small pieces followed by shearing for 1 min with the syringe. Afterwards, 2.5 ml buffer P1 were added to inactivate the collagenase and shearing was continued for 3 min. The cell suspension was then filtered through a 100 µm filter into a 50 ml falcon tube, and one drop was placed under the microscope to determine the cell quality.

For simultaneous isolation of AMCM and non-myocytes, the solution was let at 37^{0}C for 10 min, so that the cardiac myocytes sedimented. The supernatant, containing the non-myocyte population, was transferred into another 15 ml falcon tube (1).

For AMCM isolation, the sediment and the pellet were pooled in 10 ml of stop buffer P2. The suspension was transferred in a 25 ml autoclaved conical flask and calcium reconstitution was performed, gently whirling the cell suspension each time after calcium addition:

50 µl 10 mM $CaCl_2$	4 min at RT
50 µl 10 mM $CaCl_2$	4 min at RT
100 µl 10 mM $CaCl_2$	4 min at RT
30 µl 100 mM $CaCl_2$	4 min at RT
50 µl 100 mM $CaCl_2$	

The cells were transferred into a 15 ml falcon and let to sediment for 10 min. The supernatant was subsequently centrifuged for 1 min at 55 g (900 rpm).

For staining:
The pellet was pulled with the sediment in 1.5 - 1.8 ml of CM plating medium. A drop of the cell suspension was placed on a microscope slide to observe the CM quality. The laminin was then aspirated from the coverslips and 200 µl of cell suspension were seeded per coverslip and incubate for 1 h at 37^{0}C and 5% CO_2. For microscopy, the medium was carefully replaced with CM culture medium.

For RNA/protein isolation (requires pure cells):
The pellet and the sediment were pulled in 3 - 10 ml of CM plating medium and a drop of the cell suspension was pipetted on a microscope slide to determine the CM quality. The cells were then incubated in a 6 or 10 cm dish (uncoated) for 1 h at 37^{0}C and 5% CO_2. For RNA/protein extraction, the non-adherent cells were transferred into a 15 ml falcon, centrifuged for 2 min at 1200 rpm (220 g), the supernatant was aspirated and the pellet was finally frozen at -80^{0}C.

The supernatant from (1) was centrifuged with a 5702R Eppendorf centrifuge for 5 min at 4 degrees and 400 g (2).

If only the cardiac fibroblasts were of interest, the new supernatant was discarded and the pellet resuspended in the desired volume of 5% AMCF plating/ culture medium (1 - 2 ml are suitable for high density seeding for microscopy, up to 5 ml for seeding for RNA/protein extraction) and plated on 6 cm dishes. After 1 h incubation at 37^{0}C and 1% CO_2, the plates were gently washed twice with DPBS and fresh culture medium was added.

If all the non-myocyte populations were of interest, the pellet from (2) was resuspended in 1 ml erythrocyte lysis buffer and incubated at RT for 2 min. The reaction was then stopped by addition of 4 ml PBS and the suspension was further centrifuged for 5 min at 4 degrees and

400 g. The pellet was resuspended in 1 ml FACS buffer, passed through a 100 µm filter and transferred into a 1.5 ml microcentrifuge tube. This was centrifuged at 4 degrees and 400 g for 5 min, and the pellet was then resuspended in Fc block 1:50 in 200 µl FACS buffer and incubated at 4 degrees for 15 min. To stain for the different cell types, first 300 µl of FACS buffer were added to the 200 µl of the previously treated with Fc block cell suspension. The 500 µl cell suspension were now divided in following tubes:

200 µl	CD105-PE (1:50) and CD140-PE-Cy7 (1:100)
200 µl	CD105-PE (1:50) and CD140-PE-Cy7 (1:100)
25 µl	for FITC compensation
25 µl	for PE compensation
25 µl	for PE-Cy7 compensation
25 µl	unstained

The cell suspension was incubated with the antibodies for 30 min at 4 degrees, followed by a 5 min centrifugation at 4 degrees and 400 g. The pellet was then washed twice with 200 µl FACS buffer under the same conditions and the final pellet was resuspended in 500 µl FACS buffer per half heart and 200 µl FACS buffer for the 4 controls. The cells were then sorted using the S3 sorter from Bio-Rad (Hercules, CA, USA).

3.2.4 Transfection of HEK293, 3T3-NIH, A549 and NRCMs

All the above mentioned cells were transfected with 0.1, 1 and 2.5 µg of DNA plasmid per well of a 96-well, 12-well and 6-well plate, respectively using Lipofectamine 2000 according to the manufacturer's instructions, in the standard culture media but in the absence of antibiotics. 4 - 6 hours post transfection the medium was replaced with antibiotics-containing medium and the cell were either fixed or harvested for RNA/ protein isolation 48 h later.

In cases where oligonucleotides were cotransfected, they were mixed in the same tube with the plasmid DNA and Lipofectamine 2000 according to the manufacturer's instructions. In the reporter assays concerning putative targets of miR-29, the WT or the mutated - for the miR-29 binding sites - plasmids were co-transfected in HEK293 cells with 5 nM miR-control or miR-29 (Ambion, CA, USA), using Lipofectamine 2000.

In the case of primary cells, they were transfected one day after seeding, so that any dead cells could washed away, whereas the cell lines were transfected immediately upon seeding. For transfection, the cells were seeded in such a way, so that the plate was approximately 70% confluent at the time of transfection. For example, for NRCM 60000 cells were seeded per well of a 96-well plate.

3.2.5 Adeno-associated virus (AAV) production and purification

HEK293T cells were grown in triple flasks or cell factories (Thermo Fisher Scientific, Darmstadt, Germany) in standard medium (DMEM, 10% FBS, 1% penicillin/streptomycin) until reaching 70% confluency. The cells were then cotransfected with the helper plasmid (pDP6rs for AAV6 or pDP9rs for AAV9) and the transgene plasmid using PEI (Polyethyleneimine, Sigma-Aldrich, Taufkirchen, Germany). 72 h post transfection the cells were harvested, lysed and benzonase treated. The AAV was purified from the crude cell lysate using density gradient ultracentrifugation. For this purpose, 60%, 40%, 25% and 10% iodixanol gradients were generated using OptiPrep (60% Iodixanol in water, density 1.32 g/ml), and the AAV was placed on top of these gradients and centrifuged at 50000 rpm in a optima L-80 XP ultracentrifuge (Beckman Coulter, Brea, CA, USA) using a Optima L-80 XP Rotor, Type 75 Ti.

In order to exchange iodixanol with lactate, what simultaneously enabled us to concentrate the virus, the Vivaspin 20 (MWCO 100000) columns were used (Sartorius, Göttingen, Germany). The columns were washed once with lactate (5 min, 4000 g, RT), the virus was diluted 1:6 in lactate, passed through a 0.2 µm filter and then added to the Vivaspin column. The solution was centrifuged at RT and 4000 g, until 1 ml was still above the filter. This was then further diluted with 9 ml lactate and centrifuged down to 600 - 800 µl.

3.2.6 AAV titration

In order to titrate the AAV, the viral DNA had first to be released from the capsid. To achieve this, 10 µl of AAV were added to 10 µl of TE buffer in a 1.5 ml microcentrifuge tube, followed by addition of 20 µl 2 M NaOH and incubation at 56^0C for 30 min in the thermomixer. After the alkaline lysis of the capsid, 960 µl of 40 mM HCl were added, mixed and 1 µl was used for qPCR as indicated:

Component	Volume	Final concentration
AAV lysate or standard	1 µl	
10 µM primer mix	1 µl	400 nM
SYBR Green Mix 2x	12.5 µl	1X
ddH_2O	10.5 µl	

The following program was used for the qPCR:

Step	Temp.	Time	No. of steps
Initial denaturation	95^0C	10 min	1
Denaturation	95^0C	15 s	40
Elongation	60^0C	1 min	

A representative AAV titration curve is depicted in **Figure 3.2**.

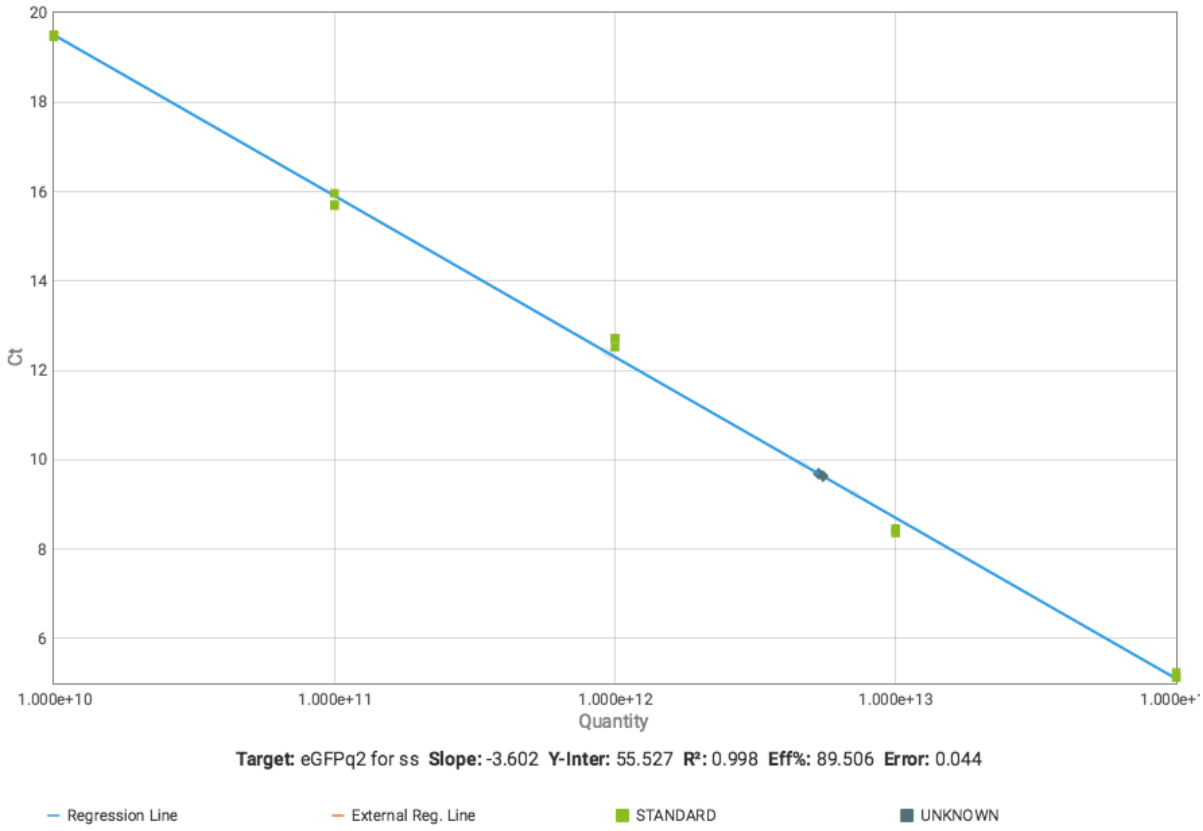

Figure 3.2 Exemplary AAV titration curve

This curve plots the transgene copy number (log, x axis) vs. the ct value of the qPCR (y axis). Five serial dilutions of a known amount of plasmid copy number were used to generate this titration curve and the unknown AAV titers could then be extrapolated. The data were analyzed using the Thermo Fisher Scientific Cloud Design and Analysis Application.

To determine the required concentration of the plasmid from which the first standard would be prepared the formula below was used and then four ten-fold dilutions were prepared:

$$\text{concentration } (g\ ml^{-1}) = \frac{\text{plasmid length } (bp) * \text{standard copies } (ml^{-1}) * 660\ (g\,mol^{-1}bp^{-1})}{6.022 * 10^{23}\ (mol^{-1})}$$

For each standard 10 µl were used and processed exactly as the AAV (see description above). After the addition of the 40 mM HCl, 1 µl of the processed standards were used for the qPCR.

3.2.7 Hypertrophy assay

To assess the cardiac myocytes cell size, 50000 NRCM per well were seeded on a 96 well plate (ibidi, Martinsried, Germany) in MEM medium containing 1% FBS. 24 hours later, the cells were washed thrice with PBS to remove the dead cells and cell debris and synthetic microRNA precursors (Ambion, CA, USA) or inhibitors (Exiqon, Vedbaek, Denmark) were transfected at the indicated concentrations, using Lipofectamine 2000. 4 - 6 hours later, the

medium was exchanged to MEM containing 0.1 % MEM. When IWR-1 (10 µM, Sigma Aldrich, Taufkirchen, Germany) or 11R-VIVIT (5 µM, Calbiochem, San Diego, CA, USA) were employed, these were added at this step. 48 h later, phenylephrine (50 µM PE, Sigma Aldrich, Taufkirchen, Germany) was added to half of the wells in MEM containing 0.1 % FBS and incubated for another 48 hours. The cells were finally washed, fixed and stained as described in the immunofluorescence section using an anti-α-actinin antibody (see the antibodies section for details). The cells were acquired using a Axio Observer.Z1 microscope (Zeiss, Oberkochen, Germany) and a Retiga 4000 DC CCD camera (QImaging, Surrey, Canada) and the cell size was determined by MetaMorph (Molecular Devices, San Jose, CA, USA) as described previously[129]. The cardiac myocytes were assigned a green, whereas the rest of the cells a red nucleus, and only the green-nuclei-containing cells were taken into account for the cell size determination.

3.2.8 NFAT and TCF/LEF luciferase assays

NFAT activity was determined by the luminescence produced from a plasmid bearing 9 binding sites for NFAT upstream of a minimal promoter driving the expression of firefly luciferase[227] (a kind gift J. Molkentin, University of Cincinnati). The signal was normalized to the total protein level.

To determine Wnt activity, a similar approach was used. In this case we used the TOPFlash plasmid (Addgene #12456) that bears binding sites for TCF/LEF upstream of the minimal promoter and its negative control, FOPFlash (Addgene #12457), which has mutated TCF/LEF binding sites[228]. Wnt3a (50 ng/ ml, Cell Guidance Systems Ltd, Cambridge, United Kingdom) was added 6 h prior the end of the experiment.

In both cases luminescence was produced using the ONE-Glo assay kit (Promega, Madison, WI, USA) and measured by the Infinite M200 plate reader (Tecan, Männedorf, Switzerland).

3.2.9 Immunofluorescence

For staining in a 96-well plate (ibidi, Martinsried, Germany), the cells were washed three times with PBS and then incubated with 100 µl 4% PFA in PBS for 10 min at RT. After washing again thrice with PBS, if the target antigen was intracellular the cells were permeabilized using 100 µl 0.2 % Triton-X for 10 min at RT. Depending on the antibodies that were used, a 1 h blocking step with either 1% BSA or 5% serum from the secondary antibody host was performed. Next, the primary antibody was added (100 µl in the dilution mentioned in the antibodies section) in blocking solution for 30 min at 37^0C or 60 min at RT in a humid chamber. The secondary antibody and DAPI were then added in blocking solution after washing the plate thrice with PBS and incubated in the dark in a humid chamber for 30 min at 37^0C. As a final step, the secondary antibody was removed by washing three times with PBS, 150 µl of 50 % glycerol in

PBS were added per well and the plate was sealed with an Alu-Sealing tape. The stained plate was kept at 4 degrees in the dark until acquisition, which had to be done within a week.

3.3 RNA methods

3.3.1 RNA isolation

To isolate RNA, adequate amount of TriFast was added to the samples (1 ml per 50 - 100 mg of tissue or a 3.5 cm culture dish), these were then homogenized (using a Turrax in the case of a tissue or by vigorously pipetting in the case of cells) and incubated at RT for 5 - 10 min to allow cell lysis. After addition of 200 µl of Chloroform per 1 ml TriFast, the cells were vortexed for 50 s and then centrifuged in a 5417R Eppendorf centrifuge at 4^0C and 12000 g for 5 min. The upper RNA-containing aqueous phase was then carefully transferred to a clean 1.5 ml microcentrifuge tube, 500 µl of isopropanol per 1 ml of TriFast were added, mixed and incubated at 4^0C for 10 min or at -20^0C overnight for maximum RNA recovery. The samples were then centrifuged for 10 min at 4^0C and 12000 g and the supernatant was discarded. The pellet was washed with 1 ml of 75% Ethanol and centrifuged for 10 min at 4^0C and 12000 g. After carefully discarding the pellet, one more washing step was performed. The RNA pellet was air-dried, resuspended in 10 - 500 µl of ddH_2O (depending on the RNA amount), heated for a few seconds at 55^0C and then kept on ice until use (for a maximum of a few hours). For storage, the RNA was kept at -80^0C.

3.3.2 Reverse transcription of total mRNA

Total RNA was retro-transcribed using the Protoscript II enzyme from New England Biolabs (Ipswich, MA, USA). First, the RNA was mixed with the following ingredients:

100 ng - 1 µg	Total RNA
1 µl	50 µM oligo dT
1 µl	10 mM dNTPs
ad. 12 µl	RNase free H_2O

The samples were then incubated at 65^0C for 5 min and then centrifuged briefly. The following mixture was added to the RNA - primer mix, incubated at 42^0C for 60 min, followed by a 5 min enzyme-inactivation step at 80^0C:

4 µl	5x Protoscript II reaction buffer
2 µl	0.1 M DTT
1 µl	Murine RNase inhibitor
1 µl	Protoscript II reverse transcriptase

The cDNA was centrifuged briefly, and then a part of it was diluted to 5 ng/ µl in a new well for further qPCR. The cDNA was stored at -20^0C.

3.3.3 Reverse transcription of miRNAs

MiRNAs were reverse-transcribed using the miRCURY LNA Universal RT microRNA PCR protocol (Exiqon, Vedbaek, Denmark). The RNA samples were adjusted to 5 ng/ µl using nuclease free water and 2 µl were added to 8 µl of the following master mix:

2 µl	5x reaction buffer
4.5 µl	nuclease free H_2O
1 µl	enzyme mix
0.5 µl	UniSp6 synthetic RNA spike-in or H_2O

The reaction was mixed by very gentle vortexing or pipetting and spin down. The samples were then incubated at 42^{0}C for 60 min, the enzyme was heat-inactivated at 95^{0}C for 5 min and the reaction was immediately cooled down to 4^{0}C and either diluted appropriately for qPCR (depending on the miRNA abundance, standard was 1:80) and frozen at -20^{0}C.

3.4 Animal experiments

3.4.1 Genomic DNA isolation

To isolate genomic DNA for genotyping, a mouse biopsy was collected with an ear punch and placed in DNA lysis buffer (see materials for recipe) containing 2.5 µl of 10 mg/ ml proteinase K and incubated at 55^{0}C and 950 rpm in a thermomixer overnight. 500 µl phenol/chloroform/isoamyl alcohol were added to the digested tails and centrifuged for 10 min at 14000 rpm in a 5417R Eppendorf centrifuge and at RT. The upper phase containing the DNA was then transferred carefully to a clean 1.5 ml microcentrifuge tube, 500 µl isopropanol were added, the tube was mixed my inversion and then centrifuged again for 10 min at 14000 rpm and 4^{0}C. The supernatant was discarded, the pellet was washed with 500 µl 70% ethanol and then centrifuged for 10 min at 14000 and 4^{0}C. After carefully discarding the supernatant, the pellet was air-dried for 10 min and the pellet was dissolved in 50 µl H_2O.

3.4.2 Genotyping of transgenic mouse lines

The genomic DNA was set to a concentration of 50 ng/ µl and following mixture was prepared:

2 µl	10x Genscript Taq buffer
0.5 µl	forward primer
0.5 µl	reverse primer
0.4 µl	dNTPs
0.1 µl	Genscript Taq polymerase
14.5 µl	nuclease free H_2O

18 µl of the mix was then added to 2 µl (100 ng) of genomic DNA and following PCR was performed:

For the *miR-29ab1* cluster:

Step	Temp.	Time	No. of steps
Initial denaturation	95^0C	5 min	1
Denaturation	95^0C	30 s	40
Annealing	58^0C	30 s	
Extension	72^0C	30 s	
Final extension	72^0C	10 min	1
Hold	4^0C	∞	-

Expected size: ~561 bp for the wildtype

~717 bp for the knockout

For the *miR-29b2c* cluster and the *miR-29b2c*$^{fl/fl}$ mice:

Step	Temp.	Time	No. of steps
Initial denaturation	95^0C	5 min	1
Denaturation	95^0C	30 s	39
Annealing	62^0C	30 s	
Extension	72^0C	45 s	
Final extension	72^0C	10 min	1
Hold	4^0C	∞	-

Expected size for the *miR-29b2c*$^{fl/fl}$ mice: ~422 bp for the wildtype

~474 bp for the floxed

3.4.3 AAV application

The various AAVs used for this study were administered to neonatal mice as described previously with minor modifications. Anesthesia was achieved to 3 - 4-day-old mice by injecting an anesthetic cocktail containing fentanyl (0.05 mg/kg), midazolam (5 mg/kg) and medetomidine (0.5 mg/kg). While being kept warm atop of a warming pad the mice were administered 50 µl of the virus close to the pericardium using a 30-gauge needle. AntimiR-control and antimiR-29 (Exiqon, Vedbaek, Denmark) were injected i.v. at 20 mg/kg. PBS-treated mice were also included as further controls. In the case of double-stranded AAV9, $5x10^{11}$, whereas in the case of single-stranded AAV9, $2\text{-}3x10^{12}$ genome copies were injected, respectively.

3.4.4 Transverse aortic constriction (TAC)

For pressure overload-induced cardiac hypertrophy, the transverse aortic constriction (TAC) model was applied as described[229] with small modifications. 8-week-old male C57BL/6N mice (Charles River, Wilmington, MA, USA) received buprenorphine (0.1 mg/kg, s.c.) one hour before anesthesia with isoflurane. The chest was disinfected and the thorax was opened between the second and third rib. The aorta was constricted by tying a nylon suture over a 27-gauge cannula and the chest was reclosed. The mice were left to recover in a warmed cage and directly supervised for the next 4 hours. For the sham mice, the same procedure was performed without the aortic constriction.

3.4.5 Echocardiography

Transthoracic echocardiography was performed with the Vevo 770 and 3100 (VisualSonics, Toronto, Canada) before TAC or sham surgery and before euthanizing the mice. Each mouse was anesthetized (2% isoflurane mixed with 0.5 L/min 100% O_2), placed atop a heating pad to maintain the body temperature in a supine position and the chest's fur was shaved and ultrasound gel was applied. The isoflurane was adjusted to maintain a constant heart rate at 450 ± 50 beats per min (bpm). First, a 2D imaging ("B-mode") was implemented, to acquire a view along the parasternal short axis. Next, a 1D imaging ("M-mode") was applied, to obtain cardiac dimensions and contractile function measurements. For confirmation of a successful TAC operation, pulse wave doppler measurements were performed and the blood flow of the left and right carotid arteries was determined. The functional parameters of the heart fractional shortening (FS %) and ejection fraction (EF %) were calculated from the left ventricular internal diameters ($LVID_s$ in systole and $LVID_d$ in diastole, respectively) and the end diastolic and end systolic volumes (EDV and ESV, respectively) as depicted:

$$FS\ \% = 100 * \frac{LVID_d - LVID_s}{LVID_d}$$

$$\text{EF } \% = 100 * \frac{\text{EDV - ESV}}{\text{EDV}}$$

3.5 Statistics

All statistical tests were performed using the software GraphPad Prism version 6. The quantitative data are presented as mean ± SEM. To compare two groups an unpaired Student's *t*-test was performed. The Shapiro-Wilk or the Kolmogorov-Smirnov test was used to test for normal distribution of the data. If differences between multiple means had to be assessed, one-way or two-way ANOVA followed by Bonferroni's post hoc test were implemented. Where the *n* numbers were too small to test for normality, non-parametric tests, such as Mann-Whitney U-test or Kruskal-Wallis test, followed by Dunn's multiple comparisons test, were used. Significant differences where designated as * $P<0.05$, ** $P<0.01$ and *** $P<0.001$. Not significant differences were assigned a "n.s." label.

4 Results

4.1 Characterization of the cardiac role of miR-29

The experiments and data described in this chapter (4.1) were conducted by P. Avramopoulos. Additionally, Y. Sassi and D. Ramanujam contributed to Figure 4.4. The *miR-29* knockout mice were generated by the group of B. De Strooper, mass spectrometry was performed by the group of M. Mayr, D. Ramanujam helped with the analysis of the secretome in Figure 4.8b and 4.8c and L. Grüter cloned the native 3'-UTRs of CTNNBIP1, HBP1 and GLIS2 in Figure 4.8e.

Essential parts of the experiments and data described in this thesis were published by the author (in shared first authorship) in the following publication: Sassi Y*, Avramopoulos P* […] and Engelhardt S.: Cardiac myocyte miR-29 promotes pathological remodeling of the heart by activating Wnt signaling. *Nature Communications*. 2017;8(1):1614. *Contributed equally

4.1.1 Global miR-29 deletion protects from cardiac remodeling

In order to test if miR-29 exerts its prohypertropic effect that we observed *in vitro* (**Figure 1.7**) also *in vivo*, we decided to subject mice with genetic deletion of miR-29 to transverse aortic constriction (TAC), a left ventricular pressure overload model. Complete deletion of all the four miR-29 alleles (located in both *miR-29 a/b1 and b2/c* clusters) was lethal for the mice, an observation also made by another group[230], who reported that the few mice survived birth died within the first month of their life. Hence, we studied mice with deletion of three or two out of four alleles, that is mice with *miR-29 ab1*$^{-/-}$ *b2c*$^{+/-}$ or *ab1*$^{+/+}$ *b2c*$^{-/-}$ genotype. As also observed by others[226,230,231], mice lacking three out of four alleles displayed smaller body weight (**Figure 4.1**) and died prematurely, while mice lacking only the *miR-29 b2c* cluster did not demonstrate such phenotypes.

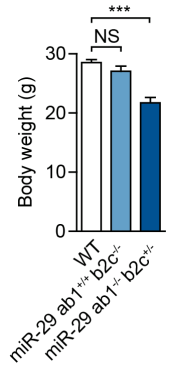

Figure 4.1. Body weight of miR-29 deficient mice

Body weight of 3 months-old wildtype mice and mice with *miR-29 ab1*$^{+/+}$ *b2c*$^{-/-}$ and *miR-29 ab1*$^{-/-}$ *b2c*$^{+/-}$ genotype, respectively. Data are from 7-11 mice per group. ***P<0.001 determined by one-way ANOVA followed by Bonferroni's post hoc test; NS: not significant. All quantitative data are reported as means ± SEM. This figure has been also used in our publication[47].

QPCR experiments showed that *miR-29 ab1*$^{-/-}$ *b2c*$^{+/-}$ and *ab1*$^{+/+}$ *b2c*$^{-/-}$ mice had only 20% and 35% of the total miR-29 remaining in the myocardium (**Figure 4.2a**), a fact that did not lead to any phenotype in sham-operated mice (**Figure 4.2b-e**). We then subjected these mice to TAC. TAC-operated *miR-29 ab1*$^{-/-}$ *b2c*$^{+/-}$ or *ab1*$^{+/+}$ *b2c*$^{-/-}$ mice were protected from cardiac hypertrophy, as assessed by improved fractional shortening (**Figure 4.2b**), decreased heart weight (**Figure 4.2c**), and smaller cardiac myocyte cross-sectional area (**Figure 4.2d)**, in comparison with wildtype littermates. Even more intriguing was the fact, that miR-29-deficient mice did not elicit signs of fibrosis after TAC, in contrast to the TAC-treated wildtype animals (**Figure 4.2e**). The protective phenotypes against cardiac hypertrophy and fibrosis were reflected at the mRNA level, where the miR-29-deficient mice exhibited decreased levels of expression of the prohypertrophic markers *Nppa*, *Myh7/Myh6*, as well as the fibrosis-related *Col1a1*, *Col1a2* and *Col3a1* genes (**Figure 4.2f**).

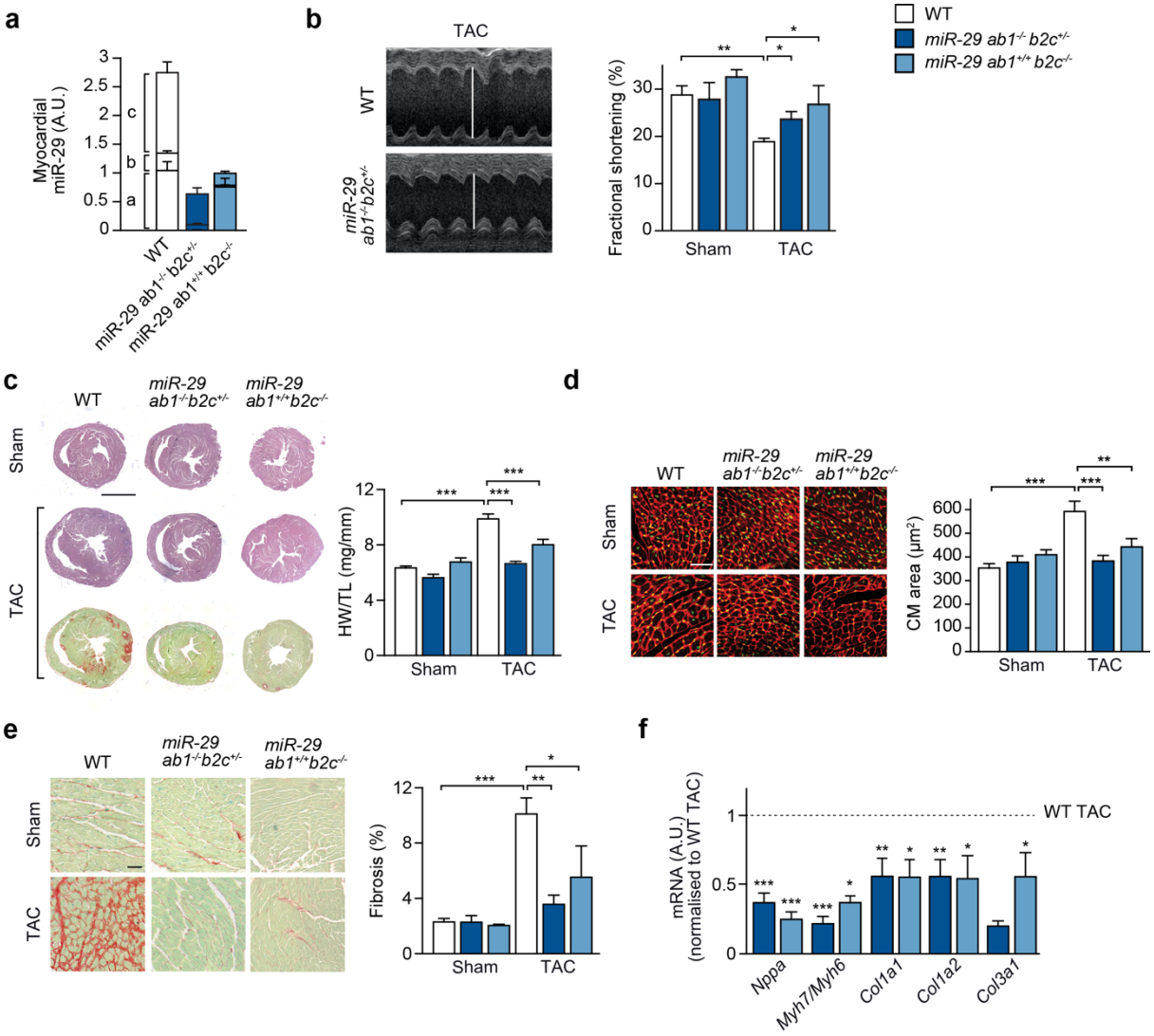

Figure 4.2. Global miR-29 deletion protects from cardiac remodeling

(**a**) Expression of miR-29 family members in left myocardium from wildtype (WT), miR-29 ab1$^{-/-}$b2c$^{+/-}$ and miR-29 ab1$^{+/+}$b2c$^{-/-}$ mice; n = 4-6 mice/group. (**b**) Echocardiographic analysis of fractional

shortening as a measure of left ventricular function; n = 4-10 mice/group. A Student's t-test was used to calculate the P values. (**c**) (Left) Representative staining of myocardial tissue from WT or the abovementioned knockout mice (tissue fixation 21 days after sham surgery or transverse aortic constriction, TAC) by hematoxylin/eosin (for hypertrophy) and Sirius Red/Fast Green staining (for fibrosis). Scale bar: 2 mm. (Right) Ratio between heart weight and tibia length (HW/TL) as a measure of cardiac hypertrophy; n = 6-14 mice/group. P values were determined by two-way ANOVA followed by Bonferroni's post hoc test. (**d**) (Left) Representative wheat germ agglutinin (WGA)-staining of midventricular sections to assess the hypertrophy of cardiac myocytes. Scale bar: 50 µm. (Right) Quantitative analysis; n =5-8 mice/group. P values were calculated using two-way ANOVA followed by Bonferroni's post hoc test (**e**) (Left) Representative image sections from Sirius Red/Fast Green-stained myocardium of the indicated groups and (Right) quantitative analysis of fibrosis; n =3-11 mice/group. P values were determined by two-way ANOVA followed by Bonferroni's post hoc test. (**f**) Real-time PCR quantification of markers for cardiac remodeling in left ventricular tissue from WT, *miR-29 ab1*$^{-/-}$*b2c*$^{+/-}$ and *miR-29 ab1*$^{+/+}$*b2c*$^{-/-}$ mice. Collagen mRNAs and the following markers of cardiac myocyte hypertrophy were assessed: Nppa, atrial natriuretic peptide; Myh7/Myh6, the ratio of mRNAs encoding β- and α-myosin heavy chain. Tissues were collected 21 d after TAC surgery; data are from 4-9 independent experiments, with 2 replicates each. WT TAC means were compared to that of *miR-29 ab1*$^{-/-}$ *b2c*$^{+/-}$ and *miR-29 ab1*$^{+/+}$ *b2c*$^{-/-}$ mice by a one-way ANOVA followed by a Bonferroni's post hoc test. *P<0.05, **P<0.01, ***P<0.001 for all panels. All quantitative data are reported as means ± SEM. This figure has been also used in our publication[47].

4.1.2 The miR-29 family is dynamically regulated

QPCR from RNA isolated from lysed left ventricular myocardium revealed that the expression of miR-29 is increased with age (**Figure 4.3a**), results that are in line with previous publications[164,232]. Even more interesting, was the fact, that miR-29 is dynamically regulated under disease conditions. In a pressure overload model, (transverse aortic constriction (TAC)), an increase of miR-29 in cardiac myocytes in the first 24-48 hours was followed by downregulation of its levels three weeks after TAC (**Figure 4.3b**). We hypothesized, that this initial boost in miR-29 expression in cardiac myocytes had to be inhibited in order to protect from impaired cardiac function. Therefore, we were interested to assess the effect of miR-29 pharmacological inhibition immediately after TAC.

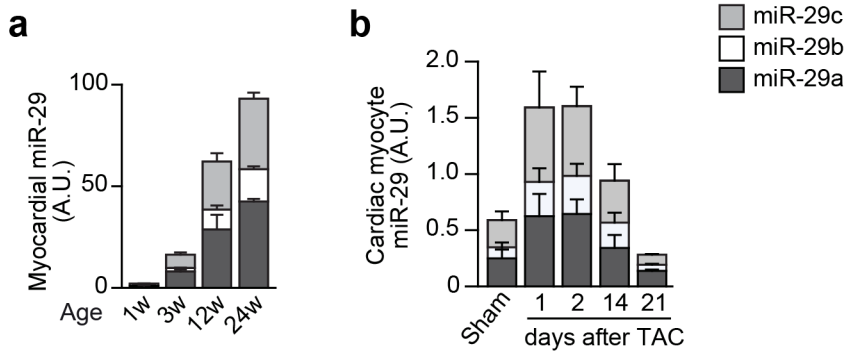

Figure 4.3. Expression of miR-29 family members in cardiac cells and their deregulation in disease

(**a**-**b**) Individual quantifications (by qPCR) of miR-29 variants a, b and c in primary cardiac cells or lysed left ventricular myocardium. (**a**) Age-dependent cardiac expression of miR-29 variants in mice (w: week); n = 4-5 mice per group. (**b**) Endogenous levels of miR-29 family members in cardiac myocytes from mice 21d after sham treatment or, for the TAC group, at denoted time points; n = 3-6 mice per group. All quantitative data are reported as means ± SEM. This figure has been also used in our publication[47].

4.1.3 Pharmacological inhibition of miR-29 prevents cardiac dysfunction

In order to test the potential of pharmacologic inhibition of miR-29, we injected intravenously (i.v.) 8 weeks old sham or TAC mice with antimiR-29 for three consecutive days after the operation, at a dose of 20 µg/g/day and sacrificed the mice three weeks later (**Figure 4.4a**).

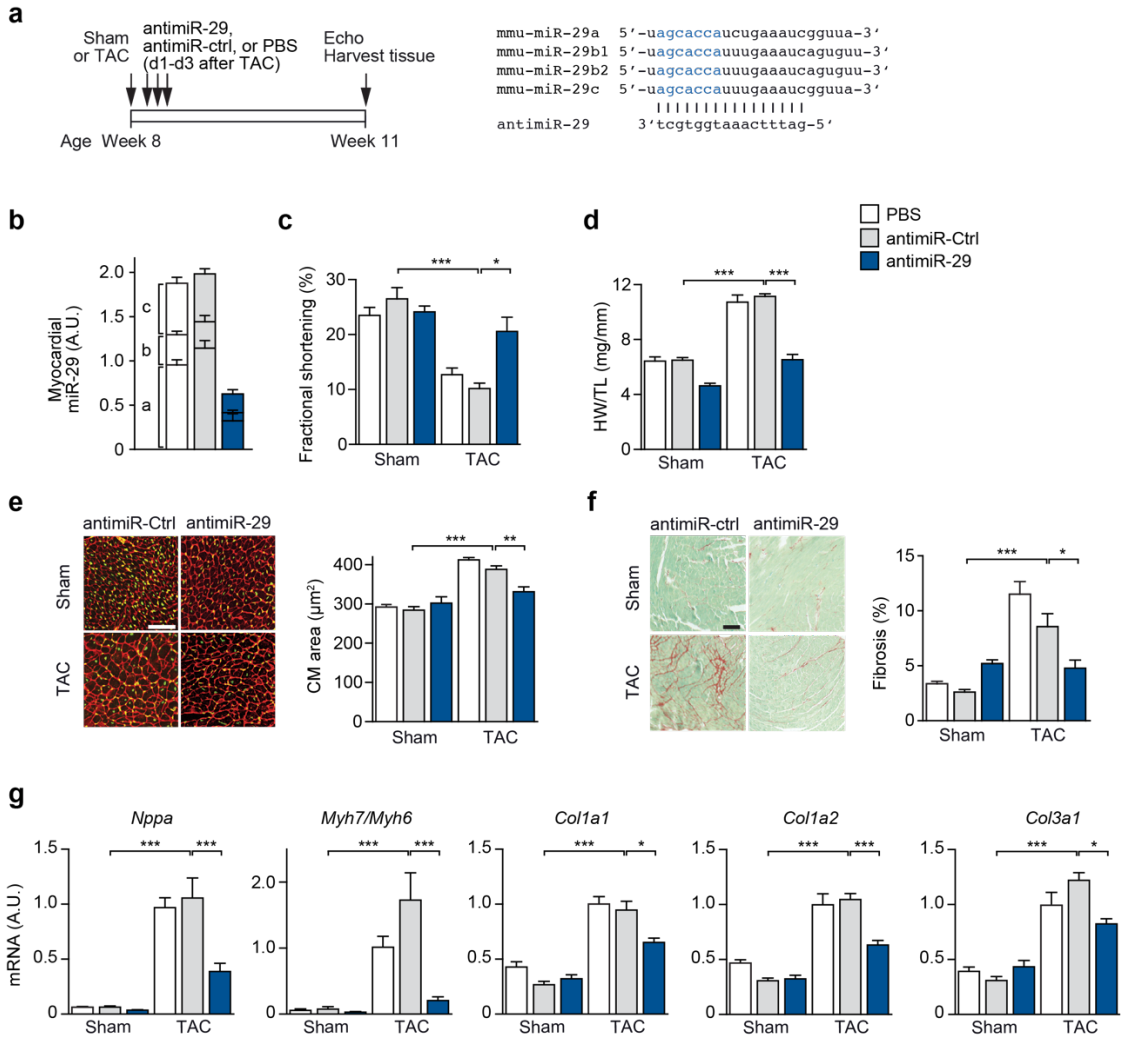

Figure 4.4. Pharmacological inhibition of miR-29 prevents cardiac remodeling and dysfunction

(**a**) (Left) Design of the study. (Right) Design of the miR-29 family inhibitor (antimiR-29). (**b**) Cardiac expression of miR-29 family members in mice, determined three weeks after the first injection of antimiR-29, a control molecule (antimiR-ctrl) or PBS. (**c**) Echocardiographic analysis of left ventricular fractional shortening in sham-/TAC-operated mice 3 weeks after injection with antimiR-29/-ctrl or PBS (determined by echocardiography), indicating reduced TAC effects in the antimiR-29-treated group. (**d**) Heart weight-to-tibia length ratio and (**e**) WGA staining of left ventricular tissue from mice described in (**c**) for determination of cardiac and CM hypertrophy. (**f**) (Left) Representative left ventricular sections stained with sirius red and picric acid/fast green of the indicated treatment groups and (right) quantification of interstitial fibrosis. (**g**) Quantitative real-time PCR analysis of molecular markers for cardiac myocyte hypertrophy (Nppa, Myh7/Myh6) and of fibrosis-associated collagens. All scale bars: 50 µm. All quantifications derive from n = 5-14 mice/group, PCR performed with 2 replicates each. All quantitative data in panels c-g are reported as means ± SEM. *P<0.05, **P<0.01, ***P<0.001 determined by two-way ANOVA followed by Bonferroni's post hoc test. This figure has been also used in our publication[47].

This led to 70% inhibition of miR-29 in the myocardium according to qPCR (**Figure 4.4b**). The antimiR-29-treated animals had preserved heart function after TAC in comparison to the control animals (**Figure 4.4c**), exhibited less hypertrophy at the whole heart level (**Figure 4.4d**) as well as the cardiac myocyte level (**Figure 4.4e**). More astonishing was the fact, that miR-29 inhibition led to a significant reduction of fibrosis after TAC in comparison to the control mice (**Figure 4.4f**). QPCR results for the hypertrophy-associated genes *Nppa*, *Myh7/Myh6*, as well as for the fibrosis-related *Col1a1*, *Col1a2* and *Col3a1*, were also in line with the protective phenotype after miR-29 inhibition (**Figure 4.4g**).

4.1.4 MiR-29 sponge inhibits cardiomyocyte hypertrophy *in vitro*

To confirm the anti-hypertrophic effect that we observed after miR-29 inhibition using an alternative methodology, we constructed several miR-29 sponges, that is, constructs bearing multiple miR-29 target sites in order to sequester and thereby inhibit active microRNA molecules. We designed sponges under the control of a strong polymerase II promoter, CMV, driving the expression of the dsRed fluorescent protein, and in its 3' 3 – 12 imperfect (or "bulged") miR-29 target sites with or without a 6-nucleotide long spacer between them. These imperfect target sites, that create a bulge at the nucleotides corresponding to the central region of the microRNA, protect from endonucleolytic cleavage by Ago2, conferring increased stability of the inhibitory complex[171]. One construct bearing 5 "perfect" miR-29 target sites was also created (**Figure 4.5a**).

Neonatal rat cardiac myocytes were transduced with AAV6 expressing each of the depicted sponges or a control construct expressing only dsRed for three days (**Figure 4.5b**), and then phenylephrine was administered to the cells to induce hypertrophy. The AAV6 transduced the majority of the cells, as seen in (**Figure 4.5b**), and assessment of the cardiac myocyte area revealed, that out of all the different designs tested, only the sponge bearing 12 imperfect miR-29 target sites inhibited phenylephrine-induced cardiomyocyte hypertrophy of neonatal rat ventricular cells (**Figure 4.5c**).

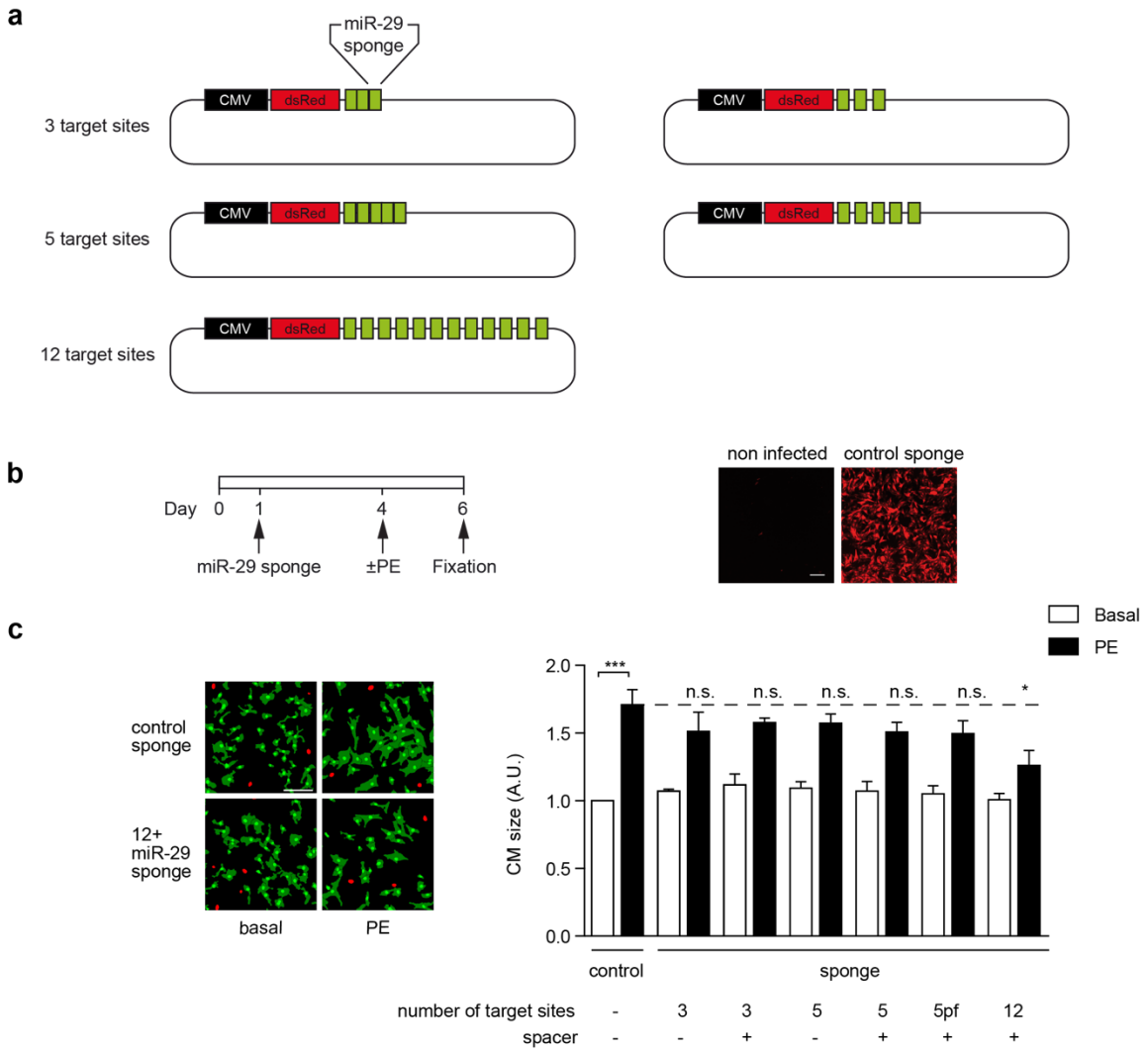

Figure 4.5. MiR-29 sponge inhibits cardiomyocyte hypertrophy *in vitro*

(**a**) Design of the miR-29 sponges. (**b**) (Left) Design of the assay. (Right) Representative images of neonatal rat cardiac myocytes depicting the high viral transduction efficacy (red is the native fluorescence of the control sponge). (**c**) A miR-29 sponge can inhibit cardiomyocyte hypertrophy *in vitro*; n=3. CM: cardiac myocyte. All quantitative data are reported as means ± SEM. *P<0.05, ***P<0.001 determined by two-way ANOVA followed by Tukey's post hoc test. Scale bar represents 100 µm.

4.1.5 MiR-29 is highly expressed in cardiac myocytes

QPCR from freshly isolated RNA from cardiac myocytes and fibroblasts revealed that miR-29 is expressed higher in the myocyte population (**Figure 4.6a**). This was an appealing finding, given the fact that miR-29 was believed to be higher expressed in fibroblasts than myocytes[44]. We could find out, that the previous characterization of miR-29 as a "fibromiR" was due to an artificial upregulation of miR-29 level in cardiac fibroblasts upon cultivation (**Figure 4.6b,c**). Our next goal was to investigate the importance of a cardiac myocyte-specific miR-29 knock down.

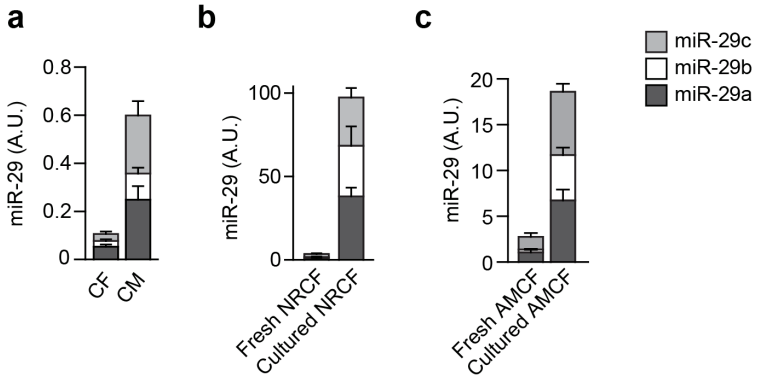

Figure 4.6. Expression of miR-29 family members in cardiac cells

(**a**) Endogenous levels of miR-29 family members expression in CM and CF freshly isolated from adult mouse myocardium; n = 12-13 independent cell isolations. (**b,c**) MiR-29 levels in (**b**) neonatal rat cardiac fibroblasts and (**c**) adult mouse cardiac fibroblasts directly after isolation and after one to two weeks of culture; n= 4-7 independents cell preparations. All quantitative data are reported as means ± SEM. This figure has been also used in our publication[47].

4.1.6 CM-specific miR-29 knockdown protects from pressure overload

To validate the hypothesis that inhibition of miR-29 in cardiac myocytes protects against cardiac hypertrophy and fibrosis, we sought to target miR-29 specifically in cardiac myocytes. Therefore, we made use of the AAV9 serotype, which within the myocardium targets primarily the cardiac myocytes (Ramanujam et al. 2016), generating a virus encoding for an improved recombinase (iCre). Intrapericardial injection to neonatal mice carrying floxed alleles of the *miR-29b2c* locus (*miR-29 b2c*$^{fl/fl}$) (**Figure 4.7a**) resulted in 50% reduction of the miR-29b and miR-29c levels (**Figure 4.7b**). Mice with cardiac myocyte-specific knockdown of miR-29 that underwent TAC showed a better heart function than the control mice (**Figure 4.7c**), less cardiac hypertrophy (**Figure 4.7d**), as well as significant less fibrosis (**Figure 4.7e**). In conclusion, targeted cardiac myocyte inhibition of miR-29 prevented cardiac dysfunction.

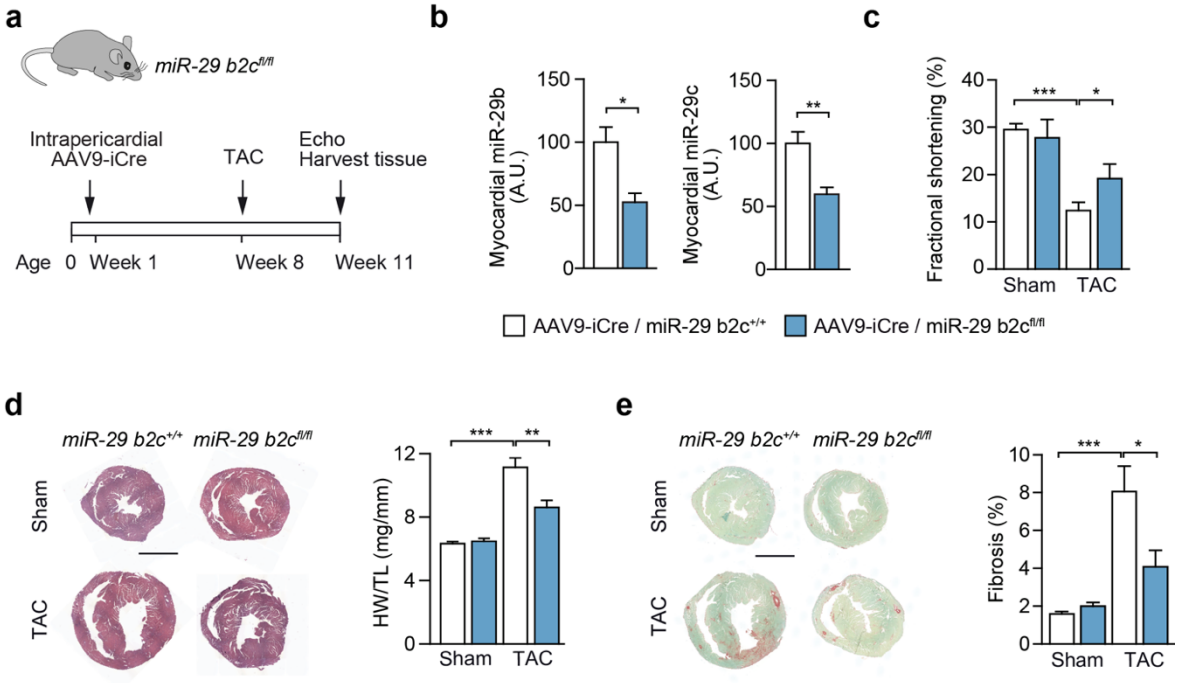

Figure 4.7. Deletion of miR-29 in cardiac myocytes *in vivo* protects from cardiac remodeling

Tropism of adeno-associated virus 9 for cardiac myocytes *in vivo* was employed to deliver improved Cre recombinase (AAV9-iCre) to miR-29 b2c$^{fl/fl}$ mice for the deletion of this cluster (with miR-29 b2c$^{+/+}$ littermates serving as controls). (**a**) Design of the study. 5x10^{11} viral particles (AAV9-iCre) were delivered to 5 days-old mice via intrapericardial injection. Seven weeks later, mice were subjected to TAC or sham surgery and sacrificed another three weeks later (after echocardiographic analysis). (**b**) Expression of miR-29b and miR-29c in cardiac tissue from mice treated as in (**a**). (**c**) Left ventricular fractional shortening as determined by echocardiographic analysis. (**d**) (Left) Representative hematoxylin eosin staining of myocardial sections; scale bar = 2 mm. (Right) Heart weight-to-tibia length ratio. (**e**) (Left) Representative myocardial sections stained for fibrosis with Sirius Red/Fast Green and (right) quantitative analysis of the results; scale bar: 2 mm. All quantitative data are reported as means ± SEM. *P<0.05, **P<0.01, ***P<0.001 as determined by Student's t-test (**b**) or two-way ANOVA followed by Bonferroni's post hoc test (**c-e**). This figure has been also used in our publication[47].

4.1.7 MiR-29 targets key components of the Wnt signaling pathway

Given the finding that manipulation of miR-29 in cardiac myocytes impacts on the activity of cardiac fibroblasts, we speculated that this should result in an altered secretome from cardiac myocytes. To analyze this, NRCM were transfected with antimiR-29 or antimiR-ctrl and their supernatant was collected 48 hours later and analyzed by mass spectrometry (**Figure 4.8a**). Most of the significant downregulated secreted factors upon miR-29 inhibition in NRCM had a reported profibrotic role (**Figure 4.8b**). Moreover, among the significantly deregulated secreted factors, we found an enrichment for TCF/LEF and NFAT binding sites (**Figure 4.8c**). Binding sites for these transcription factors indicates the involvement of the Wnt signaling pathway[233].

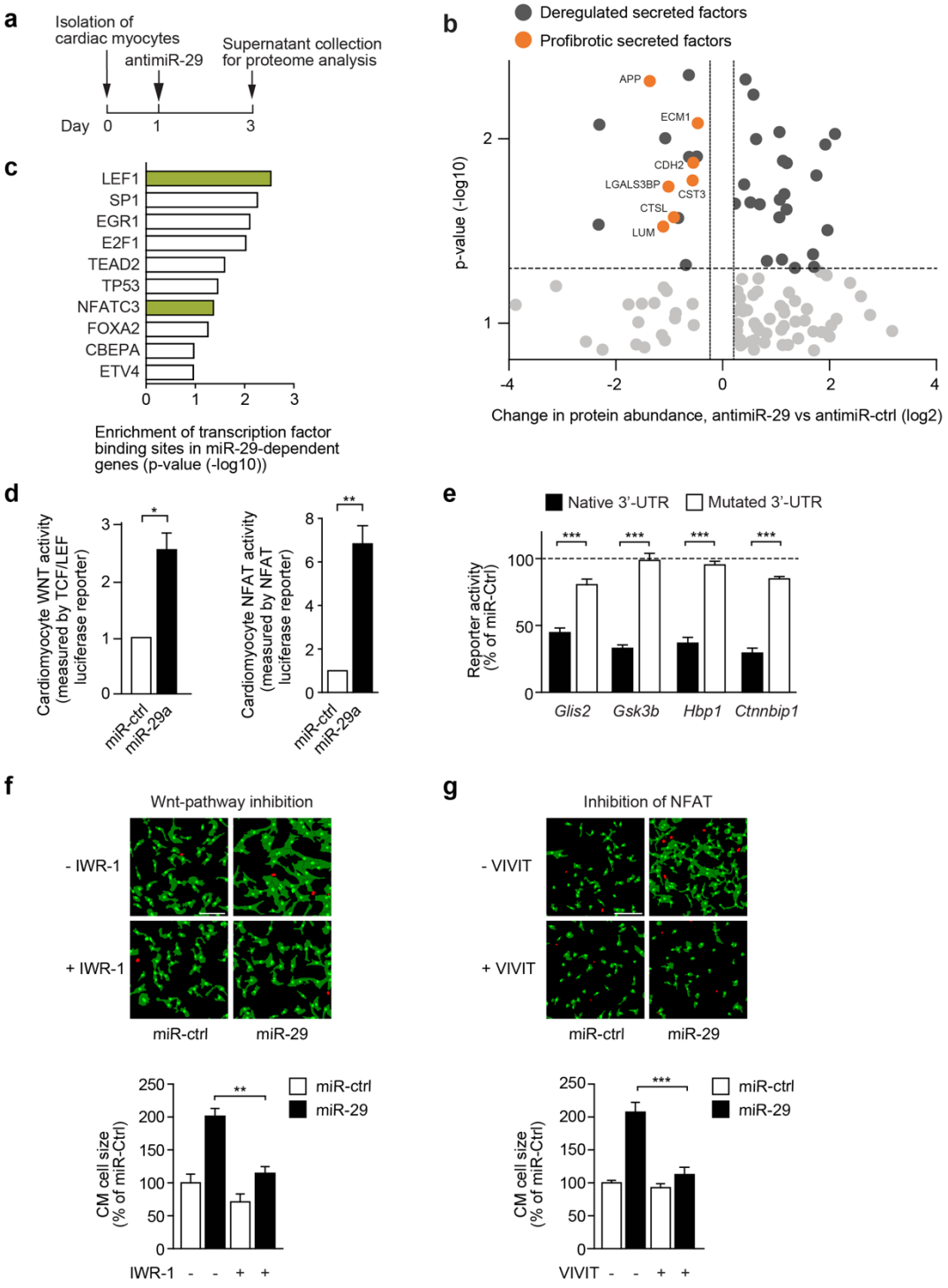

Figure 4.8. MiR-29 targets key components of the Wnt signaling pathway

(**a**) Design of the study. (**b**) Volcano-plot of fold changes of individual proteins from NRCM transfected with antimiR-29 or antimiR-ctrl. Dark grey symbols highlight significantly deregulated proteins ($p<0.05$) and orange symbols those with known or predicted profibrotic function. LUM, Lumican; CTSL, Cathepsin L; LGALS3BP, Galectin 3 Binding Protein; CST3, Cystatin C; CDH2, Cadherin 2; ECM1, Extracellular Matrix Protein 1; APP, Amyloid Beta Precursor Protein. (**c**) Significant GO enrichment of transcription factor binding sites in the deregulated secreted factors. (**d**) (Left) Wnt activity using a TCF/LEF reporter assay in NRCM 48 h after transfection with miR-29a or miR-ctrl. (Right) NFAT activity in NRCM 48 h after transfection with miR-29a miR-ctrl; 4-5 independent experiments in triplicate. (**e**) MiR-29 directly regulates the Gsk3β, Ctnnbip1, Hbp1 and Glis2 3'-UTRs. HEK293 cells were transfected with miR-29a or miR-ctrl. Ratiometric analysis of fluorescent emissions from a dual fluorescent reporter carrying the Gsk3β, Ctnnbip1, Hbp1 and Glis2 3'-UTRs or seed mutants. (**f**) The

Wnt-inhibitor IWR-1 (10 µM for 96 h) prevented miR-29-induced cardiac myocyte hypertrophy. (Up) Representative segmentation images of NRCM transfected with either miR-29 or miR-ctrl in the presence or absence of IWR-1 scale bar: 100 µm. NRCM were identified based on α-actinin detection (green) and are assigned green nuclei, whereas non-myocytes were identified by red nuclei. (Down) Quantitative analysis of the results. (**g**) The NFAT-inhibitor VIVIT prevents miR-29 from inducing cardiac myocyte hypertrophy. (Up) Representative image segmentations of NRCM after transfection with synthetic miR-29 (or miR-ctrl) and addition of 11R-VIVIT (5 µM for 48 h); scale bar: 100 µm. (Down) Quantitative analysis of the results. Data are from 6 independent experiments each performed in triplicate. All quantitative data are reported as means ± SEM. *P<0.05, **P<0.01, ***P<0.001 as determined by Student's *t*-test (**d, e**) or two-way ANOVA followed by Bonferroni's post hoc test (**f,g**). This figure has been also used in our publication[47].

Indeed, miR-29 transfection in NRCM induced Wnt ligand-induced as well as NFAT pathways activation (**Figure 4.8d**). We next screened for direct miR-29 targets implicated in the Wnt pathway and could successfully identify and validate four Wnt pathway inhibitors, namely GSK3β, ICAT/CTNNBIP1, HBP1 and GLIS2 as direct miR-29 targets (**Figure 4.8e**). In order to show that miR-29 induces hypertrophy through the Wnt pathway, we used a small molecule inhibitor of the Wnt pathway, IWR-1. In the absence of the Wnt pathway inhibitor, miR-29 transfection in NRCM induced cardiac myocyte hypertrophy, what was significantly blunted in the presence of IWR-1 (**Figure 4.8f**). Moreover, VIVIT, a specific NFAT inhibitor, was able to inhibit the miR-29-induced CM hypertrophy (**Figure 4.8g**). Ultimately, our findings provide evidence, that the prohypertrophic effect of miR-29 is mediated through the Wnt signaling pathway. Due to the reported profibrotic role of Wnt signaling[233–235] our data indicate that the cardiac myocyte miR-29 is functionally dominating in the myocardium as a system.

4.2 Development of a sensor for microRNA activity *in vitro* and *in vivo*

4.2.1 Design and development of the microRNA sensor for *in vivo* delivery

In order to measure microRNA activity, we constructed a dual fluorescent sensor, encoding tdTomato under the control of a CMV enhancer element followed by a CMV promoter as a normalization gene, and divergent to it, a second CMV enhancer – CMV promoter pair driving the expression of eGFP (enhanced Green Fluorescent Protein), in the 3' of whose lied a microRNA binding site, or a scrambled sequence as a control (**Figure 4.9a**). This sensor was then cloned in an AAV vector and single-stranded AAV was produced. Mice that were administered the AAV9-control sensor, did express strong eGFP signal, but almost no red fluorescence (**Figure 4.9a**).

Since recombination of repetitive sequences, such as the two CMV enhancer – CMV promoter pairs or the two tandem Tomato copies (of tdTomato), is a well-studied phenomenon in retroviruses[236,237], we suspected that this could also be the case for AAVs. In order for the AAV to express both fluorescent proteins, we designed several variants of our sensor, either repla-

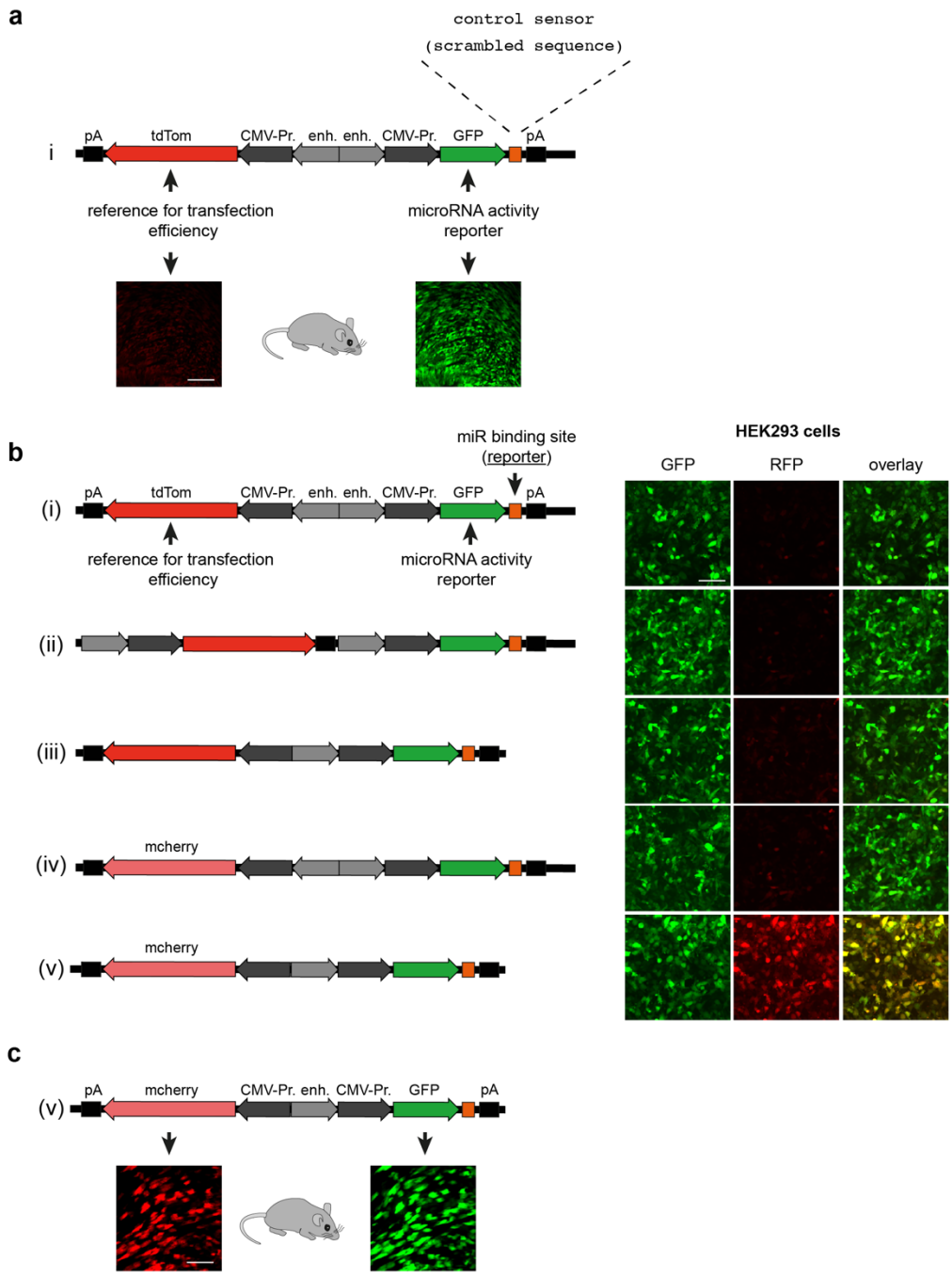

Figure 4.9. Design and development of the microRNA sensor for *in vivo* delivery

(**a**) Up: Design and principle of the microRNA activity sensor; pA: polyA tail, tdTom: tdTomato, CMV-Pr.: Cytomegalovirus promoter, enh.: CMV enhancer, GFP: Green Fluorescent Protein, RFP: Red Fluorescent Protein. Down: Representative images from 5 µm thick cryosections of cardiac tissue. Neonatal mice were injected with the AAV9-control sensor expressing tdTomato under the control of a CMV enhancer and CMV promoter and the tissues were collected 6-7 weeks later. Scale bar 200 µm. (**b**) Representative images of HEK293 cells transduced with $2x10^5$ copies of AAV6 of the denoted AAVs. Scale bar represents 100 µm. (**c**) Representative images of 5-µm-thick cryosections of mice that had been administered with the optimized AAV9-control sensor (v). Scale bar is 100 µm.

cing the tandem Tomato red fluorescent protein with mcherry, or removing one of the CMV enhancers, or changing the direction of the one expression cassette, or combinations of the mentioned possibilities (**Figure 4.9b ii-v**). AAVs expressing these variants were used to

transduce HEK293cells, with only one construct expressing both red and green fluorescent proteins (**Figure 4.9b v**).

Mice injected with the optimized AAV-control sensor exhibited high transduction of the cardiac myocytes, and expressed bright red and green signals (**Figure 4.9c**). This optimization step of the sensor's configuration was necessary before starting to test the capability of the sensor to detect and measure microRNA activity *in vivo*.

4.2.2 Validation of the microRNA activity sensor *in vitro*

We next set out to validate the microRNA activity sensor *in vitro*. A miR-29a complementary binding site was cloned for that purpose in the 3' of the eGFP sequence. Sufficient microRNA activity should repress eGFP expression (and therefore the corresponding signal), whereas low or no microRNA activity should lead to high GFP expression levels.

Mir-29 was chosen with regard to its characterization in cardiac myocytes which, as part of this thesis, has revealed a role of this microRNA in cardiac remodeling[47]. The sequence of the miR-29 family members as well as the sequence of a 16-mer antisense oligonucleotide inhibitor of miR-29 purchased from Exiqon are presented in **Figure 4.10a** (left). The low miR-29 expression level in HEK293 cells, allowed us for testing the sensor's performance upon external microRNA supplementation, whereas the high miR-29 expression in 3T3 mouse fibroblasts rendered them suitable for miR-29 inhibition experiments. The *in vitro* study design is depicted in **Figure 4.10a** (right).

For microRNA supplementation experiments, HEK-293 cells were co-transfected with i.) the miR-29a or a control sensor, and ii.) serial dilutions of a synthetic miR-29a precursor molecule (Ambion) or a scrambled control, using the transfection reagent Lipofectamine 2000. 48 hours later, cells were fixed with 4% Paraformaldehyde (PFA) and the plate was acquired by an epifluorescent microscope. At concentrations of 1-10 pM no decrease in the GFP/RFP could be observed, whereas at 1 nM the GFP expression was almost completely repressed. On the left-hand side of **Figure 4.10c** representative fluorescent images of HEK293 cells transfected with 1 nM of either a scrambled sequence (miR-control/ MC) or a miR-29a precursor (miR-29a) are presented, whereas the concentration-response curve concerning the effect of miR-29a on the miR-29 sensor is depicted on the right-hand side. This experiment revealed that this miR-29 sensor has a sensitivity window of two orders of magnitude regarding the microRNA concentration.

For microRNA inhibition experiments, 3T3 cells were transfected with the same sensor as described in the previous section, together with a synthetic antisense inhibitor of miR-29 (antimiR-29, Exiqon; see **Figure 4.10a** for sequence).

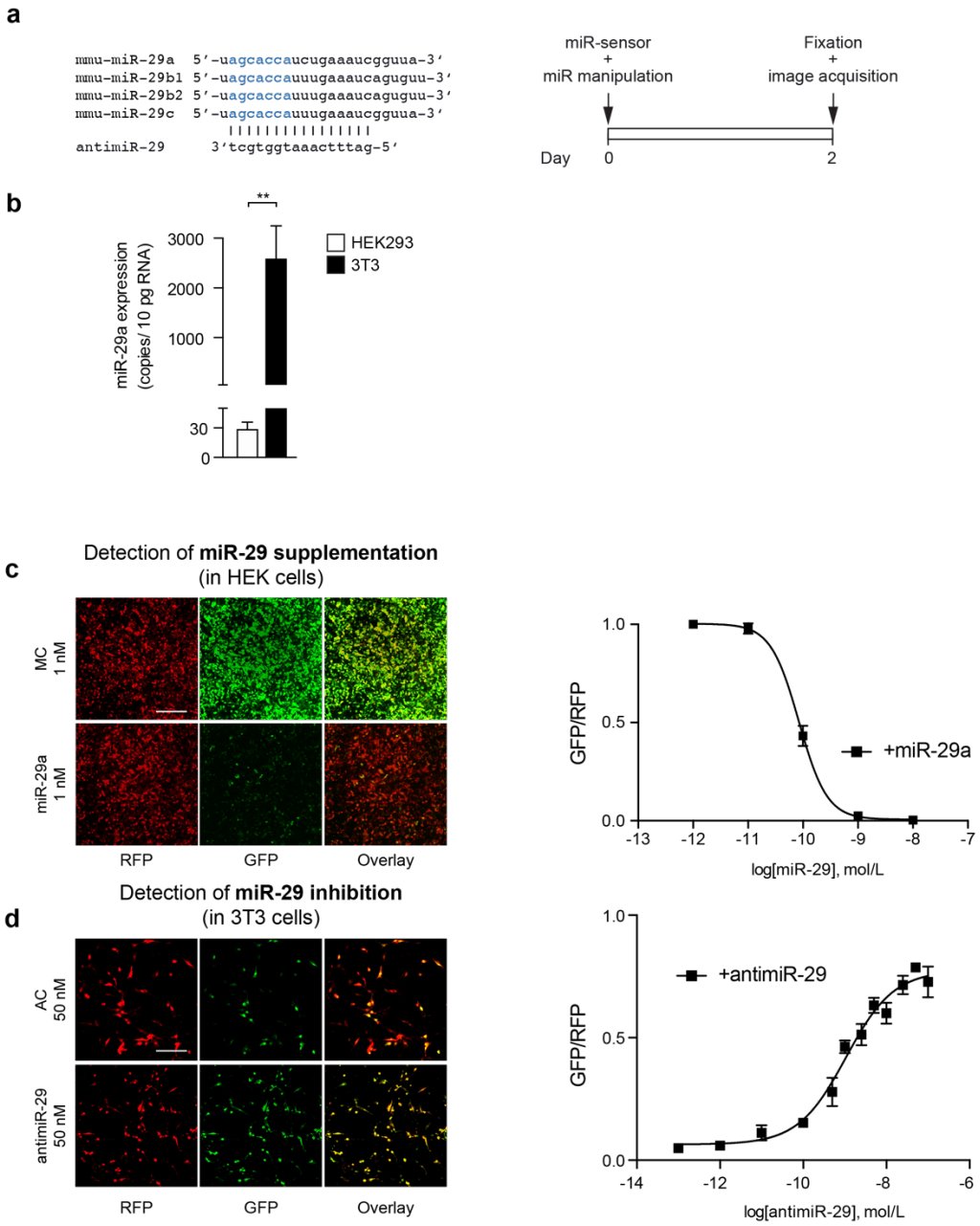

Figure 4.10. MicroRNA activity sensor validation *in vitro*

(**a**) (Left) Design of the miR-29 family inhibitor (antimiR-29). Sequences of miR-29a, b1, b2 and c display a high degree of sequence similarity with identical seed regions (depicted in blue), thus permitting the design of a single antimiR molecule. (Right) Design of the study. (**b**) Quantification of miR-29a in HEK293 and 3T3 cells by qPCR; n=6. (**c**) (Left) Representative images of HEK cells transfected with 1 nM miR-ctrl (MC) or a synthetic miR-29a precursor (miR-29a) and the miR-29 activity sensor and fixed 48 hours post-transfection. (Right) Dose-response curve of miR-29a. (**d**) (Left) Representative images of 3T3 mouse fibroblasts transfected with 50nM antimiR-ctrl (AC) or antimiR-29 and the miR-29 activity sensor and fixed 48 hours post-transfection. (Right) Dose-response curve of antimiR-29. Scale bars represent 100 µm. **P<0.01, as determined by Student's *t*-test. All quantitative data are reported as means ± SEM.

As expected, a non-functional control antimiR (AC) did not affect miR-29, a thus high endogenous expression of miR-29 allowed for a pronounced suppression of the GFP mRNA. By contrast, antimiR-29 led to an inhibition of the miR-29 activity and subsequently to the

derepression of the GFP expression (**Figure 4.10d left**). The corresponding dose-response curve of the antimiR-29 effect on the sensor signal (**Figure 4.10d right**) reveals that concentrations in the range of nM are required for the sensor to detect a change in the microRNA activity, despite the assisted –by Lipofectamine 2000- uptake of the antimiR.

4.2.3 Specificity of the sensor for microRNA family members

As the miR-29 family members only differ by one to few nucleotides to each other, we wanted to investigate the specificity of different sensors carrying binding sites for miR-29a, miR-29b, miR-29c, or one binding site of each of them.

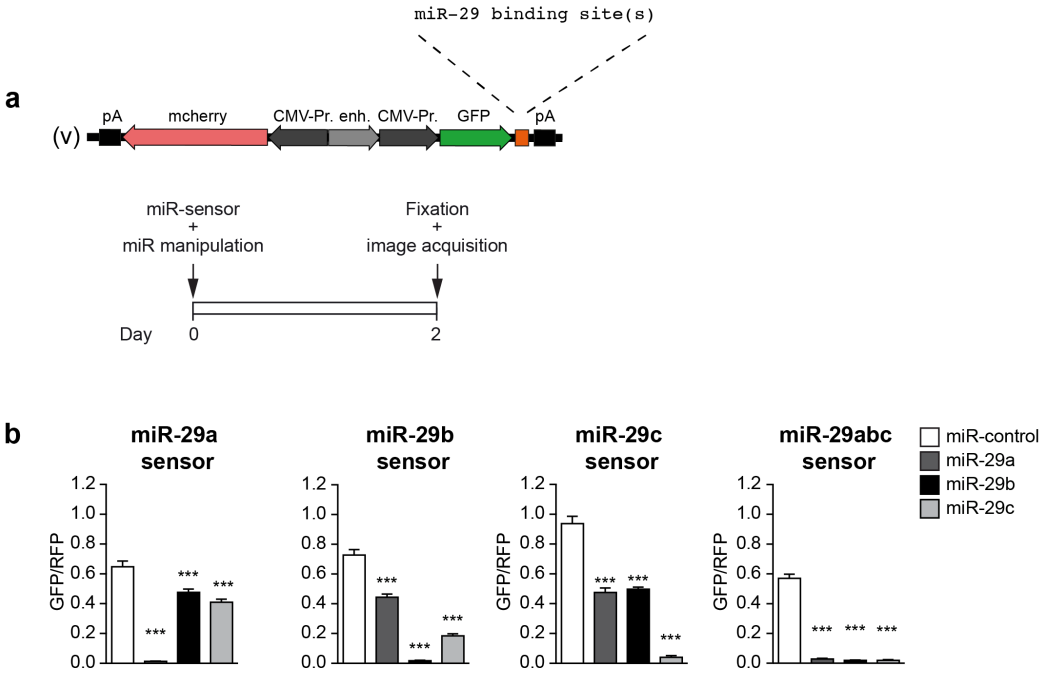

Figure 4.11. Specificity of the sensor for microRNA family members

Neonatal rat cardiac myocytes (NRCM) were transfected with miR-29a, miR-29b, miR-29c or miR-29abc sensor and miR-29a miR-29b or miR-29c mimics. The cells were fixed 48 hours post-transfection and then the GFP and RFP fluorescence were acquired. (**a**) Sensor and experiment design. (**b**) Quantitative representation of the results; n=8. All quantitative data are reported as means ± SEM. ***P<0.001 versus miR-control, as determined by one-way ANOVA followed by Sidak's post hoc test.

Each of the four different sensors or a control sensor was co-transfected in neonatal rat ventricular cardiac myocytes (NRCM) cells with high concentration of miR-29a, miR-29b or miR-29c synthetic microRNA precursors (50 nM) and the cells were fixed 48 hours later. The sensor and study design is depicted in **Figure 4.11a**. Transfection of miR-29a led to complete repression, about 45%, or 50% repression of the GFP in the case of miR-29a, miR-29b, or miR-29c sensor, respectively. The analogous suppression of the GFP of the three sensors, when miR-29b was transfected, was 25%, 35%, and 50%, whereas transfection of miR-29c led to 50%, 50%, and above 95% depletion of the GFP, accordingly. Transfection of any of the

three miR-29 sequences led to complete repression of the GFP, when the miR-29abc sensor was utilized, as shown in **Figure 4.11b**.

This data brought us to the conclusion , that the miR-29a sensor was the most specific for one miR-29 family member that the other sensors, and that the miR-29abc sensor could be employed, if the activity of all the miR-29 family was to be measured.

4.2.4 Validation of the microRNA activity sensor *in vivo*

Adeno-associated viruses (AAVs) are an excellent tool for gene transfer and are even used in clinical trials for gene therapy[238]. To deliver the microRNA activity sensor to cardiac myocytes,

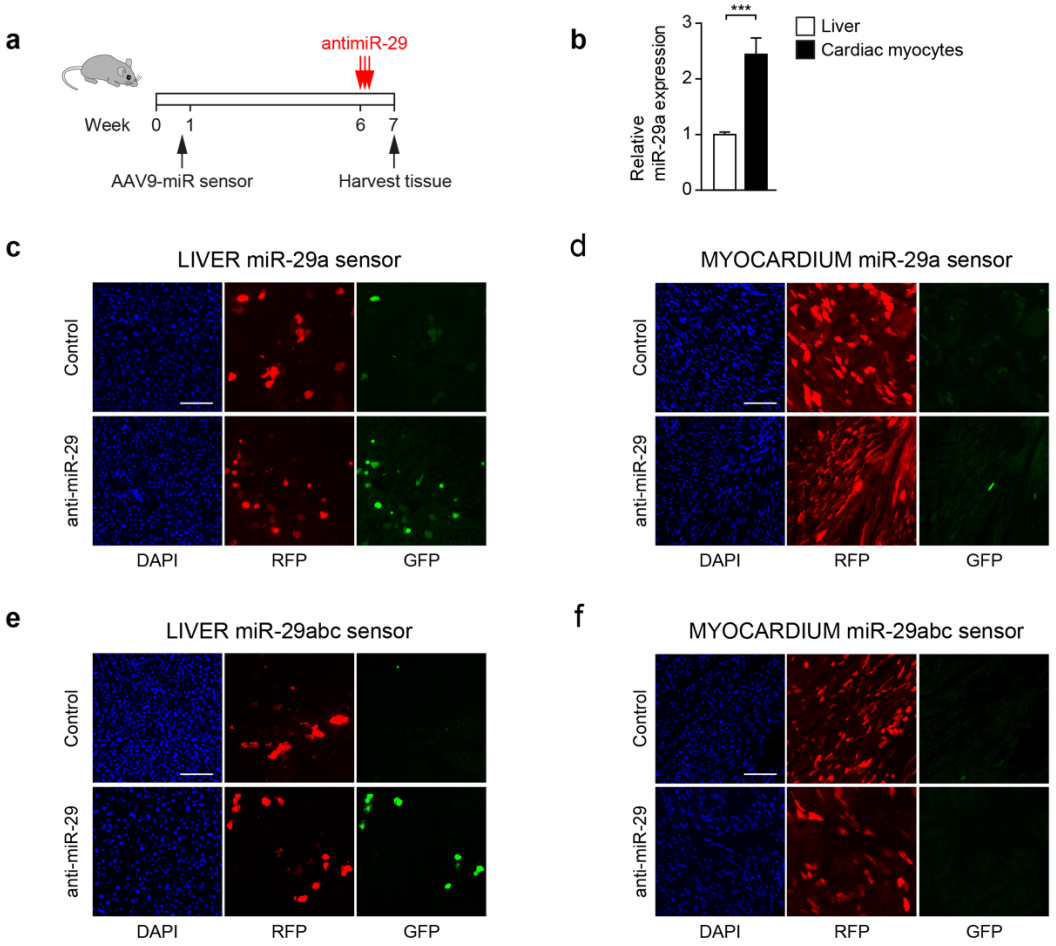

Figure 4.12. MicroRNA activity sensor validation *in vivo*

(**a**) Design of the antimiR-29 study. (**b**) qPCR for miR-29a expression in liver and adult mouse cardiac myocytes; n=5-6. (**c,d**) Representative images of the fluorescent expression of the miR-29a activity sensor *in vivo* from liver (**c**) and myocardium tissue (**d**) of mice either administered antimiR-29 or control littermates; n=5. (**e,f**) The miR-29abc sensor was used here to detect miR-29 inhibition as on (**c,d**); n=4. Scale bars represent 100 µm.***P<0.001, as determined by Student's t-test. All quantitative data are reported as means ± SEM.

serotype 9 of the AAV (AAV9) was chosen, since it has the highest tropism for the heart and, therein, especially for cardiac myocytes[239,240].

AAV9 expressing the optimized miR-29a or the miR-29abc activity sensors (**Figure 4.9b v**) was injected intrapericardially in 3-4 days old mice and five weeks later antimiR-29 at a dose of 20 µg/g/day was administered in the tail vein of the mice for three consecutive days. One week after the first injection the mice were sacrificed and their organs were PFA-perfused (**Figure 4.12a**). We found miR-29a to be expressed higher in isolated cardiac myocytes than in liver lysates (**Figure 4.12b**). Both the miR-29a and the miR-29abc activity sensors successfully detected the miR-29 inhibition by the antimiR-29 in the liver, as seen by the increased green fluorescence in comparison to the control mice that did not express almost any green because of the high endogenous miR-29 activity (**Figure 4.12c,e**). The RFP expression indicated successful delivery of the sensor in both cases. In the case of the cardiac myocytes though, the miR-29 activity sensor did not detect any change in the miR-29 activity upon antimiR-29 injection (**Figure 4.12d,f**), presumably due to the much higher antimiR uptake by the liver cells in comparison to the cardiac myocytes and the subsequent different degree of miR-29 inhibition.

The CMV promoter has been reported to drive high transcription and expression for a few weeks, followed by an inactivation[241,242], especially in the liver[217,240]. The small percentage of the sensor-expressing cells in the liver after five weeks of transduction is in line with these observations. Mice that were administered with the same control sensor and with the same titer, but were sacrificed at a shorter timepoint (two weeks after infection), displayed much higher percentage of transduced cells in the liver (**Figure 4.13a**). The CMV promoter was at the same timepoint resulting in robust transduction of the myocardium (**Figure 4.13b**).

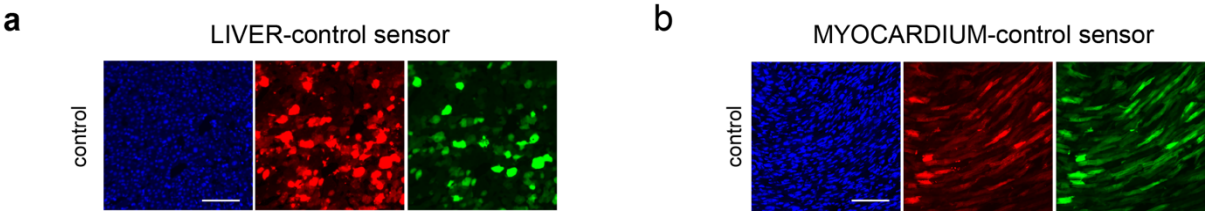

Figure 4.13. High transduction efficiency of AAV9-control sensor in both liver and heart

Neonatal mice were administered with AAV9-control sensor and their tissues were harvested two weeks later. Representative images of cryosections from mouse liver (**a**) and heart (**b**) show a high transduction efficiency in both organs. Scale bars represent 100 µm.

4.2.5 Generation of a transgenic mouse expressing a microRNA activity sensor

To ubiquitously express a microRNA activity sensor *in vivo*, recombinase-mediated cassette exchange was applied to embryonic stem cells from mice. The control microRNA activity construct containing a scrambled microRNA binding site was first cloned in a pRMCE plasmid kindly provided by Prof. Dr. Ralf Kühn. Subsequently, embryonic stem (ES) cells harboring a pre-engineered Rosa26 docking site (IDG3.2 R26.10-3 ES cells[243]) were electroporated with our construct and a plasmid expressing the φC31 integrase (**Figure 4.14a**), mediating

successful recombination. Positive ES-cell colonies were selected on the basis of antibiotic resistance plus expression of the two fluorescent proteins, sent to our collaborator Mr. Ronald Naumann at the Max-Planck-Institute (MPI) in Dresden, blastocyst injections took place and chimeras were generated. Despite the fact that germline transmission could be confirmed by fluorescent microscopy and genotyping, transgenic progenies died in the first two weeks after birth. This finding may be best explained by the reported toxicity of high expression levels of eGFP[244–246] (**Figure 4.14b**). At the same time, we found out that the microRNA activity sensor needed further optimization for detection of microRNA inhibition in the myocardial tissue, so we did not proceed with new trials for generation of a transgenic mouse expressing the microRNA activity sensor.

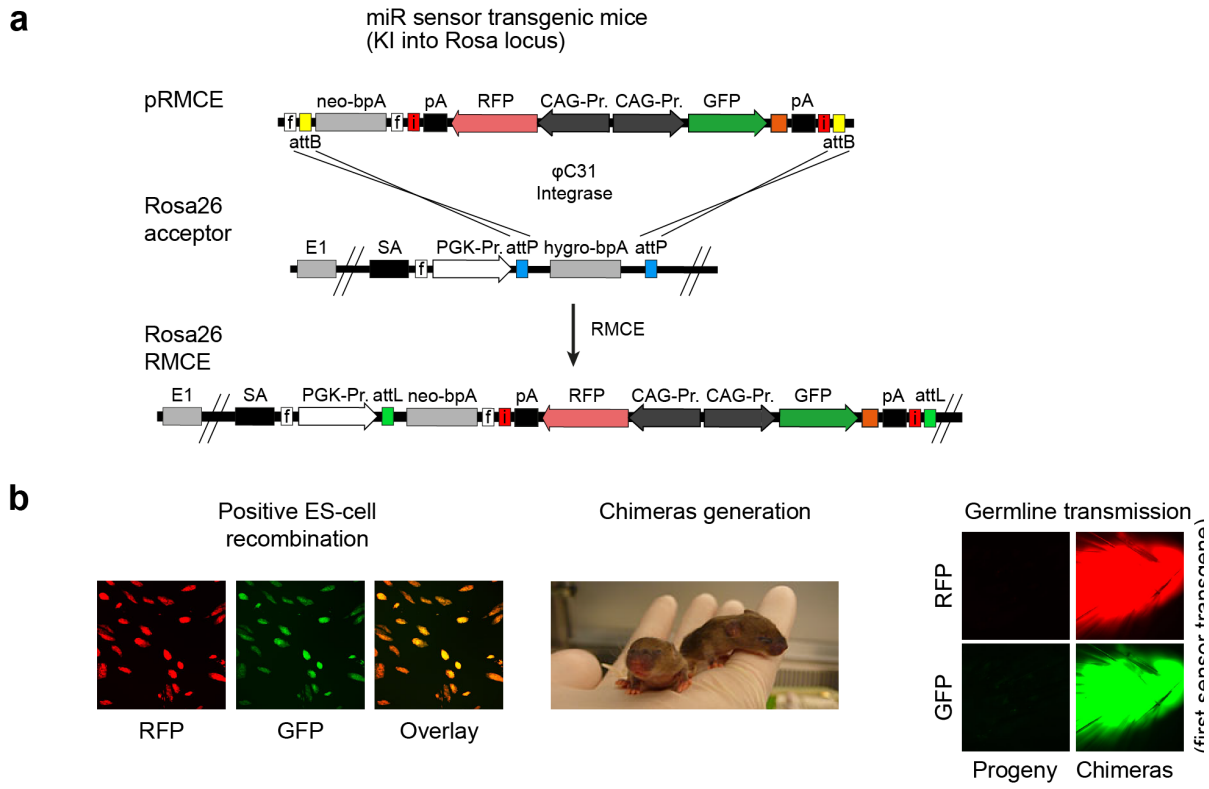

Figure 4.14. Generation of a knock-in mouse expressing a microRNA sensor ubiquitously

(**a**) Schematic representation of the Recombinase-Mediated Cassette Exchange (RMCE) method. A control sensor (with a scrambled- instead of a microRNA-binding site) was cloned in the pRMCE plasmid and this construct was electroporated together with a plasmid encoding the φC31 Integrase in the Rosa26 acceptor ES cells. (**b**) Positive ES-cell recombination was observed and clones positive for the control sensor were used to generate chimeras, which exhibited abnormally high levels of RFP and GFP express (The right panel presents tail biopsies from progenies and chimeras under an epifluorescent microscope; exposure time 10 ms).

4.2.6 Correlation analysis of microRNA expression and sensor suppression as a means to select the best microRNA candidate sensor *in vivo*

As we could not detect a derepression of the sensor in the myocardium upon antimiR-29 administration (**Figure 4.12**), we hypothesized that our sensor could not detect a partial

inhibition of miR-29, due to the high endogenous expression of miR-29. We reasoned that a suitable sensor should only partially be suppressed by the endogenous levels of the microRNA of interest, so that partial microRNA inhibition by an antimiR would lead to the maximum derepression of the sensor's GFP expression. In order to identify the best microRNA candidates for the sensor we performed a series of experiments to correlate the absolute expression of a microRNA to its activity. Knowing the range of expression of a microRNA that would lead to partial suppression of its sensor would allow us to select from a microRNA sequencing database the most promising microRNAs.

The miR-29 sensor was brought to expression in cells with low (HEK), medium (NRCM cultured for 3, 6 or 9 days), high (A549) or very high (3T3) miR-29 expression. The GFP and RFP intensities acquired by an epifluorescent microscope were used to correlate the activity of miR-29 in each cell type with its absolute expression as determined by qPCR and plotted in **Figure 4.15a**. Any expression above approximately 1000 miR-29a copies per 10 pg RNA (that roughly corresponds to one cell) led to a GFP/RFP expression of almost zero, being suggestive that we need to find a microRNA that is expressed at lower than 1000 copies per 10 pg RNA in the myocardium. In order to select candidates from a small RNA sequencing database from cardiac cell types performed in our lab, the output of this database (reads per million, RPM) had to be correlated to the qPCR output (copies per 10 pg RNA). RNA was isolated from cardiac myocytes, endothelial cells and leukocytes (all cell types were FACS-sorted using standard antibodies), reverse transcriptase (RT) was performed in the presence of synthetic microRNA spike-ins of known concentrations and qPCR was performed for two exemplary microRNAs, miR-29a and miR-30c. For each microRNA a good correlation could be observed between the copies per 10 pg RNA and RPM (**Figure 4.15b**). As the microRNA copies per 10 pg RNA in every case lied between 39% and 85% of the corresponding RPM, and miR-29a has 1401 RPM in cardiac myocytes (Ramanujam D., unpublished data), what was previously shown in this thesis to be too high for a partial inhibition by an antimiR to be detected by a sensor, we chose to investigate microRNAs whose expression lie between 200 and 1000 RPM in at least three out of four main cardiac cell types (cardiac myocytes, fibroblasts, endothelial cells and leukocytes). That criterion was fulfilled by 17 microRNAs (**Figure 4.15c**).

We then excluded microRNAs that were part of a microRNA family, because these would have the drawback not be able to be used later to compare different antimiR chemistries, that would target either one family member or the entire family. That narrowed the list of possible candidates down to five, whose absolute expression was then determined by qPCR from RNA isolated from cardiac myocytes and liver of 8-weeks-old mice (**Figure 4.15d**). We then applied a further stringent expression criterion: the microRNA should express at least 400 copies per 10 pg RNA (dashed line in (**Figure 4.15d**)). Only two microRNAs, miR-191-5p and miR-151-5p, fulfilled all the above mentioned prerequisites.

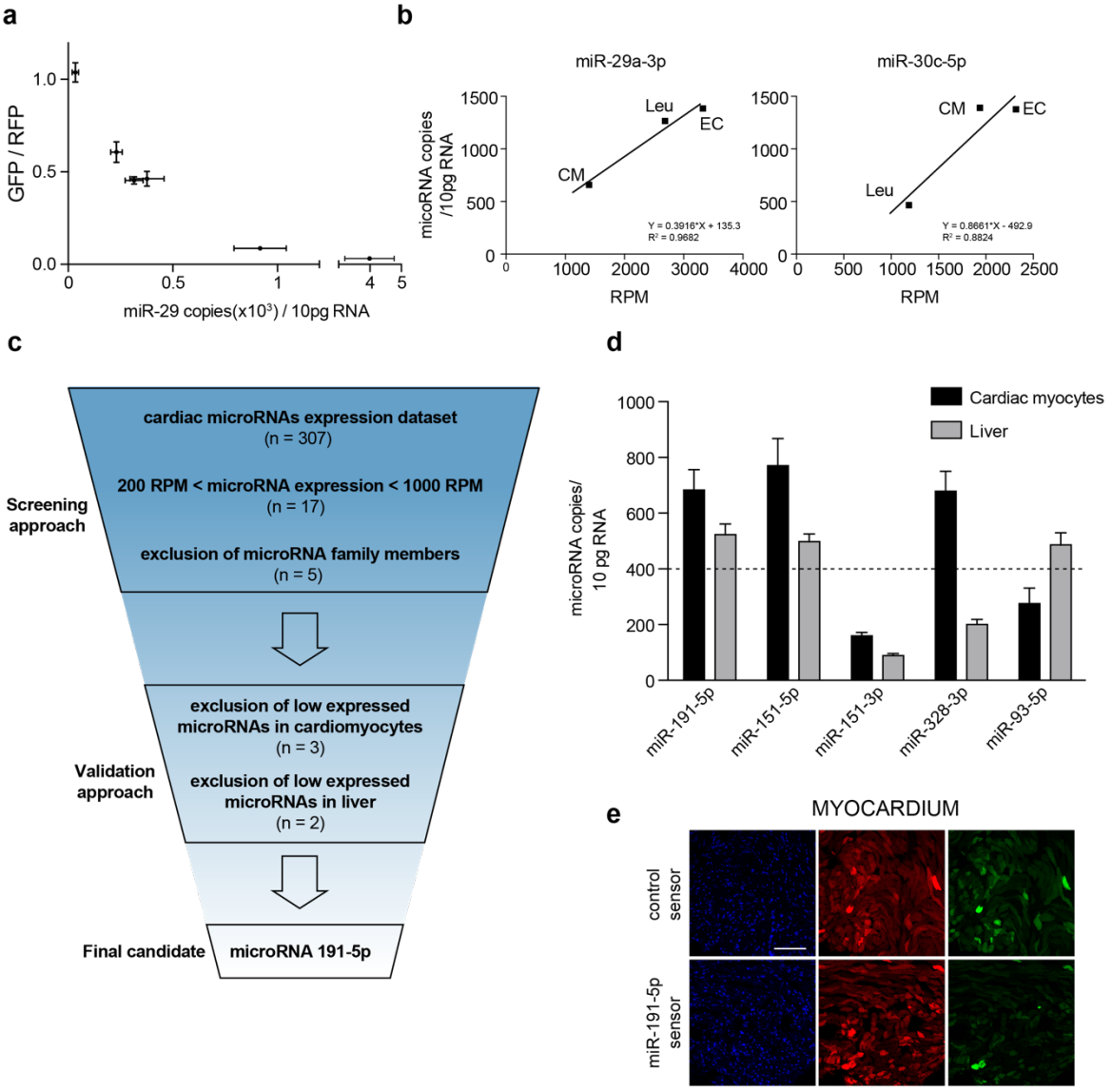

Figure 4.15. Correlation of microRNA expression to activity reveals candidates for a suitable sensor for *in vivo* microRNA inhibition detection

(**a**) Correlation of miR-29 expression and activity. The miR-29 sensor was expressed in cells with low (HEK), medium (NRCM), high (A549) or very high (3T3) miR-29 expression. The GFP and RFP intensities acquired by an epifluorescent microscope were used to correlate the activity of miR-29 in each cell type with its absolute expression as determined by qPCR. (**b**) Correlation of small RNA sequencing expression (in reads per million; RPM) to the expression determined by qPCR (in miR-29 copies per 10 pg RNA). Cardiac myocytes (CM), endothelial cells (EC) and leukocytes (Leu) were isolated by FACS, RNA was isolated and qPCR was performed for the indicated microRNAs. (**c**) Selection strategy for the best microRNA candidate for the microRNA activity sensor with the highest sensitivity for microRNA inhibition. (**d**) Absolute quantification of the expression level of the 5 microRNAs selected from the screening approach in (**c**) in both isolated mouse cardiac myocytes and liver tissue. The dashed line indicates the threshold set in (**c**) in order to exclude lowly expressed microRNAs. (**e**) Representative images of the fluorescent expression of the miR-191 activity sensor *in vivo* from myocardial tissue. Scale bar represents 100 µm. All quantitative data are reported as means ± SEM.

Since miR-151-5p is very highly expressed in endothelial cells of the myocardium (4414 RPM, Ramanujam D., unpublished data), we chose to construct the sensor for the miR-191-5p. Its homogeneous expression within the desired expression range in all the main cardiac cell types, as well as in the liver, would render it suitable for generating a knock-in mouse expressing ubiquitously this microRNA activity sensor. Mice administered with AAV9-miR-191 sensor did indeed express some basal green above background, but substantially less compared to the control sensor, what renders this sensor ideal for an antimiR-191 uptake study (**Figure 4.15e**).

5 Discussion and outlook

5.1 Characterization of the cardiac role of miR-29

Concerning the biological role of miR-29, we could show its implication in cardiac remodeling both concerning cardiac hypertrophy and fibrosis. MiR-29 has been studied extensively and was shown to be downregulated in a mouse MI model, as well as in infarcted hearts of human patients[44]. In addition, its higher expression in cardiac fibroblasts than cardiac myocytes, together with the property of miR-29 to directly target Elastin, Fibrillin and Collagens 1a1, 1a2 and 3a1, led the authors to the conclusion that the decreased expression of miR-29 in a disease model constitutes a pathological event. These observations were supported by other studies, which verified that miR-29 can target various collagens and ECM molecules, both in the myocardium[124,164], as well as in the lung[247], liver[248], and kidney[249]. We were therefore initially surprised by the results of a screening for hypertrophy-modulating microRNAs from our laboratory, that ranked miR-29 as one of the most prohypertrophic microRNAs[129]. In a validation experiment, transfection of all miR-29 family members could robustly induce cardiomyocyte hypertrophy of NRCM[47]. Based on this initial observation, we decided to characterize the role of miR-29 in cardiac remodeling using a pressure overload model (TAC).

5.1.1 MiR-29 expression and regulation

MiR-29 is expressed at low levels in early life, but this changes dramatically with ageing. Kamran et al. first observed, that tissue development and miR-29 expression are associated, the more mature and older the tissue, the higher the miR-29 expression[232]. Boon et al. also revealed, that miR-29 is expressed at higher levels in the aortas of aged mice[164]. Our findings are in accordance to these data, as we also appreciated a remarkable increase in the myocardial miR-29 levels with age. Although it was believed, that miR-29 is expressed much higher in cardiac fibroblasts than cardiac myocytes[44], we were able to find out that these data were a result of prolonged cultivation, whereas in freshly isolated cells miR-29 is predominant expressed in cardiac myocytes of mice.

The dynamic regulation of the miR-29 expression in cardiac myocytes in response to TAC, with an initial boost of miR-29 levels as an immediate response, provides a better insight into the role of miR-29 in cardiac remodeling. Of note, miR-29a and miR-29b were also downregulated in myocardium from aortic stenosis patients (**Figure 5.1**)[47]. Similarly, miR-29 was also downregulated after myocardial infarction in mice, as well as in the border zone of the infarcted region from human patients receiving heart transplants[44].

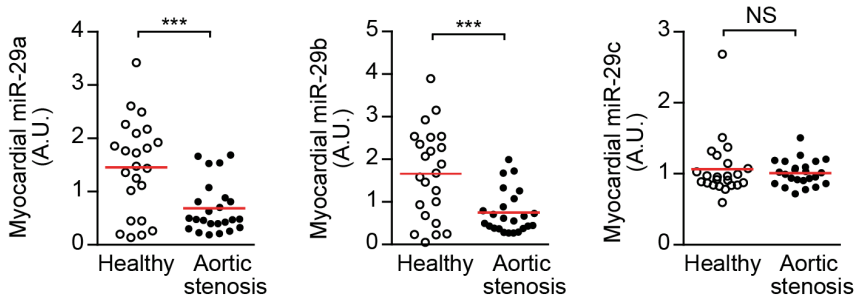

Figure 5.1. Expression of miR-29 family members in aortic valve stenosis patients

Quantification of miR-29 family levels in human left ventricular myocardium from healthy individuals or from patients with aortic valve stenosis. All quantitative data are reported as means ± SEM. ***P<0.001 calculated using Student's t-test. This figure has been also used in our publication[47].

Although several studies have proposed TGF-β to decrease the miR-29 level[44,249], a recent publication shows that TGF-β signaling triggers senescence via miR-29-mediated loss of H4K20me3, resulting in cardiac ageing[250].

5.1.2 Global miR-29 deletion protects from cardiac remodeling

MiR-29 is a microRNA family comprising four members, miR-29a, miR-29b1, miR-29b2, and miR-29c1, that all share the same seed sequence. Moreover, the mature miR-29b1 and miR-29b2 have exactly the same sequence, but are transcribed from two different clusters. MiR-29b1 is organized in one cluster with miR-29a on chromosome 7 in humans and 6 in mice, whereas miR-29b2 is transcribed together with miR-29c and located on chromosome 1, both in humans and mice[9,251,252]. All miR-29 clusters are on the [-] strand, so all miR-29 members are characterized as 3p.

We could also verify what was reported by others[226,230,231], that mice triple allelic knockout for miR-29 display smaller body weight and die prematurely, while we could not obtain any mice with a complete miR-29 KO. In contrast, another group obtained miR-29 KO mice, although, these mice died during their first month of life[230]. On the other hand, mice which lacked only the *miR-29 b2c* cluster did not exhibit any overt abnormalities.

The miR-29-deficient mice were protected from cardiac hypertrophy and fibrosis, in contrast to the TAC-operated wildtype animals. Moreover, the fibrosis-related genes *Col1a1*, *Col1a2* and *Col3a1* were also found to be downregulated in the KO mice after TAC in comparison with their wildtype littermates, despite the fact that they have been shown to be direct targets of miR-29[44,124,247]. This might well be a result of a paracrine effect triggered by the protected – after miR-29 inhibition – cardiac myocytes, in contrast to published reports, where miR-29 transfection directly in cardiac fibroblasts led to decrease in the collagen levels.

5.1.3 Pharmacological inhibition of miR-29 prevents cardiac dysfunction

In order to exclude genetic compensation[253], an antisense approach employing a LNA-based antimiR-29 targeting all the miR-29 members was adopted. Intravenous administration of antimiR-29 immediately after TAC and for three consecutive days led to preserved heart function and abrogated fibrosis compared to the control animals. Of note, a study using antagomiR-29b after aortic binding reported increased perivascular fibrosis, without any decline in heart function[123]. The differences in the observations of the two studies concerning the miR-29-associated fibrosis could depend on the difference in the inhibitor chemistries used in the two studies (antagomiR versus LNA/DNA mixmer); different antimiR chemistries have exerted contradictory results also in other cases[42,121]. Other possible explanations for the opposing phenotypes of the two microRNA inhibitors are the targeted miR-29 member (miR-29b in the Abonnenc study versus all miR-29 family members in our study), or the reported nuclear localization of miR-29b[254,255]. Intriguingly, Lyu et al.[250] found the expression of miR-29a and miR-29c to be increased after TGF-β induction, whereas the expression of miR-29b was nearly unchanged, supporting the notion, that microRNA family members might have different functions, despite the fact, that they share the same seed sequence.

5.1.4 MiR-29 sponge inhibits cardiomyocyte hypertrophy *in vitro*

A microRNA sponge is an alternative to antimiRs, and is transcribed and produced by the cell as a transgene consisting of multiple microRNA target sites in tandem[171]. This microRNA binding sites are usually imperfect, introducing a bulge at the position that corresponds to nt 9-12 of the microRNA, to prevent AGO2 cleavage of the sponge mRNA[27,28], so that the microRNA can be sequestered and thereby inactive for a longer time. According to standard practice[124,171,173,175], we constructed a series of miR-29 sponges, in order to test whether any of them could protect from cardiomyocyte hypertrophy. We could show, that the miR-29 sponge bearing 12 miR-29 binding sites in tandem (including 6 nt spacers between each target site) was able to significantly blunt the PE-induced cardiomyocyte hypertrophy in NRCM. Dawson et al. used a sponge targeting miR-29b in fibroblasts and observed increase in *Col1a1*. The difference between the two studies is the different cell type targeted each time.

5.1.5 CM-specific miR-29 knockdown protects from pressure overload

In order to knockdown the miR-29 specifically in the cardiomyocytes, we decided to use a combination of the AAV9, that in our setup targets primarily the cardiomyocytes within the heart[55], and a codon-improved Cre recombinase, iCre[256]. A similar approach, using AAV9 and iCre, but in adult mice, also showed cardiomyocyte-specific recombination[257]. In that study, the authors used both the a LacZ reporter mouse[258], where Cre-mediated excision of a stop cassette lead to activation of LacZ transcription, and a serum response factor (SRF)

conditional KO[259], whose excision led to severe cardiomyopathy. In our study, intrapericardial injection of neonatal mice floxed for the *miR-29b2c* locus (*miR-29 b2c*$^{fl/fl}$) resulted in a robust reduction of the miR-29b and miR-29c expression. This percutaneous way of injecting a virus in the pericardial cavity, was introduced by Zhang et al. who injected adenoviruses expressing either luciferase or LacZ resulting in robust local transduction of the myocardium[260]. When we knocked down miR-29 levels specifically in cardiomyocytes using this approach, the mice displayed better myocardial function and less fibrosis after TAC, compared to control animals.

5.1.6 MiR-29 targets key components of the Wnt signaling pathway

Proteomics analysis of the secretome of cardiac myocytes, whose miR-29 levels were manipulated, revealed that miR-29 can induce the activation of TCF/LEF and NFAT transcription factors. These are both involved in the well-described Wnt signaling pathway[71–73].

We were able to prove the direct interaction between miR-29 and four members of the Wnt signaling pathway, leading to increased activity of TCF/LEF and NFAT. These are GSK3β, CTNNBIP1, HBP1 and GLIS2. Studies by two independent groups using a transgenic mouse, whose GSK3β was mutated to produce a constantly active molecule and subjecting it to various models of cardiac hypertrophy, demonstrated that activation of GSK3β resulted in a protected phenotype[93,94].

Using a small molecule inhibitor of the Wnt signaling pathway, that acts through stabilization of the member of the destruction complex Axin[261], we could inhibit the miR-29-induced cardiomyocyte hypertrophy.

Under various conditions Ca^{2+} concentration can be increased in the cytoplasm, resulting in dephosphorylation of NFAT by calcineurin, stimulating its translocation to the nucleus and transcriptional activation of NFAT-responsive genes[86]. Activation of NFAT has been shown to drive maladaptive cardiac hypertrophy and hear tfailure[95].

Adopting a similar approach as we did with IWR-1 to inhibit the Wnt signaling, we employed a highly selective NFAT inhibitor, VIVIT[262], and showed that the miR-29 induced hypertrophy is mediated through NFAT activation.

GSK3β in contrast, phosphorylates and deactivates NFAT, preventing it from translocating to the nucleus[87]. Furthermore, genetic modification of NFAT in a way to prevent its phosphorylation by GSK3β, was constitutively active, inducing calcineurin-independent cardiac hypertrophy[95]. Of note, a transgenic mouse overexpressing GSK3β displayed impaired cardiac contractile function and smaller cardiomyocytes, underlining the role of this molecule in the regulation of normal cardiac growth and function[263]. Moreover, in a hypertrophic cardiomyopathy (HCM) mouse model caused by a mutation in myosin heavy chain, GSK3β

was found to be inhibited, but interestingly, exercise was able to return the GSK3β phosphorylation levels to normal and on the same time the HCM phenotype could be prevented or even reversed[264,265].

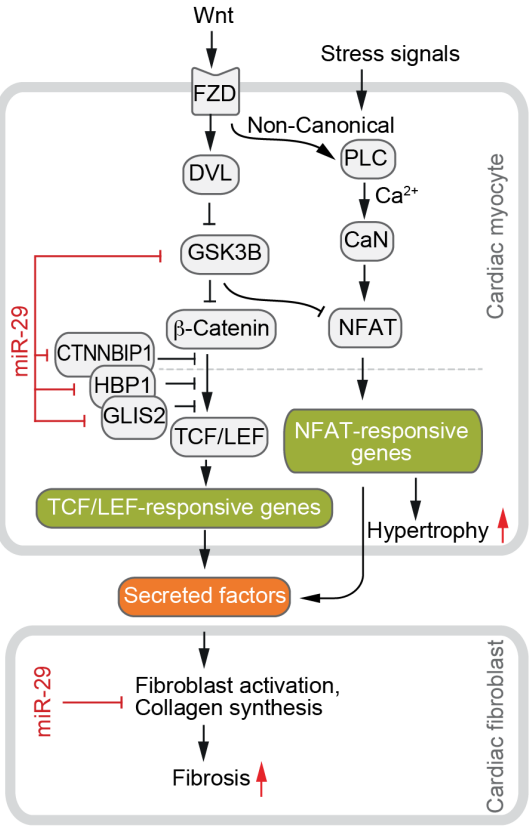

Figure 5.2. Proposed mechanism how miR-29 promotes Wnt signaling in CM and signals to fibroblasts

In cardiac myocytes, miR-29 (by targeting Gsk3β, Ctnnbip1, Hbp1 and Glis2) activates the Wnt signaling pathway, as well as NFAT activity. Activation of Wnt and NFAT signaling pathways promotes cardiac myocyte hypertrophy and secretion of profibrotic factors, which act in cardiac fibroblasts. Pharmacological inhibition or genetic deletion of miR-29 in cardiomyocytes prevents cardiac hypertrophy and fibrosis. This figure has been also used in our publication[47].

CTNNBIP1 (or ICAT) was shown to interact with β-catenin preventing it from binding to TCF/LEF[98]. Deficiency of ICAT has been shown to cause cardiac hypertrophy[100]. HBP1 acts in a similar way, also preventing TCF/LEF from activating the Wnt pathway[99], and its lack also resulted in cardiac hypertrophy[100]. GLIS2 interacts with β-catenin leading to negative regulation of the Wnt signaling pathway and its target gene *Cyclin D1*[101].

Taken together, our data suggest the activation of the Wnt pathway by miR-29 through direct targeting of four pathway members: GSK3β, CTNNBIP1 (or ICAT), HBP1, and GLIS2. Despite the well-established protective role of GSK3β against cardiac hypertrophy[266,267], potential therapies targeting this molecule should proceed with caution, as its overexpression in healthy mice has been shown to negatively impact the cardiac growth and function[263]. Interestingly,

reports on miR-29 in fibrosis disease models in other organs such as liver, lung and kidney have demonstrated the potential benefit of elevating miR-29 levels[247–249]. In contrast to these findings, we show that inhibition or genetic deficiency of miR-29 *in vivo* prevents (rather than promotes) myocardial fibrosis in a cardiac disease model, and propose a dominating role of miR-29 in CM over that in CF. These data highlight the importance of tissue- and cell type-specific miR-29 manipulation.

5.2 Development of a sensor for microRNA activity *in vitro* and *in vivo*

Despite the exponential increase in the knowledge about microRNAs and their function during the last decades since their discovery[3], quantification of a miRNA's level or in the best case of its target genes still remains the most commonly used measure for miRNA activity. The mild effects that most of the microRNAs exert on their targets either at the mRNA level[203,204], or at the protein level[205,206], force most scientists to use the measurable microRNA amount left after antimiR application as an indicator of the antimiRs potency. Even if the targetome of a specific microRNA could be identified and quantified with high confidence, its different targetome in different cell types, in combination with the distinct expression profile of the microRNA itself and its targets in discrete cell types, would render a direct comparison of the antimiRs potency in the different cell types almost impossible.

As already mentioned in the respective introduction chapter, LNA/DNA, LNA/2'-O-Me and 2'-F/MOE, which have high affinity for their cognate microRNAs, stereochemical inhibit the target microRNA[135,136,140,165,167,207], while 2'-O-Me, 2'-MOE and cholesterol-conjugated 2'-O-Me modified antagomiRs, that comprise lower affinity chemistries, lead to microRNA degradation[134,137,140,168,207]. Several hybridization-based techniques used for microRNA detection or/and quantification, such as northern blotting or ISH, might not be useful to interpret antimiR-induced microRNA inhibition, due to the inability of the probe to replace the antimiR in the miR : antimiR duplex[140]. Additionally, standard RNA isolation methods might lead to misleading results, due to retention of a portion of the miR : antimiR duplex in the supernatant after the isopropanol-based precipitation step[140,155,208,209]. Likewise, antimiR that is either inactive a cellular compartment, or even extracellular, can artificially bind to its target microRNA during cell lysis and RNA extraction, interfering with the subsequent reverse transcription and qPCR[210].

Some workarounds for these obstacles concerning northern blotting have been proposed, such as using harsh denaturing conditions during electrophoresis[134], using LNA probes[135,136,165,167] or including a competitor decoy with the same sequence as the miRNA before electrophoresis to replace the microRNA in the miR : antimiR duplex[140,207]. As there is

no solution to prevent the artificial miR : antimiR binding during RNA isolation, the direct measurements of microRNA levels after its inhibition should be interpreted with caution and always complemented with functional data, such as target derepression.

Fluorescence- or radioactive isotope-based labeled antimiRs have been employed to investigate the tissue and cell type distribution of antimiRs[42,165]. The lack of assessment of the potency of the antimiR in this case, however, as well as the potential differential uptake and distribution caused by the label itself, constitute the main disadvantages of these methods.

In order to investigate the antimiR's potency in inhibiting a microRNAs function, as well as its distribution, we decided to develop a microRNA activity sensor.

5.2.1 Design and development of the microRNA sensor for *in vivo* delivery

Some recent reports developed microRNA activity sensors that use a so-termed "ON-system", where increased microRNA activity leads to an increased signal of the reporter, in contrast to the traditional "OFF- system", where increased microRNA activity leads to suppression of the reporter[218,219]. In that alternative strategy, the microRNA target sites are located in the 3' UTR of a repressor gene, that is controlling the expression of a following reporter cassette. In these cases, the reported sensitivity for microRNA detection was limited, as 1nM was the minimum required microRNA concentration, in order to get a positive signal. Moreover, the concentration range of detection did not even cover two orders of magnitude, and only very highly expressed microRNAs, such as the miR-133 and miR-1 for muscle and miR-122 for liver, were used as proof of principle. In addition, as we were primarily interested in generating a signal by the reporter after microRNA inhibition, we decided to use the traditional "OFF-system", where microRNA binding sites would be cloned in the 3' UTR of a reporter gene, so that antimiR-mediated microRNA inhibition would lead to a derepression of the reporter gene.

The most widely used reporter genes are the luciferase and fluorescent genes. Luciferases do not require light but a substrate in order to produce a signal, what minimizes the autofluorescence of tissues resulting in low- to no-background[268]. For whole-animal bioluminescence experiments, both the Firefly (Fluc) and the Renilla (Rluc) luciferases, require the injection of their substrates, in contrast to the fluorescent proteins that can be readily detected. Fluc requires D-luciferin, while Rluc needs coelenterazine as a substrate[269]. Luciferase has a dynamic range of expression and high sensitivity because of its enzyme-base reporter nature, and a quick turnover, with a half-life of approximately three hours[270]. On the other hand, fluorescent proteins have a half-life of approximately 26 h, which can be reduced dramatically by genetic modifications[271]. Rather than the turnover of the reporter gene, in our case, more important was the maturation time of the fluorescent protein, that is the time from translation to fluorescence, as we were interested in the generation of a signal after microRNA

inhibition. The maturation time of a fluorescent protein can vary from minutes to hours[272]. The biggest advantage of the fluorescent proteins versus luciferase though, is the possibility to perform single-cell analysis of the signal, whereas the bioluminescence does not provide information about the individual cells and thereby also cell types, but rather generates only one signal from a whole cell population. As we were interested in developing a tool for determining antimiR's potency in different cell types, we decided to use fluorescent genes for our sensor.

For our construct, we initially chose as a control gene tdTomato[272], a red fluorescent protein with excitation and emission peaks at 554/581 nm, and as reporter gene eGFP[273], a green fluorescent protein, with excitation and emission peaks at 488/509 nm. We chose these two fluorescent proteins, as they are very bright, stable, and do not bleach quickly[272]. It is noteworthy that the enhanced GFP variant eGFP is 16-fold brighter than its wildtype version[273].

Our dual fluorescent reporter consisted of two cassettes in a back-to-back configuration, each under the control of a distinct CMV enhancer-CMV promoter pair (**Figure 4.9a**). In order to first test the ability of this construct to express in the cardiomyocytes *in vivo*, we decided to use AAV9, that has been shown to efficiently transduce the myocardium[55,239]. Since the transgene capacity of a self-complementary (or double-stranded) AAV is only 2.5 kbp and our transgene was far longer in size (4.3 kbp including the inverted terminal repeats (ITRs), that are necessary for the proper packaging of the virus), we produced a single-stranded AAV, whose capacity is up to 4.7 kb[274]. Mice injected with this virus encoding for a control sensor, where a scrambled binding site was located in the 3' UTR of the eGFP sequence, displayed high transduction, as indicated by the green fluorescence in cardiac sections, but the red fluorescence, that was supposed to serve as a reference, was almost absent (**Figure 4.9a**).

We supposed that this could be a result of the recombination of a repetitive sequence, a known issue in retroviruses[236,237]. To address this, we cloned several variants of the control sensor, where the two CMV enhancer-CMV promoters pairs were either located in a greater distance (**Figure 4.9b ii**), or the one enhancer element before the tdTomato was removed (**Figure 4.9b iii**), or the two tandem Tomato copies (of tdTomato) were replaced by mcherry (**Figure 4.9b iv**), or a combination of variants iii and iv (**Figure 4.9b v**). We then utilized the ability of AAV6 to efficiently transduce HEK293 cells[275] to test whether some of the above mentioned constructs were expressing both fluorescent genes. Only the control sensor lacking the CMV enhancer before the red fluorescent protein, which was the mcherry and not the tdTomato, was able to express both RFP and GFP at high levels (**Figure 4.9b v**). Mcherry has slightly different excitation and emission spectra than tdTomato, with its peak being at 587/610 nm, is very photostable, and has a quicker maturation time in comparison to tdTomato ($T_{0.5}$ maturation 15 min vs. 1 h) [272]. This optimized sensor also successfully transduced the myocardium, resulting in bright red and green fluorescence in cardiac slices (**Figure 4.9c**). Our

results indicate that the recombination of same sequences can also occur in AAV-mediated transgene delivery, an important point to take into account for future studies.

5.2.2 Validation and characterization of the microRNA sensor *in vitro*

As we were interested in the role of miR-29 in the myocardium[47], we decided to use a complementary binding site for miR-29a, in order to characterize the sensor *in vitro*.

Transfection of synthetic miR-29a in HEK293 cells, which endogenously barely express miR-29a (**Figure 4.10b**), led to a dose-dependent suppression of the reporter, as assessed by the gradual decrease in GFP/RFP (**Figure 4.10c**). Appealing was the observation, that 100 pM of synthetic miR-29a could repress more than 50% the sensor, while 1 nM resulted in almost complete silencing of the reporter, revealing the superior sensitivity of this system in comparison to the "ON-system" sensors, whose detection limit is approximately 1 nM[219].
Similarly, transfection of antimiR-29 in 3T3 cells, that endogenously have a high miR29a abundance (**Figure 4.10b**), resulted in a dose-dependent derepression of the sensor (**Figure 4.10d**). A difference in comparison to the microRNA supplementation experiment is that for antimiR-mediated inhibition, 1 nM of the synthetic inhibitor only led to approximately 50% derepression of the sensor. It might well be, that the high endogenous miR-29a abundance in 3T3 cells require more inhibitor, compared to what would be needed for inhibiting a microRNA with lower abundance. Moreover, the sensor seems to have higher sensitivity for detecting microRNA supplementation than inhibition, as determined by the hill slopes. The hill slope for the microRNA supplementation was determined to be -1.693, while the one for the microRNA inhibition 0.755. The hill slope is a measure for the steepness of the curve. A positive hill slope corresponds to an increasing curve as x increases, whereas a negative value means, that the curve decreases with the x-axis. A hill slope of 1.0 refers to a standard sigmoidal dose-response curve, and lower absolute values correspond to more shallow curves, while higher absolute values are linked with steeper curves. One alternative explanation for the more shallow curve upon microRNA inhibition, that would also explain the fact that even with the highest concentration used the sensor did not derepress to the level of the control sensor (GFP/RFP ~ 0.8 vs. 1), is the fact that the antimiR-29 was designed to perfectly target miR-29b and miR-29c, but has 1 nucleotide mismatch for the miR-29a (**Figure 4.10a**). The antimiR was designed that way in order to target 2/3 mature sequences perfectly, as if a perfect complementary antimiR against miR-29a would be used, then only 1/3 family members would be completely inhibited.

Testing microRNA activity sensors bearing target sites for each one of the miR-29 family members, or a combination of all of them, by transfecting miR-29a, miR-29b or miR-29c synthetic microRNA precursors in NRCM, led to the conclusion that the miR-29a sensor is less

prone to detect miR-29b and miR-29c than the rest of the sensors, whereas the miR-29abc sensor could equally detect all miR-29 family members.

This data prove that the miR-29a sensor was the most specific for one miR-29 family member that the others, whilst the miR-29abc sensor could be used in order to measure the activity of the whole miR-29 family. As a consequence, the miR-29a sensor should be used in order to determine miR-29a inhibition, taking into accounts that different antimiR chemistries target either the whole sequence of the microRNA and thereby are specific for only one family member[134], or only a smaller part of the microRNA and can that way inhibit a whole microRNA family[165]. In the case of the miR-29abc sensor, inhibition for example only of miR-29c would not be able to be detected, as miR-29a and miR-29b would still be able to repress the sensor. Only in the case of a family inhibitor, such as the LNA/DNA 16-mer used in this study, the miR-29abc sensor could also be useful to detect antimiR-mediated microRNA inhibition.

5.2.3 MicroRNA activity sensor validation *in vivo*

In order to determine the antimiR potency, we administered antimiR-29 intravenously for three consecutive days to mice expressing the miR-29a or miR-29abc sensor, that were previously delivered employing a single-stranded AAV9. Both sensors could robustly detect the antimiR-29-mediated miR-29 inhibition in the liver, as assessed by the derepression of the sensor (increased green fluorescence) in comparison to the untreated group (**Figure 4.12c,e**). Concerning the myocardium, none of both miR-29 sensors was able to detect any change in the miR-29 activity in the antimiR-treated mice (**Figure 4.12d,f**). This could have several reasons. First, it has been shown that the antimiR is accumulated in the liver and kidneys after systemic administration[134,135,165]. Moreover, we showed that miR-29a is higher expressed in the cardiomyocytes than in liver lysates (**Figure 4.12b**), what renders its inhibition even more cumbersome.

We attributed the relatively low transduction efficiency of the liver demonstrated in **Figure 4.12c,e** to CMV promoter silencing, a phenomenon that has been reported to lead to inactivation of the transcription in the long term[241,242], particularly in the liver[217,240]. Indeed, mice that were sacrificed two weeks after AAV9 administration, displayed great transduction efficiency, even in the liver (**Figure 4.13a**). These mice also displayed highly efficient transduction of the myocardium (**Figure 4.13b**).

5.2.4 Generation of mice transgenic for a microRNA activity sensor

For ubiquitous expression of our microRNA activity sensor *in vivo*, we utilized the recombinase-mediated cassette exchange technique. Although we successfully managed to recombine our sensor in embryonic stem cells with a pre-engineered Rosa26 docking site (IDG3.2 R26.10-3 ES cells[243]) and chimeras with very high expression of our transgene were generated, these

mice died in the first two weeks after birth. This finding may be explained by the reported toxicity caused by high expression levels of eGFP[244–246] (**Figure 4.14b**), which in combination with the CAG promoter, one of the strongest ubiquitous promoters available[276], might exacerbate its deleterious effects. In order to minimize the toxic effects of very strong expression of two fluorescent proteins, another ubiquitous but less strong promoter should be used. PGK-1 can drive ubiquitous but not uniform expression in transgenic mice[277], while EF-1a, though being a strong promoter, has been reported to fail to drive transgene expression, when arranged in a back-to-back configuration[278]. The ubiquitin C promoter could be a good candidate, since it drives ubiquitous expression in mice[279], and both mcherry and eGFP transgenic mice have been generated under its control[280].

5.2.5 Correlation of microRNA expression and sensor suppression as a means to select the best microRNA candidate sensor *in vivo*

We hypothesized that our miR-29a and miR-29abc sensors did not detect any antimiR potency in the myocardium because of the high basal expression and activity of miR-29. Moreover, activity of a microRNA above a certain threshold, would constantly suppress the sensor. In most of the cases, only the highest expressed microRNAs are studied, because they are more likely to have a biological function[212,281]. Since an enormous microRNA inhibition in the myocardium after systemic antimiR administration is certainly not the case, we next decided to identify a microRNA, whose activity would be at the most sensitive - for assessing antimiR-mediated microRNA inhibition - level.

There are studies reporting, that the microRNA expression correlates with its activity[282,283], and while this does not hold true for all the microRNAs[212,284], it was a straight-forward approach to screen microRNAs based on their expression and validate them based on their activity. Possible reasons why some microRNAs' activity does not reflect their expression are the subcellular localization of some miRs, the role of other factors such as RNA binding proteins and the ratio miR : target mRNAs[212,284]. In order to determine the sensitivity of the sensor for microRNA inhibition, we performed a serial of experiments that allowed us to roughly correlate the expression of a microRNA to its activity. When miR-29 was expressed at a level of 1000 copies per 10 pg RNA (that roughly correlates to one cell) or higher, it was able to completely repress a sensor bearing a complementary binding site for it (**Figure 4.15a**). Therefore, we screened for a microRNA whose expression would lie lower than this threshold -if possible in most of the cardiac cell types-, so that a sensor for this microRNA would allow to detect differences in the delivery of several antimiR chemistries even after a modest microRNA inhibition. Setting a window of expression from a small RNA sequencing database, 17 microRNAs were found to be expressed at the desired level in at least three out of four main cardiac cell types (**Figure 4.15c**). After excluding microRNA family members, the remaining

five candidate microRNAs were validated for their absolute expression in CM and liver lysates (**Figure 4.15d**). We further narrowed down the expression window by applying a minimum expression level of 400 copies/10 pg RNA in both the CM and liver, what resulted in only two microRNAs fulfilling that criteria, miR-191-5p and miR-151-5p. Because of the very high expression of miR-151-5p in endothelial cells of the myocardium (4414 RPM, Ramanujam D., unpublished data), we chose to create the sensor for the miR-191-5p, whose expression lied within the desired expression range in all the main cardiac cell types, as well as in the liver. This feature of miR-191-5p makes it the ideal candidate for the generation of a knock-in mouse ubiquitously expressing this microRNA activity sensor. AAV9-miR-191 sensor was indeed shown to be suppressed to the desired extent in the myocardium of mice, rendering it optimal for an antimiR-191 uptake study (**Figure 4.15e**).

There are reports supporting that oligonucleotide uptake is enhanced under stress conditions[169,285]. Therefore, one could also assess antimiR-mediated microRNA inhibition under a disease condition, such as TAC or MI. The presumably inefficient uptake of the charged synthetic antimiRs by the cardiac myocytes in contrast to the liver cells might be improved by increasing the half-life of the antimiRs, improving their cell penetrance and/or by targeted delivery.

5.2.6 Delivery strategies of oligonucleotides to improve tissue enrichment

A simple and straightforward way to achieve tissue enrichment of the delivered oligonucleotide is its local application. Hinkel et al. compared the effect of regional application, using a catheter, to the systemic administration of antimiR-92a in an ischemia/ reperfusion injury model in pigs[286]. The catheter-based administration - but not the intravenous infusion- of antimiR-92a lead to improved ejection fraction and smaller infarct size, compared to antimiR-control treated pigs. Despite the fact that the effect on the myocardium was improved with the local application, miR-92a levels were also decreased in the liver and kidney of the treated animals. In order to avoid the systemic effects, one could inject the antimiR intramuscularly. As this application method restricts the diffusion of the oligonucleotide to the close proximity of the injection site, multiple injections would be needed to achieve efficient delivery. Alternatively, balloons or drug-eluting stents could be employed. Wang et al. used antimiR-21-eluting stents in an in-stent restenosis (ISR) model in rats. The antimiR-21-eluting stents reduced vascular smooth muscle cell proliferation, and mitigated myointimal hyperplasia and ISR. Notably, no miR-21 reduction was observed in other organs, such as liver, kidney, heart and lung, in contrast to systemic antimiR-21 administration.

Another group used light-inducible antimiR-92a to improve the wound healing in diabetic mice[287]. In this case, photolabile groups, called “cages”, were used to abrogate the antimiR activity. Light activation of intradermally injected caged antimiR-92a led to similar effects as

systemically injected antimiR-92a, without reducing miR-92a expression in other organs. However, in order to target internal organs, such as the heart, future optimization experiments are necessary.

Receptor-mediated endocytosis is also gaining ground concerning oligonucleotide delivery. N-acetylgalactosamine (or GalNAc) conjugation can be used to deliver antimiRs to the liver, taking into advantage the ligand-receptor relationship of GalNAc and the asialoglycoprotein receptor (ASGPR), which is highly expressed in hepatocytes[169]. This modification is currently being used in clinical trials to treat HCV patients[170]. In addition, microRNAs can be conjugated to aptamers, or "chemical antibodies", which are RNA molecules that bind to specific receptors resulting in cell-type specific delivery of the conjugated antimiR. In a recent study, antimiR-21 was combined with an epidermal growth factor receptor (EGFR) aptamer and a fluorescent dye to target cancer cells in a triple-negative breast cancer mouse model[288]. This multifunctional RNA structure, that used a three-way junction from bacteriophage ϕ29 as a molecular scaffold, led to accumulation and internalization of the antimiR-21 in the cancer cells, and inhibition of the tumor growth. Of note, the antimiR conjugate was not found in other organs. A schematic representation of this assembly is depicted in **Figure 5.3**[289].

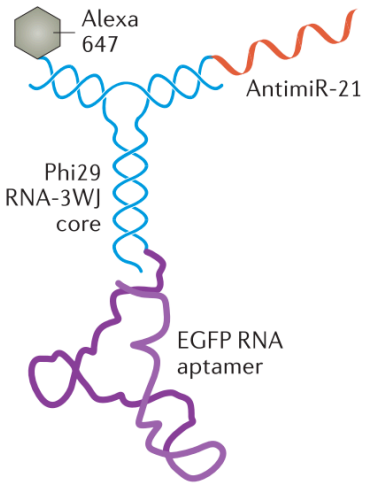

Figure 5.3. Three-way-junction-aptamer-antimiR RNA conjugate

The trifunctional RNA structure is comprised of an antimiR-21 sequence, an epidermal growth factor receptor aptamer, and Alexa647 for imaging, using a three-way junction (3WJ) motif as a molecular scaffold. Figure adapted from Zhou & Rossi (2017)[289].

Following internalization, any cargo gets into early endosomes, followed by either recycling of its content to the cell surface, or to late endosomes. In the latter case, the cargo is then transferred to lysosomes, where it gets degraded. Consequently, various methods have been developed to promote the endosomal escape of the cargo. To this end, Wagenaar et al. observed increased antimiR-21 uptake from cancer cells when two key components of the endosomal sorting complex required for transport (ESCRT-I), which is responsible for the

maturation and trafficking of endosomal content, were knocked down[290]. An alternative strategy is the conjugation of the cargo to pH-sensitive molecules, that become protonated in mature endosomes (pH < 6), causing an osmotic swelling of the endosomes also known as “proton sponge effect”, enhancing the endosomal escape of the cargo. Liu et al. took advantage of this property, conjugating an aptamer-siRNA complex to a pH-sensitive polyhistidine, resulting in increased cytosolic release and activity of the aptamer-siRNA complex[291]. As aptamer-mediated delivery of oligonucleotides has been mainly used to target cancer and endothelial cells to date[292], future studies using aptamer-antimiR complexes in the cardiovascular field are necessary.

A prominent strategy to increase the cellular uptake of the -in most cases- negatively charged oligonucleotides is to encapsulate them. Bellera et al. administered antimiR-92a encapsulated in microspheres (9 µm poly-D,-lactide-co-glycolide [PLGA]) intracoronary in a pig model of perfused acute myocardial infarction (AMI)[293]. This resulted in local downregulation of miR-92a, and prevention from remodeling in the infarct area, without reduction of miR-92a levels in other organs. Li et al. loaded antimiR-155 in mesoporous silica nanoparticles (MSNs) modified with polymerized dopamine (PDA) and AS1411 aptamer for targeting colorectal cancer in mice. AS1411 is a ligand for nucleolin, a cell surface receptor overexpressed in colorectal cancer[294]. This approach resulted in enriched delivery of the microRNA inhibitor to the tumor cells and enhanced therapeutic effects. Lesizza et al. employed lipid formulations to deliver miR-199a and miR-590 mimics to mice by a single intracardiac injection[182]. The result of their attempt was improved cardiac function after acute myocardial infarction with minimal distribution to other organs.

Despite the plethora of delivery options for oligonucleotides, targeting the heart is still challenging, because of the high dosages required to reach this organ, in contrast to liver and kidney. Combination of the above mentioned methods, as well as developing novel strategies to achieve enrichment of antimiR in the heart, and more specifically to defined cell types, will provide great therapeutic benefits and decrease of off-target effects.

6 Summary

MicroRNAs (miRNAs or miRs) are noncoding RNA molecules of 18-22 nucleotides length that regulate gene expression at the posttranscriptional level by inducing the degradation or translational suppression of their target mRNAs. MicroRNAs are involved in the control of key steps in development, metabolism and disease, including diseases of the cardiovascular system. With regard to the role of miR-29 in cardiac remodeling, we were surprised to identify miR-29 among the most potent prohypertrophic microRNAs in an unbiased screening of hypertrophy-modulating microRNAs, given the previous reports that characterized miR-29 as a beneficial – for the inhibition of fibrosis- molecule. We therefore first validated the prohypertrophic potential of miR-29 *in vitro*. Transfection of isolated cardiac myocytes with a synthetic miR-29 precursor led to significant hypertrophy, whereas employment of a miR-29 sponge prevented from phenylephrine-induced cardiomyocyte hypertrophy. We could demonstrate that miR-29 is expressed substantially higher in cardiac myocytes than in fibroblasts. Importantly, pharmacological inhibition by an (locked nucleic acids containing) LNA-antimiR-29 protected mice from cardiac dysfunction in a disease model for chronic cardiac pressure overload. In further support, cardiac myocyte-specific, genetic deficiency for miR-29 - conferred by Cre recombinase-mediated deletion of miR-29 alleles - prevented cardiac hypertrophy and fibrosis in mice. Mechanistically, we found miR-29 to activate the canonical and non-canonical Wnt signaling pathway by directly targeting four of its members. Our findings suggest that miR-29 in cardiac myocytes functionally dominates during cardiac remodeling over the other cell types in the myocardium.

Cloning a miRNA binding site into the 3'-UTR of a reporter gene is a sensitive way to quantitatively measure microRNA activity. To this end, we first optimized and validated microRNA activity sensors for miR-29 *in vitro*. We then brought the miR-29 sensor to expression *in vivo*. Using this sensor, inhibition of miR-29 by systemically administered antimiR could be detected in the liver, but not in the heart. To achieve a constant expression of the sensor, a knock-in mouse line was also generated. However, these mice died in the first two weeks after birth, presumably due to toxicity effects of the high GFP[244–246]. Additional experiments suggested that the sensitivity of the sensor strongly depends on the expression level of the endogenous microRNA. Therefore, several endogenous microRNAs were quantified and categorized for their expression strength. Based on these results, microRNA candidates within the optimal expression range for detection of microRNA inhibition were identified and validated for their expression and activity in cardiomyocytes. MiR-191-5p was selected as the best candidate for microRNA inhibition assessment and will be the focus of further investigations.

7 References

1. Venter JC, Adams MD, Myers EW, Li PW, Mural RJ, Sutton GG, Smith HO, Yandell M, Evans CA, Holt RA, Gocayne JD, Amanatides P, Ballew RM, Huson DH, Wortman JR, Zhang Q, Kodira CD, Zheng XH, Chen L, Skupski M, Subramanian G, Thomas PD, Zhang J, Miklos GLG, Nelson C, Broder S, Clark AG, Nadeau J, Mckusick VA, Zinder N, Levine AJ, Roberts RJ, Simon M, Slayman C, Hunkapiller M, Bolanos R, Delcher A, Dew I, Fasulo D, Flanigan M, Florea L, Halpern A, Hannenhalli S, Kravitz S, Levy S, Mobarry C, Reinert K, Remington K, Abu-threideh J, Beasley E, Biddick K, Bonazzi V, Brandon R, Cargill M, Chandramouliswaran I, Charlab R, Chaturvedi K, Deng Z, Francesco V Di, Dunn P, Eilbeck K, Evangelista C, Gabrielian AE, Gan W, Ge W, Gong F, Gu Z, Guan P, Heiman TJ, Higgins ME, Ji R, Ke Z, Ketchum KA, Lai Z, Lei Y, Li Z, Li J, Liang Y, Lin X, Lu F, Merkulov G V, Milshina N, Moore HM, Naik AK, Narayan VA, Neelam B, Nusskern D, Rusch DB, Salzberg S, Shao W, Shue B, Yao A, Ye J, Zhan M, Zhang W, Zhang H, Zhao Q, Zheng L, et al. The sequence of the human genome. *Science*. 2001;291:1–38.

2. Consortium EP, Dunham I, Kundaje A, Aldred SF, Collins PJ, Davis CA, Doyle F, Epstein CB, Frietze S, Harrow J, Kaul R, Khatun J, Lajoie BR, Landt SG, Lee BK, Pauli F, Rosenbloom KR, Sabo P, Safi A, Sanyal A, Shoresh N, Simon JM, Song L, Trinklein ND, Altshuler RC, Birney E, Brown JB, Cheng C, Djebali S, Dong X, Ernst J, Furey TS, Gerstein M, Giardine B, Greven M, Hardison RC, Harris RS, Herrero J, Hoffman MM, Iyer S, Kellis M, Kheradpour P, Lassmann T, Li Q, Lin X, Marinov GK, Merkel A, Mortazavi A, Parker SCJ, Reddy TE, Rozowsky J, Schlesinger F, Thurman RE, Wang J, Ward LD, Whitfield TW, Wilder SP, Wu W, Xi HS, Yip KY, Zhuang J, Bernstein BE, Green ED, Gunter C, Snyder M, Pazin MJ, Lowdon RF, Dillon LAL, Adams LB, Kelly CJ, Zhang J, Wexler JR, Good PJ, Feingold EA, Crawford GE, Dekker J, Elnitski L, Farnham PJ, Giddings MC, Gingeras TR, Guigó R, Hubbard TJ, Kent WJ, Lieb JD, Margulies EH, Myers RM, Stamatoyannopoulos JA, Tenenbaum SA, Weng Z, White KP, Wold B, Yu Y, Wrobel J, Risk BA, Gunawardena HP, Kuiper HC, Maier CW, Xie L, et al. An integrated encyclopedia of DNA elements in the human genome. *Nature*. 2012;489:57–74.

3. Lee RC, Feinbaum RL, Ambros V. The C. elegans heterochronic gene lin-4 encodes small RNAs with antisense complementarity to lin-14. *Cell*. 1993;75:843–854.

4. Reinhart BJ, Slack FJ, Basson M, Pasquinelli AE, Bettinger JC, Rougvie AE, Horvitz HR, Ruvkun G. The 21-nucleotide let-7 RNA regulates developmental timing in Caenorhabditis elegans. *Nature*. 2000;403:901–906.

5. Pasquinelli AE, Reinhart BJ, Slack F, Martindale MQ, Kuroda MI, Maller B, Hayward DC, Ball EE, Degnan B, Müller P, Spring J, Srinivasan A, Fishman M, Finnerty J, Corbo J, Levine M, Leahy P, Davidson E, Ruvkun G. Conservation of the sequence and temporal expression of let-7 heterochronic regulatory RNA. *Nature*. 2000;408:86–89.

6. Lagos-Quintana M, Rauhut R, Lendeckel W, Tuschl T. Identification of novel genes coding for small expressed RNAs. *Science*. 2001;294:853–858.

7. Lau NC. An abundant class of tiny RNAs with probable regulatory roles in Caenorhabditis elegans. *Science*. 2001;294:858–862.

8. Lee RC. An extensive class of small RNAs in Caenorhabditis elegans. *Science*. 2001;294:862–864.

9. Griffiths-Jones S, Saini HK, van Dongen S, Enright AJ. miRBase: tools for microRNA genomics. *Nucleic Acids Res*. 2007;36:D154–D158.

10. Lee Y. MicroRNA maturation: stepwise processing and subcellular localization. *EMBO J*. 2002;21:4663–4670.

11. CAI X. Human microRNAs are processed from capped, polyadenylated transcripts that can also function as mRNAs. *RNA*. 2004;10:1957–1966.

12. Lee Y, Kim M, Han J, Yeom K-H, Lee S, Baek SH, Kim VN. MicroRNA genes are transcribed by RNA polymerase II. *EMBO J*. 2004;23:4051–4060.

13. Nguyen TA, Jo MH, Choi Y-G, Park J, Kwon SC, Hohng S, Kim VN, Woo J-S. Functional anatomy of the human microprocessor. *Cell*. 2015;161:1374–1387.

14. Lee Y, Ahn C, Han J, Choi H, Kim J, Yim J, Lee J, Provost P, Rådmark O, Kim S, Kim VN. The nuclear RNase III Drosha initiates microRNA processing. *Nature*. 2003;425:415–419.

15. Yi R. Exportin-5 mediates the nuclear export of pre-microRNAs and short hairpin RNAs. *Genes Dev*. 2003;17:3011–3016.

16. Lund E. Nuclear export of microRNA precursors. *Science*. 2004;303:95–98.

17. Grishok A, Pasquinelli AE, Conte D, Li N, Parrish S, Ha I, Baillie DL, Fire A, Ruvkun G, Mello CC. Genes and mechanisms related to RNA interference regulate expression of the small temporal RNAs that control C. elegans developmental timing. *Cell*. 2001;106:23–34.

18. Zhang H, Kolb FA, Jaskiewicz L, Westhof E, Filipowicz W. Single processing center models for human Dicer and bacterial RNase III. *Cell*. 2004;118:57–68.

19. Hammond SM, Bernstein E, Beach D, Hannon GJ. An RNA-directed nuclease mediates

post-transcriptional gene silencing in Drosophila cells. *Nature*. 2000;404:293–296.

20. Martinez J, Patkaniowska A, Urlaub H, Lührmann R, Tuschl T. Single-stranded antisense siRNAs guide target RNA cleavage in RNAi. *Cell*. 2002;110:563–574.

21. Bartel DP. MicroRNAs: Genomics, biogenesis, mechanism, and function. *Cell*. 2004;116:281–297.

22. Lim LP, Lau NC, Garrett-Engele P, Grimson A, Schelter JM, Castle J, Bartel DP, Linsley PS, Johnson JM. Microarray analysis shows that some microRNAs downregulate large numbers of target mRNAs. *Nature*. 2005;433:769–773.

23. Khvorova A, Reynolds A, Jayasena SD. Functional siRNAs and miRNAs exhibit strand bias. *Cell*. 2003;115:209–216.

24. Bartel DP. Metazoan MicroRNAs. *Cell*. 2018;173:20–51.

25. Bartel DP. MicroRNAs: Target recognition and regulatory functions. *Cell*. 2009;136:215–233.

26. Wightman B, Ha I, Ruvkun G. Posttranscriptional regulation of the heterochronic gene lin-14 by lin-4 mediates temporal pattern formation in C. elegans. *Cell*. 1993;75:855–862.

27. Liu J. Argonaute2 is the catalytic engine of mammalian RNAi. *Science*. 2004;305:1437–1441.

28. Meister G, Landthaler M, Patkaniowska A, Dorsett Y, Teng G, Tuschl T. Human Argonaute2 mediates RNA cleavage targeted by miRNAs and siRNAs. *Mol Cell*. 2004;15:185–197.

29. Filipowicz W, Bhattacharyya SN, Sonenberg N. Mechanisms of post-transcriptional regulation by microRNAs: are the answers in sight? *Nat Rev Genet*. 2008;9:102–114.

30. Lewis BP, Burge CB, Bartel DP. Conserved seed pairing, often flanked by adenosines, indicates that thousands of human genes are microRNA targets. *Cell*. 2005;120:15–20.

31. Friedman RC, Farh KKH, Burge CB, Bartel DP. Most mammalian mRNAs are conserved targets of microRNAs. *Genome Res*. 2009;19:92–105.

32. Ketting RF. Dicer functions in RNA interference and in synthesis of small RNA involved in developmental timing in C. elegans. *Genes Dev*. 2001;15:2654–2659.

33. Poy MN, Hausser J, Trajkovski M, Braun M, Collins S, Rorsman P, Zavolan M, Stoffel M. MiR-375 maintains normal pancreatic alpha- and beta-cell mass. *Proc Natl Acad Sci*. 2009;106:5813–5818.

34. Latreille M, Hausser J, Stützer I, Zhang Q, Hastoy B, Gargani S, Kerr-Conte J, Pattou

F, Zavolan M, Esguerra JLS, Eliasson L, Rülicke T, Rorsman P, Stoffel M. MicroRNA-7a regulates pancreatic β cell function. *J Clin Invest*. 2014;124:2722–2735.

35. Iorio M V., Ferracin M, Liu C-G, Veronese A, Spizzo R, Sabbioni S, Magri E, Pedriali M, Fabbri M, Campiglio M, Ménard S, Palazzo JP, Rosenberg A, Musiani P, Volinia S, Nenci I, Calin GA, Querzoli P, Negrini M, Croce CM. MicroRNA gene expression deregulation in human breast cancer. *Cancer Res*. 2005;65:7065–7070.

36. Johnson SM, Grosshans H, Shingara J, Byrom M, Jarvis R, Cheng A, Labourier E, Reinert KL, Brown D, Slack FJ. RAS is regulated by the let-7 microRNA family. *Cell*. 2005;120:635–647.

37. Asangani IA, Rasheed SAK, Nikolova DA, Leupold JH, Colburn NH, Post S, Allgayer H. MicroRNA-21 (miR-21) post-transcriptionally downregulates tumor suppressor Pdcd4 and stimulates invasion, intravasation and metastasis in colorectal cancer. *Oncogene*. 2008;27:2128–2136.

38. Hebert SS, Horre K, Nicolai L, Papadopoulou AS, Mandemakers W, Silahtaroglu AN, Kauppinen S, Delacourte A, De Strooper B. Loss of microRNA cluster miR-29a/b-1 in sporadic Alzheimer's disease correlates with increased BACE1/ -secretase expression. *Proc Natl Acad Sci*. 2008;105:6415–6420.

39. Kim J, Inoue K, Ishii J, Vanti WB, Voronov S V., Murchison E, Hannon G, Abeliovich A. A microRNA feedback circuit in midbrain dopamine neurons. *Science*. 2007;317:1220–1224.

40. Du C, Liu C, Kang J, Zhao G, Ye Z, Huang S, Li Z, Wu Z, Pei G. MicroRNA miR-326 regulates TH-17 differentiation and is associated with the pathogenesis of multiple sclerosis. *Nat Immunol*. 2009;10:1252–1259.

41. Jopling CL. Modulation of hepatitis C virus RNA abundance by a liver-specific microRNA. *Science*. 2005;309:1577–1581.

42. Thum T, Gross C, Fiedler J, Fischer T, Kissler S, Bussen M, Galuppo P, Just S, Rottbauer W, Frantz S, Castoldi M, Soutschek J, Koteliansky V, Rosenwald A, Basson MA, Licht JD, Pena JTR, Rouhanifard SH, Muckenthaler MU, Tuschl T, Martin GR, Bauersachs J, Engelhardt S. MicroRNA-21 contributes to myocardial disease by stimulating MAP kinase signalling in fibroblasts. *Nature*. 2008;456:980–984.

43. Carè A, Catalucci D, Felicetti F, Bonci D, Addario A, Gallo P, Bang M-L, Segnalini P, Gu Y, Dalton ND, Elia L, Latronico MVG, Høydal M, Autore C, Russo M a, Dorn GW, Ellingsen Ø, Ruiz-Lozano P, Peterson KL, Croce CM, Peschle C, Condorelli G. MicroRNA-133 controls cardiac hypertrophy. *Nat Med*. 2007;13:613–618.

44. van Rooij E, Sutherland LB, Thatcher JE, DiMaio JM, Naseem RH, Marshall WS, Hill JA, Olson EN. Dysregulation of microRNAs after myocardial infarction reveals a role of miR-29 in cardiac fibrosis. *Proc Natl Acad Sci*. 2008;105:13027–13032.

45. Ucar A, Gupta SK, Fiedler J, Erikci E, Kardasinski M, Batkai S, Dangwal S, Kumarswamy R, Bang C, Holzmann A, Remke J, Caprio M, Jentzsch C, Engelhardt S, Geisendorf S, Glas C, Hofmann TG, Nessling M, Richter K, Schiffer M, Carrier L, Napp LC, Bauersachs J, Chowdhury K, Thum T. The miRNA-212/132 family regulates both cardiac hypertrophy and cardiomyocyte autophagy. *Nat Commun*. 2012;3:1078.

46. Ganesan J, Ramanujam D, Sassi Y, Ahles A, Jentzsch C, Werfel S, Leierseder S, Loyer X, Giacca M, Zentilin L, Thum T, Laggerbauer B, Engelhardt S. MiR-378 controls cardiac hypertrophy by combined repression of Mitogen-activated protein kinase pathway factors. *Circulation*. 2013;127:2097–2106.

47. Sassi Y, Avramopoulos P, Ramanujam D, Grüter L, Werfel S, Giosele S, Brunner A-D, Esfandyari D, Papadopoulou AS, De Strooper B, Hübner N, Kumarswamy R, Thum T, Yin X, Mayr M, Laggerbauer B, Engelhardt S. Cardiac myocyte miR-29 promotes pathological remodeling of the heart by activating Wnt signaling. *Nat Commun*. 2017;8:1614.

48. Mendis S, Puska P, Norrving B. Global atlas on cardiovascular disease prevention and control. Geneva: World Health Organization; 2011.

49. Pfeffer JM, Pfeffer MA, Braunwald E. Influence of chronic captopril therapy on the infarcted left ventricle of the rat. *Pharmacol Res*. 1985;57:84–95.

50. Cohn JN, Ferrari R, Sharpe N. Cardiac remodeling-concepts and clinical implications: A consensus paper from an International Forum on Cardiac Remodeling. *J Am Coll Cardiol*. 2000;35:569–582.

51. Braunwald E. Heart failure. *JACC Hear Fail*. 2013;1:1–20.

52. van Rooij E, Sutherland LB, Qi X, Richardson J a, Hill J, Olson EN. Control of stress-dependent cardiac growth and gene expression by a microRNA. *Science*. 2007;316:575–579.

53. Duisters RF, Tijsen AJ, Schroen B, Leenders JJ, Lentink V, van der Made I, Herias V, van Leeuwen RE, Schellings MW, Barenbrug P, Maessen JG, Heymans S, Pinto YM, Creemers EE. MiR-133 and miR-30 regulate connective tissue growth factor: implications for a role of microRNAs in myocardial matrix remodeling. *Circ Res*. 2009;104:170–178.

54. Matkovich SJ, Wang W, Tu Y, Eschenbacher WH, Dorn LE, Condorelli G, Diwan A,

Nerbonne JM, Dorn GW. MicroRNA-133a protects against myocardial fibrosis and modulates electrical repolarization without affecting hypertrophy in pressure-overloaded adult hearts. *Circ Res*. 2010;106:166–175.

55. Ramanujam D, Sassi Y, Laggerbauer B, Engelhardt S. Viral vector-based targeting of miR-21 in cardiac nonmyocyte cells reduces pathologic remodeling of the heart. *Mol Ther*. 2016;24:1939–1948.

56. Mone SM, Sanders SP, Colan SD. Control mechanisms for physiological hypertrophy of pregnancy. *Circulation*. 1996;94:667–672.

57. Heineke J, Molkentin JD. Regulation of cardiac hypertrophy by intracellular signalling pathways. *Nat Rev Mol Cell Biol*. 2006;7:589–600.

58. Frey N, Olson EN. Cardiac Hypertrophy: The Good, the Bad, and the Ugly. *Annu Rev Physiol*. 2003;65:45–79.

59. Razeghi P, Young ME, Alcorn JL, Moravec CS, Frazier OH, Taegtmeyer H. Metabolic gene expression in fetal and failing human heart. *Circulation*. 2001;104:2923–2931.

60. Nakamura M, Sadoshima J. Mechanisms of physiological and pathological cardiac hypertrophy. *Nat Rev Cardiol*. 2018;15:387–407.

61. Kawaguchi M, Takahashi M, Hata T, Kashima Y, Usui F, Morimoto H, Izawa A, Takahashi Y, Masumoto J, Koyama J, Hongo M, Noda T, Nakayama J, Sagara J, Taniguchi S, Ikeda U. Inflammasome activation of cardiac fibroblasts is essential for myocardial ischemia/reperfusion injury. *Circulation*. 2011;123:594–604.

62. Travers JG, Kamal FA, Robbins J, Yutzey KE, Blaxall BC. Cardiac fibrosis: The fibroblast awakens. *Circ Res*. 2016;118:1021–40.

63. Weber KT. Fibrosis and hypertensive heart disease. *Curr Opin Cardiol*. 2000;15:264–72.

64. Gray M. Angiotensin II stimulates cardiac myocyte hypertrophy via paracrine release of TGF-β1 and endothelin-1 from fibroblasts. *Cardiovasc Res*. 1998;40:352–363.

65. Yue L, Xie J, Nattel S. Molecular determinants of cardiac fibroblast electrical function and therapeutic implications for atrial fibrillation. *Cardiovasc Res*. 2011;89:744–753.

66. Isoyama S, Nitta-Komatsubara Y. Acute and chronic adaptation to hemodynamic overload and ischemia in the aged heart. *Heart Fail Rev*. 2002;7:63–9.

67. Nusse R, van Ooyen A, Cox D, Fung YK, Varmus H. Mode of proviral activation of a putative mammary oncogene (int-1) on mouse chromosome 15. *Nature*. 1984;307:131–6.

68. Schneider VA. Wnt antagonism initiates cardiogenesis in Xenopus laevis. *Genes Dev*. 2001;15:304–315.

69. Tzahor E. Wnt signals from the neural tube block ectopic cardiogenesis. *Genes Dev*. 2001;15:255–260.

70. Malekar P, Hagenmueller M, Anyanwu A, Buss S, Streit MR, Weiss CS, Wolf D, Riffel J, Bauer A, Katus HA, Hardt SE. Wnt signaling is critical for maladaptive cardiac hypertrophy and accelerates myocardial remodeling. *Hypertension*. 2010;55:939–945.

71. Moon RT. The promise and perils of Wnt signaling through beta -catenin. *Science*. 2002;296:1644–1646.

72. Veeman MT, Axelrod JD, Moon RT. A second canon. Functions and mechanisms of beta-catenin-independent Wnt signaling. *Dev Cell*. 2003;5:367–77.

73. Sheldahl LC, Slusarski DC, Pandur P, Miller JR, Kühl M, Moon RT. Dishevelled activates Ca 2+ flux, PKC, and CamKII in vertebrate embryos. *J Cell Biol*. 2003;161:769–777.

74. Rao TP, Kuhl M. An updated overview on Wnt signaling pathways: A prelude for more. *Circ Res*. 2010;106:1798–1806.

75. Liu C, Li Y, Semenov M, Han C, Baeg GH, Tan Y, Zhang Z, Lin X, He X. Control of beta-catenin phosphorylation/degradation by a dual-kinase mechanism. *Cell*. 2002;108:837–47.

76. Liu C, Kato Y, Zhang Z, Do VM, Yankner B a, He X. Beta-Trcp couples beta-catenin phosphorylation-degradation and regulates Xenopus axis formation. *Proc Natl Acad Sci*. 1999;96:6273–6278.

77. Pinson KI, Brennan J, Monkley S, Avery BJ, Skarnes WC. An LDL-receptor-related protein mediates Wnt signalling in mice. *Nature*. 2000;407:535–538.

78. Cliffe A, Hamada F, Bienz M. A role of Dishevelled in relocating Axin to the plasma membrane during Wingless signaling. *Curr Biol*. 2003;13:960–966.

79. van de Schans VAM, van den Borne SWM, Strzelecka AE, Janssen BJA, van der Velden JLJ, Langen RCJ, Wynshaw-Boris A, Smits JFM, Blankesteijn WM. Interruption of Wnt signaling attenuates the onset of pressure overload-induced cardiac hypertrophy. *Hypertension*. 2007;49:473–480.

80. Mirotsou M, Zhang Z, Deb A, Zhang L, Gnecchi M, Noiseux N, Mu H, Pachori A, Dzau V. Secreted frizzled related protein 2 (Sfrp2) is the key Akt-mesenchymal stem cell-released paracrine factor mediating myocardial survival and repair. *Proc Natl Acad Sci*. 2007;104:1643–1648.

81. Blankesteijn WM, Essers-Janssen YPG, Ulrich MMW, Smits JFM. Increased expression of a homologue of drosophila tissue polarity gene “frizzled” in left ventricular hypertrophy in the rat, as identified by subtractive hybridization. *J Mol Cell Cardiol*. 1996;28:1187–1191.

82. de Jaime-Soguero A, Abreu de Oliveira W, Lluis F. The pleiotropic effects of the canonical Wnt pathway in early development and pluripotency. *Genes (Basel)*. 2018;9:93.

83. Slusarski DC, Corces VG, Moon RT. Interaction of Wnt and a Frizzled homologue triggers G-protein-linked phosphatidylinositol signalling. *Nature*. 1997;390:410–413.

84. Berridge MJ, Irvine RF. Inositol phosphates and cell signalling. *Nature*. 1989;341:197–205.

85. Berridge MJ. Inositol trisphosphate and calcium signalling. *Nature*. 1993;361:315–325.

86. Kohn AD, Moon RT. Wnt and calcium signaling: β-Catenin-independent pathways. *Cell Calcium*. 2005;38:439–446.

87. Frey N. Hypertrophy of the heart: A new therapeutic target? *Circulation*. 2004;109:1580–1589.

88. He X. LDL receptor-related proteins 5 and 6 in Wnt/ -catenin signaling: Arrows point the way. *Development*. 2004;131:1663–1677.

89. Habas R, Kato Y, He X. Wnt/Frizzled activation of Rho regulates vertebrate gastrulation and requires a novel formin homology protein Daam1. *Cell*. 2001;107:843–854.

90. Winter CG, Wang B, Ballew A, Royou A, Karess R, Axelrod JD, Luo L. Drosophila Rho-associated kinase (Drok) links Frizzled-mediated planar cell polarity signaling to the actin cytoskeleton. *Cell*. 2001;105:81–91.

91. Boutros M, Paricio N, Strutt DI, Mlodzik M. Dishevelled activates JNK and discriminates between JNK pathways in planar polarity and wingless signaling. *Cell*. 1998;94:109–118.

92. Tufan AC, Daumer KM, DeLise AM, Tuan RS. AP-1 transcription factor complex is a target of signals from both WNT-7a and N-Cadherin-dependent cell–cell adhesion complex during the regulation of limb mesenchymal chondrogenesis. *Exp Cell Res*. 2002;273:197–203.

93. Antos CL, McKinsey TA, Frey N, Kutschke W, McAnally J, Shelton JM, Richardson JA, Hill JA, Olson EN. Activated glycogen synthase-3 suppresses cardiac hypertrophy in vivo. *Proc Natl Acad Sci*. 2002;99:907–912.

94. Matsuda T, Zhai P, Maejima Y, Hong C, Gao S, Tian B, Goto K, Takagi H, Tamamori-Adachi M, Kitajima S, Sadoshima J. Distinct roles of GSK-3alpha and GSK-3beta phosphorylation in the heart under pressure overload. *Proc Natl Acad Sci*. 2008;105:20900–20905.

95. Molkentin JD, Lu J-R, Antos CL, Markham B, Richardson J, Robbins J, Grant SR, Olson EN. A Calcineurin-dependent transcriptional pathway for cardiac hypertrophy. *Cell*. 1998;93:215–228.

96. Krishnan V. Regulation of bone mass by Wnt signaling. *J Clin Invest*. 2006;116:1202–1209.

97. Malinauskas T. Docking of fatty acids into the WIF domain of the human Wnt inhibitory factor-1. *Lipids*. 2008;43:227–230.

98. Tago K, Nakamura T, Nishita M, Hyodo J, Nagai S, Murata Y, Adachi S, Ohwada S, Morishita Y, Shibuya H, Akiyama T. Inhibition of Wnt signaling by ICAT, a novel beta-catenin-interacting protein. *Genes Dev*. 2000;14:1741–9.

99. Sampson EM. Negative regulation of the Wnt-beta-catenin pathway by the transcriptional repressor HBP1. *EMBO J*. 2001;20:4500–4511.

100. Eppig JT, Blake JA, Bult CJ, Kadin JA, Richardson JE. The Mouse Genome Database (MGD): facilitating mouse as a model for human biology and disease. *Nucleic Acids Res*. 2015;43:D726–D736.

101. Kim Y-S, Kang HS, Jetten AM. The Krüppel-like zinc finger protein Glis2 functions as a negative modulator of the Wnt/β-catenin signaling pathway. *FEBS Lett*. 2007;581:858–864.

102. Fang Y, Yu X, Liu Y, Kriegel AJ, Heng Y, Xu X, Liang M, Ding X. MiR-29c is downregulated in renal interstitial fibrosis in humans and rats and restored by HIF-α activation. *Am J Physiol Physiol*. 2013;304:F1274–F1282.

103. Roderburg C, Urban G-W, Bettermann K, Vucur M, Zimmermann H, Schmidt S, Janssen J, Koppe C, Knolle P, Castoldi M, Tacke F, Trautwein C, Luedde T. Micro-RNA profiling reveals a role for miR-29 in human and murine liver fibrosis. *Hepatology*. 2011;53:209–18.

104. Wang L, Zhou L, Jiang P, Lu L, Chen X, Lan H, Guttridge DC, Sun H, Wang H. Loss of miR-29 in myoblasts contributes to dystrophic muscle pathogenesis. *Mol Ther*. 2012;20:1222–33.

105. Maurer B, Stanczyk J, Jüngel A, Akhmetshina A, Trenkmann M, Brock M, Kowal-Bielecka O, Gay RE, Michel B a, Distler JHW, Gay S, Distler O. MicroRNA-29, a key

regulator of collagen expression in systemic sclerosis. *Arthritis Rheum*. 2010;62:1733–1743.

106. Cushing L, Kuang PP, Qian J, Shao F, Wu J, Little F, Thannickal VJ, Cardoso W V., Lü J. MiR-29 is a major regulator of genes associated with pulmonary fibrosis. *Am J Respir Cell Mol Biol*. 2011;45:287–294.

107. Lagos-Quintana M, Rauhut R, Yalcin A, Meyer J, Lendeckel W, Tuschl T. Identification of tissue-specific microRNAs from mouse. *Curr Biol*. 2002;12:735–739.

108. Sayed D, Hong C, Chen I-Y, Lypowy J, Abdellatif M. MicroRNAs play an essential role in the development of cardiac hypertrophy. *Circ Res*. 2007;100:416–424.

109. Ikeda S, He A, Kong SW, Lu J, Bejar R, Bodyak N, Lee K-H, Ma Q, Kang PM, Golub TR, Pu WT. MicroRNA-1 negatively regulates expression of the hypertrophy-associated Calmodulin and Mef2a genes. *Mol Cell Biol*. 2009;29:2193–2204.

110. Elia L, Contu R, Quintavalle M, Varrone F, Chimenti C, Russo MA, Cimino V, De Marinis L, Frustaci A, Catalucci D, Condorelli G. Reciprocal regulation of microRNA-1 and insulin-like growth factor-1 signal transduction cascade in cardiac and skeletal muscle in physiological and pathological conditions. *Circulation*. 2009;120:2377–2385.

111. Li Q, Song X-W, Zou J, Wang G-K, Kremneva E, Li X-Q, Zhu N, Lappalainen P, Yuan W-J, Qin Y-W, Jing Q. Attenuation of microRNA-1 derepresses the cytoskeleton regulatory protein twinfilin-1 to provoke cardiac hypertrophy. *J Cell Sci*. 2010;123:2680–2680.

112. Karakikes I, Chaanine AH, Kang S, Mukete BN, Jeong D, Zhang S, Hajjar RJ, Lebeche D. Therapeutic cardiac-targeted delivery of miR-1 reverses pressure overload-induced cardiac hypertrophy and attenuates pathological remodeling. *J Am Heart Assoc*. 2013;2:e000078–e000078.

113. Chen JF, Mandel EM, Thomson JM, Wu Q, Callis TE, Hammond SM, Conlon FL, Wang DZ. The role of microRNA-1 and microRNA-133 in skeletal muscle proliferation and differentiation. *Nat Genet*. 2006;38:228–233.

114. Dong D-L, Chen C, Huo R, Wang N, Li Z, Tu Y-J, Hu J-T, Chu X, Huang W, Yang B-F. Reciprocal repression between microRNA-133 and calcineurin regulates cardiac hypertrophy: A novel mechanism for progressive cardiac hypertrophy. *Hypertension*. 2010;55:946–952.

115. Callis TE, Pandya K, Seok HY, Tang R-H, Tatsuguchi M, Huang Z-P, Chen J-F, Deng Z, Gunn B, Shumate J, Willis MS, Selzman CH, Wang D-Z. MicroRNA-208a is a regulator of cardiac hypertrophy and conduction in mice. *J Clin Invest*. 2009;119:2772–

2786.

116. Xu X-D, Song X-W, Li Q, Wang G-K, Jing Q, Qin Y-W. Attenuation of microRNA-22 derepressed PTEN to effectively protect rat cardiomyocytes from hypertrophy. *J Cell Physiol*. 2012;227:1391–1398.

117. Huang Z-P, Chen J, Seok HY, Zhang Z, Kataoka M, Hu X, Wang D-Z. MicroRNA-22 regulates cardiac hypertrophy and remodeling in response to stress. *Circ Res*. 2013;112:1234–1243.

118. Knezevic I, Patel A, Sundaresan NR, Gupta MP, Solaro RJ, Nagalingam RS, Gupta M. A novel cardiomyocyte-enriched microRNA, miR-378, targets insulin-like growth factor 1 receptor. *J Biol Chem*. 2012;287:12913–12926.

119. Li Z, Song Y, Liu L, Hou N, An X, Zhan D, Li Y, Zhou L, Li P, Yu L, Xia J, Zhang Y, Wang J, Yang X. MiR-199a impairs autophagy and induces cardiac hypertrophy through mTOR activation. *Cell Death Differ*. 2017;24:1205–1213.

120. da Costa Martins PA, Salic K, Gladka MM, Armand A-S, Leptidis S, el Azzouzi H, Hansen A, Coenen-de Roo CJ, Bierhuizen MF, van der Nagel R, van Kuik J, de Weger R, de Bruin A, Condorelli G, Arbones ML, Eschenhagen T, De Windt LJ. MicroRNA-199b targets the nuclear kinase Dyrk1a in an auto-amplification loop promoting calcineurin/NFAT signalling. *Nat Cell Biol*. 2010;12:1220–1227.

121. Patrick DM, Montgomery RL, Qi X, Obad S, Kauppinen S, Hill JA, van Rooij E, Olson EN. Stress-dependent cardiac remodeling occurs in the absence of microRNA-21 in mice. *J Clin Invest*. 2010;120:3912–3916.

122. Roy S, Khanna S, Hussain SRA, Biswas S, Azad A, Rink C, Gnyawali S, Shilo S, Nuovo GJ, Sen CK. MicroRNA expression in response to murine myocardial infarction: MiR-21 regulates fibroblast metalloprotease-2 via phosphatase and tensin homologue. *Cardiovasc Res*. 2009;82:21–29.

123. Abonnenc M, Nabeebaccus AA, Mayr U, Barallobre-Barreiro J, Dong X, Cuello F, Sur S, Drozdov I, Langley SR, Lu R, Stathopoulou K, Didangelos A, Yin X, Zimmermann W-H, Shah AM, Zampetaki A, Mayr M. Extracellular matrix secretion by cardiac fibroblasts: Role of microRNA-29b and microRNA-30c. *Circ Res*. 2013;113:1138–1147.

124. Dawson K, Wakili R, Ordog B, Clauss S, Chen Y, Iwasaki Y, Voigt N, Qi XY, Sinner MF, Dobrev D, Kaab S, Nattel S. MicroRNA29: A mechanistic contributor and potential biomarker in atrial fibrillation. *Circulation*. 2013;127:1466–1475.

125. Ji X, Takahashi R, Hiura Y, Hirokawa G, Fukushima Y, Iwai N. Plasma miR-208 as a biomarker of myocardial injury. *Clin Chem*. 2009;55:1944–1949.

126. D'Alessandra Y, Devanna P, Limana F, Straino S, Di Carlo A, Brambilla PG, Rubino M, Carena MC, Spazzafumo L, De Simone M, Micheli B, Biglioli P, Achilli F, Martelli F, Maggiolini S, Marenzi G, Pompilio G, Capogrossi MC. Circulating microRNAs are new and sensitive biomarkers of myocardial infarction. *Eur Heart J*. 2010;31:2765–2773.

127. Adachi T, Nakanishi M, Otsuka Y, Nishimura K, Hirokawa G, Goto Y, Nonogi H, Iwai N. Plasma microRNA 499 as a biomarker of acute myocardial infarction. *Clin Chem*. 2010;56:1183–1185.

128. Tijsen AJ, Creemers EE, Moerland PD, de Windt LJ, van der Wal AC, Kok WE, Pinto YM. MiR423-5p as a circulating biomarker for heart failure. *Circ Res*. 2010;106:1035–1039.

129. Jentzsch C, Leierseder S, Loyer X, Flohrschütz I, Sassi Y, Hartmann D, Thum T, Laggerbauer B, Engelhardt S. A phenotypic screen to identify hypertrophy-modulating microRNAs in primary cardiomyocytes. *J Mol Cell Cardiol*. 2012;52:13–20.

130. Janssen HLA, Reesink HW, Lawitz EJ, Zeuzem S, Rodriguez-Torres M, Patel K, van der Meer AJ, Patick AK, Chen A, Zhou Y, Persson R, King BD, Kauppinen S, Levin AA, Hodges MR. Treatment of HCV infection by targeting microRNA. *N Engl J Med*. 2013;368:1685–1694.

131. Gomez IG, MacKenna DA, Johnson BG, Kaimal V, Roach AM, Ren S, Nakagawa N, Xin C, Newitt R, Pandya S, Xia T, Liu X, Borza D, Grafals M, Shankland SJ, Himmelfarb J, Portilla D, Liu S, Chau BN, Duffield JS. Anti–microRNA-21 oligonucleotides prevent Alport nephropathy progression by stimulating metabolic pathways. *J Clin Invest*. 2015;125:141–156.

132. Esau CC. Inhibition of microRNA with antisense oligonucleotides. *Methods*. 2008;44:55–60.

133. Lennox K a, Behlke M a. Chemical modification and design of anti-miRNA oligonucleotides. *Gene Ther*. 2011;18:1111–1120.

134. Krützfeldt J, Rajewsky N, Braich R, Rajeev KG, Tuschl T, Manoharan M, Stoffel M. Silencing of microRNAs in vivo with 'antagomirs.' *Nature*. 2005;438:685–689.

135. Elmén J, Lindow M, Schütz S, Lawrence M, Petri A, Obad S, Lindholm M, Hedtjärn M, Hansen HF, Berger U, Gullans S, Kearney P, Sarnow P, Straarup EM, Kauppinen S. LNA-mediated microRNA silencing in non-human primates. *Nature*. 2008;452:896–899.

136. Lanford RE, Hildebrandt-Eriksen ES, Petri A, Persson R, Lindow M, Munk ME, Kauppinen S, Orum H. Therapeutic silencing of microRNA-122 in primates with chronic hepatitis C virus infection. *Science*. 2010;327:198–201.

137. Krützfeldt J, Kuwajima S, Braich R, Rajeev KG, Pena J, Tuschl T, Manoharan M, Stoffel M. Specificity, duplex degradation and subcellular localization of antagomirs. *Nucleic Acids Res*. 2007;35:2885–2892.

138. Bumcrot D, Manoharan M, Koteliansky V, Sah DWY. RNAi therapeutics: a potential new class of pharmaceutical drugs. *Nat Chem Biol*. 2006;2:711–719.

139. Davis S, Lollo B, Freier S, Esau C. Improved targeting of miRNA with antisense oligonucleotides. *Nucleic Acids Res*. 2006;34:2294–2304.

140. Davis S, Propp S, Freier SM, Jones LE, Serra MJ, Kinberger G, Bhat B, Swayze EE, Bennett CF, Esau C. Potent inhibition of microRNA in vivo without degradation. *Nucleic Acids Res*. 2009;37:70–77.

141. Lennox K a., Behlke M a. A direct comparison of anti-microRNA oligonucleotide potency. *Pharm Res*. 2010;27:1788–1799.

142. Fabani MM, Abreu-Goodger C, Williams D, Lyons PA, Torres AG, Smith KGC, Enright AJ, Gait MJ, Vigorito E. Efficient inhibition of miR-155 function in vivo by peptide nucleic acids. *Nucleic Acids Res*. 2010;38:4466–4475.

143. Stenvang J, Petri A, Lindow M, Obad S, Kauppinen S. Inhibition of microRNA function by antimiR oligonucleotides. *Silence*. 2012;3:1.

144. Khvorova A, Watts JK. The chemical evolution of oligonucleotide therapies of clinical utility. *Nat Biotechnol*. 2017;35:238–248.

145. Petersen M, Wengel J. LNA: a versatile tool for therapeutics and genomics. *Trends Biotechnol*. 2003;21:74–81.

146. Esau CC, Monia BP. Therapeutic potential for microRNAs. *Adv Drug Deliv Rev*. 2007;59:101–114.

147. Stenvang J, Kauppinen S. MicroRNAs as targets for antisense-based therapeutics. *Expert Opin Biol Ther*. 2008;8:59–81.

148. Koshkin AA, Singh SK, Nielsen P, Rajwanshi VK, Kumar R, Meldgaard M, Olsen CE, Wengel J. LNA (Locked Nucleic Acids): Synthesis of the adenine, cytosine, guanine, 5-methylcytosine, thymine and uracil bicyclonucleoside monomers, oligomerisation, and unprecedented nucleic acid recognition. *Tetrahedron*. 1998;54:3607–3630.

149. Obika S, Nanbu D, Hari Y, Andoh J, Morio K, Doi T, Imanishi T. Stability and structural features of the duplexes containing nucleoside analogues with a fixed N-type conformation, 2′-O,4′-C-methyleneribonucleosides. *Tetrahedron Lett*. 1998;39:5401–5404.

150. Braasch D a, Corey DR. Locked nucleic acid (LNA): fine-tuning the recognition of DNA and RNA. *Chem Biol*. 2001;8:1–7.

151. Seth PP, Vasquez G, Allerson CA, Berdeja A, Gaus H, Kinberger GA, Prakash TP, Migawa MT, Bhat B, Swayze EE. Synthesis and biophysical evaluation of 2′,4′-constrained 2′ O -methoxyethyl and 2′,4′-constrained 2′ O -ethyl nucleic acid analogues. *J Org Chem*. 2010;75:1569–1581.

152. Brown DA, Kang SH, Gryaznov SM, DeDionisio L, Heidenreich O, Sullivan S, Xu X, Nerenberg MI. Effect of phosphorothioate modification of oligodeoxynucleotides on specific protein binding. *J Biol Chem*. 1994;269:26801–26805.

153. Levin AA. A review of issues in the pharmacokinetics and toxicology of phosphorothioate antisense oligonucleotides. *Biochim Biophys Acta - Gene Struct Expr*. 1999;1489:69–84.

154. Lennox KA, Sabel JL, Johnson MJ, Moreira BG, Fletcher CA, Rose SD, Behlke MA, Laikhter AL, Walder JA, Dagle JM. Characterization of modified antisense oligonucleotides in Xenopus laevis embryos. *Oligonucleotides*. 2006;16:26–42.

155. Fabani MM, Gait MJ. MiR-122 targeting with LNA/2'-O-methyl oligonucleotide mixmers, peptide nucleic acids (PNA), and PNA-peptide conjugates. *RNA*. 2007;14:336–346.

156. Babar IA, Cheng CJ, Booth CJ, Liang X, Weidhaas JB, Saltzman WM, Slack FJ. Nanoparticle-based therapy in an in vivo microRNA-155 (miR-155)-dependent mouse model of lymphoma. *Proc Natl Acad Sci*. 2012;109:E1695–E1704.

157. Torres AG, Fabani MM, Vigorito E, Williams D, Al-Obaidi N, Wojciechowski F, Hudson RHE, Seitz O, Gait MJ. Chemical structure requirements and cellular targeting of microRNA-122 by peptide nucleic acids anti-miRs. *Nucleic Acids Res*. 2012;40:2152–2167.

158. Martello G, Zacchigna L, Inui M, Montagner M, Adorno M, Mamidi A, Morsut L, Soligo S, Tran U, Dupont S, Cordenonsi M, Wessely O, Piccolo S. MicroRNA control of nodal signalling. *Nature*. 2007;449:183–188.

159. Flynt AS, Li N, Thatcher EJ, Solnica-Krezel L, Patton JG. Zebrafish miR-214 modulates Hedgehog signaling to specify muscle cell fate. *Nat Genet*. 2007;39:259–263.

160. Kloosterman WP, Lagendijk AK, Ketting RF, Moulton JD, Plasterk RHA. Targeted inhibition of miRNA maturation with morpholinos reveals a role for miR-375 in pancreatic islet development. *PLoS Biol*. 2007;5:e203.

161. Egholm M, Buchardt O, Nielsen PE, Berg RH. Peptide Nucleic Acids (PNA). Oligonucleotide analogues with an achiral peptide backbone. *J Am Chem Soc*.

1992;114:1895–1897.

162. van Rooij E, Kauppinen S. Development of microRNA therapeutics is coming of age. *EMBO Mol Med*. 2014;6:851–64.

163. Montgomery RL, Hullinger TG, Semus HM, Dickinson BA, Seto AG, Lynch JM, Stack C, Latimer PA, Olson EN, van Rooij E. Therapeutic inhibition of miR-208a improves cardiac function and survival during heart failure. *Circulation*. 2011;124:1537–1547.

164. Boon RA, Seeger T, Heydt S, Fischer A, Hergenreider E, Horrevoets AJG, Vinciguerra M, Rosenthal N, Sciacca S, Pilato M, van Heijningen P, Essers J, Brandes RP, Zeiher AM, Dimmeler S. MicroRNA-29 in aortic dilation: Implications for aneurysm formation. *Circ Res*. 2011;109:1115–1119.

165. Obad S, dos Santos CO, Petri A, Heidenblad M, Broom O, Ruse C, Fu C, Lindow M, Stenvang J, Straarup EM, Hansen HF, Koch T, Pappin D, Hannon GJ, Kauppinen S. Silencing of microRNA families by seed-targeting tiny LNAs. *Nat Genet*. 2011;43:371–378.

166. Garchow BG, Bartulos Encinas O, Leung YT, Tsao PY, Eisenberg RA, Caricchio R, Obad S, Petri A, Kauppinen S, Kiriakidou M. Silencing of microRNA-21 in vivo ameliorates autoimmune splenomegaly in lupus mice. *EMBO Mol Med*. 2011;3:605–615.

167. Elmén J, Lindow M, Silahtaroglu A, Bak M, Christensen M, Lind-Thomsen A, Hedtjärn M, Hansen JB, Hansen HF, Straarup EM, McCullagh K, Kearney P, Kauppinen S. Antagonism of microRNA-122 in mice by systemically administered LNA-antimiR leads to up-regulation of a large set of predicted target mRNAs in the liver. *Nucleic Acids Res*. 2008;36:1153–1162.

168. Esau C, Davis S, Murray SF, Yu XX, Pandey SK, Pear M, Watts L, Booten SL, Graham M, McKay R, Subramaniam A, Propp S, Lollo B a., Freier S, Bennett CF, Bhanot S, Monia BP. MiR-122 regulation of lipid metabolism revealed by in vivo antisense targeting. *Cell Metab*. 2006;3:87–98.

169. Juliano RL. The delivery of therapeutic oligonucleotides. *Nucleic Acids Res*. 2016;44:6518–6548.

170. van der Ree MH, de Vree JM, Stelma F, Willemse S, van der Valk M, Rietdijk S, Molenkamp R, Schinkel J, van Nuenen AC, Beuers U, Hadi S, Harbers M, van der Veer E, Liu K, Grundy J, Patick AK, Pavlicek A, Blem J, Huang M, Grint P, Neben S, Gibson NW, Kootstra NA, Reesink HW. Safety, tolerability, and antiviral effect of RG-101 in patients with chronic hepatitis C: a phase 1B, double-blind, randomised controlled trial.

Lancet. 2017;389:709–717.

171. Ebert MS, Neilson JR, Sharp P a. MicroRNA sponges: competitive inhibitors of small RNAs in mammalian cells. *Nat Methods*. 2007;4:721–726.

172. Ebert MS, Sharp PA. MicroRNA sponges: Progress and possibilities. *RNA*. 2010;16:2043–2050.

173. Ebert MS, Sharp PA. Emerging roles for natural microRNA sponges. *Curr Biol*. 2010;20:R858–R861.

174. Bader AG, Brown D, Stoudemire J, Lammers P. Developing therapeutic microRNAs for cancer. *Gene Ther*. 2011;18:1121–1126.

175. Garzon R, Marcucci G, Croce CM. Targeting microRNAs in cancer: rationale, strategies and challenges. *Nat Rev Drug Discov*. 2010;9:775–789.

176. Thorsen SB, Obad S, Jensen NF, Stenvang J, Kauppinen S. The therapeutic potential of microRNAs in cancer. *Cancer J*. 2012;18:275–284.

177. Po YC, Weinmann L, Gaidatzis D, Pei Y, Zavolan M, Tuschl T, Meister G. Strand-specific 5′-O-methylation of siRNA duplexes controls guide strand selection and targeting specificity. *Rna*. 2008;14:263–274.

178. Chiu YL, Rana TM. siRNA function in RNAi: A chemical modification analysis. *RNA*. 2003;9:1034–1048.

179. Pramanik D, Campbell NR, Karikari C, Chivukula R, Kent OA, Mendell JT, Maitra A. Restitution of tumor suppressor microRNAs using a systemic nanovector inhibits pancreatic cancer growth in mice. *Mol Cancer Ther*. 2011;10:1470–1480.

180. Ibrahim AF, Weirauch U, Thomas M, Grunweller A, Hartmann RK, Aigner A. MicroRNA replacement therapy for miR-145 and miR-33a is efficacious in a model of colon carcinoma. *Cancer Res*. 2011;71:5214–5224.

181. Takeshita F, Patrawala L, Osaki M, Takahashi RU, Yamamoto Y, Kosaka N, Kawamata M, Kelnar K, Bader AG, Brown D, Ochiya T. Systemic delivery of synthetic microRNA-16 inhibits the growth of metastatic prostate tumors via downregulation of multiple cell-cycle genes. *Mol Ther*. 2010;18:181–187.

182. Lesizza P, Prosdocimo G, Martinelli V, Sinagra G, Zacchigna S, Giacca M. Single-dose intracardiac injection of pro-regenerative microRNAs improves cardiac function after myocardial infarction. *Circ Res*. 2017;120:1298–1304.

183. Peacock H, Fucini R V., Jayalath P, Ibarra-Soza JM, Haringsma HJ, Flanagan WM, Willingham A, Beal PA. Nucleobase and ribose modifications control immunostimulation

by a microRNA-122-mimetic RNA. *J Am Chem Soc*. 2011;133:9200–9203.

184. Ramkissoon SH, Mainwaring LA, Sloand EM, Young NS, Kajigaya S. Nonisotopic detection of microRNA using digoxigenin labeled RNA probes. *Mol Cell Probes*. 2006;20:1–4.

185. Valoczi A. Sensitive and specific detection of microRNAs by northern blot analysis using LNA-modified oligonucleotide probes. *Nucleic Acids Res*. 2004;32:e175–e175.

186. Hunt EA, Broyles D, Head T, Deo SK. MicroRNA detection: Current technology and research strategies. *Annu Rev Anal Chem*. 2015;8:217–237.

187. Bustin SA, Benes V, Garson JA, Hellemans J, Huggett J, Kubista M, Mueller R, Nolan T, Pfaffl MW, Shipley GL, Vandesompele J, Wittwer CT. The MIQE guidelines: Minimum information for publication of quantitative Real-Time PCR Experiments. *Clin Chem*. 2009;55:611–622.

188. Yin JQ, Zhao RC, Morris K V. Profiling microRNA expression with microarrays. *Trends Biotechnol*. 2008;26:70–76.

189. van Rooij E. The art of microRNA research. *Circ Res*. 2011;108:219–234.

190. Ambros V, Bartel B, Bartel D, Burge CB, Carrington J, Chen X, Dreyfuss G, Eddy S, Griffiths-Jones S, Marshal M, Matzke M, Ruvkun G, Tuschl T. A uniform system for microRNA annotation. *RNA*. 2003;9:277–279.

191. Zuker M. Mfold web server for nucleic acid folding and hybridization prediction. *Nucleic Acids Res*. 2003;31:3406–3415.

192. Kloosterman WP, Wienholds E, de Bruijn E, Kauppinen S, Plasterk RHA. In situ detection of miRNAs in animal embryos using LNA-modified oligonucleotide probes. *Nat Methods*. 2006;3:27–29.

193. Tuddenham L, Wheeler G, Ntounia-Fousara S, Waters J, Hajihosseini MK, Clark I, Dalmay T. The cartilage specific microRNA-140 targets histone deacetylase 4 in mouse cells. *FEBS Lett*. 2006;580:4214–4217.

194. Obernosterer G, Martinez J, Alenius M. Locked nucleic acid-based in situ detection of microRNAs in mouse tissue sections. *Nat Protoc*. 2007;2:1508–1514.

195. Silahtaroglu AN, Nolting D, Dyrskjøt L, Berezikov E, Møller M, Tommerup N, Kauppinen S. Detection of microRNAs in frozen tissue sections by fluorescence in situ hybridization using locked nucleic acid probes and tyramide signal amplification. *Nat Protoc*. 2007;2:2520–2528.

196. Song R, Ro S, Yan W. In situ hybridization detection of microRNAs. *Methods Mol Biol*.

2010;629:285–292.

197. Porichis F, Hart MG, Griesbeck M, Everett HL, Hassan M, Baxter AE, Lindqvist M, Miller SM, Soghoian DZ, Kavanagh DG, Reynolds S, Norris B, Mordecai SK, Nguyen Q, Lai C, Kaufmann DE. High-throughput detection of miRNAs and gene-specific mRNA at the single-cell level by flow cytometry. *Nat Commun*. 2014;5:5641.

198. Urbanek M, Nawrocka A, Krzyzosiak W. Small RNA detection by in situ hybridization methods. *Int J Mol Sci*. 2015;16:13259–13286.

199. Dong H, Jin S, Ju H, Hao K, Xu L-P, Lu H, Zhang X. Trace and label-free microRNA detection using oligonucleotide encapsulated silver nanoclusters as probes. *Anal Chem*. 2012;84:8670–8674.

200. Johnson BN, Mutharasan R. Sample preparation-free, real-time detection of microRNA in human serum using piezoelectric cantilever biosensors at attomole level. *Anal Chem*. 2012;84:10426–10436.

201. Fang S, Lee HJ, Wark AW, Corn RM. Attomole microarray detection of microRNAs by nanoparticle-amplified SPR imaging measurements of surface polyadenylation reactions. *J Am Chem Soc*. 2006;128:14044–14046.

202. Johnson BN, Mutharasan R. Biosensor-based microRNA detection: techniques, design, performance, and challenges. *Analyst*. 2014;139:1576.

203. Hendrickson DG, Hogan DJ, McCullough HL, Myers JW, Herschlag D, Ferrell JE, Brown PO. Concordant regulation of translation and mRNA abundance for hundreds of targets of a human microRNA. *PLoS Biol*. 2009;7:25–29.

204. Guo H, Ingolia NT, Weissman JS, Bartel DP. Mammalian microRNAs predominantly act to decrease target mRNA levels. *Nature*. 2010;466:835–840.

205. Selbach M, Schwanhäusser B, Thierfelder N, Fang Z, Khanin R, Rajewsky N. Widespread changes in protein synthesis induced by microRNAs. *Nature*. 2008;455:58–63.

206. Baek D, Villén J, Shin C, Camargo FD, Gygi SP, Bartel DP. The impact of microRNAs on protein output. *Nature*. 2008;455:64–71.

207. Torres AG, Threlfall RN, Gait MJ. Potent and sustained cellular inhibition of miR-122 by lysine-derivatized peptide nucleic acids (PNA) and phosphorothioate locked nucleic acid (LNA)/2'-O-methyl (OMe) mixmer anti-miRs in the absence of transfection agents. *Artif DNA PNA XNA*. 2011;2:71–78.

208. Chomczynski P, Sacchi N. The single-step method of RNA isolation by acid guanidinium thiocyanate–phenol–chloroform extraction: twenty-something years on. *Nat Protoc*.

2006;1:581–585.

209. Lu Y, Xiao J, Lin H, Bai Y, Luo X, Wang Z, Yang B. A single anti-microRNA antisense oligodeoxyribonucleotide (AMO) targeting multiple microRNAs offers an improved approach for microRNA interference. *Nucleic Acids Res*. 2009;37:e24–e24.

210. Thomson DW, Bracken CP, Szubert JM, Goodall GJ. On measuring miRNAs after transient transfection of mimics or antisense inhibitors. *PLoS One*. 2013;8:e55214.

211. Ko HY, Hwang DW, Lee DS, Kim S. A reporter gene imaging system for monitoring microRNA biogenesis. *Nat Protoc*. 2009;4:1663–1669.

212. Mullokandov G, Baccarini A, Ruzo A, Jayaprakash AD, Tung N, Israelow B, Evans MJ, Sachidanandam R, Brown BD. High-throughput assessment of microRNA activity and function using microRNA sensor and decoy libraries. *Nat Methods*. 2012;9:840–846.

213. Förstemann K, Horwich MD, Wee L, Tomari Y, Zamore PD. Drosophila microRNAs are sorted into functionally distinct Argonaute complexes after production by Dicer-1. *Cell*. 2007;130:287–297.

214. Mansfield JH, Harfe BD, Nissen R, Obenauer J, Srineel J, Chaudhuri A, Farzan-Kashani R, Zuker M, Pasquinelli AE, Ruvkun G, Sharp PA, Tabin CJ, McManus MT. MicroRNA-responsive “sensor” transgenes uncover Hox-like and other developmentally regulated patterns of vertebrate microRNA expression. *Nat Genet*. 2004;36:1079–1083.

215. Brown BD, Venneri MA, Zingale A, Sergi LS, Naldini L. Endogenous microRNA regulation suppresses transgene expression in hematopoietic lineages and enables stable gene transfer. *Nat Med*. 2006;12:585–591.

216. Lee JY, Kim S, Hwang DW, Jeong JM, Chung J-K, Lee MC, Lee DS. Development of a dual-luciferase reporter system for in vivo visualization of microRNA biogenesis and posttranscriptional regulation. *J Nucl Med*. 2008;49:285–294.

217. Wang G, Dong X, Hu J, Tian W, Yuchi J, Wang Y, Wu X. Long-term ex vivo monitoring of in vivo microRNA activity in liver using a secreted luciferase sensor. *Sci China Life Sci*. 2011;54:418–425.

218. Amendola M, Giustacchini A, Gentner B, Naldini L. A double-switch vector system positively regulates transgene expression by endogenous microRNA expression (miR-ON vector). *Mol Ther*. 2013;21:934–946.

219. Ezzine S, Vassaux G, Pitard B, Barteau B, Malinge J-M, Midoux P, Pichon C, Baril P. RILES, a novel method for temporal analysis of the in vivo regulation of miRNA expression. *Nucleic Acids Res*. 2013;41:e192–e192.

220. Schmidt A, Tief K, Foletti A, Hunziker A, Penna D, Hummler E, Beermann F. lacZ

transgenic mice to monitor gene expression in embryo and adult. *Brain Res Brain Res Protoc*. 1998;3:54–60.

221. Fraga H. Firefly luminescence: a historical perspective and recent developments. *Photochem Photobiol Sci*. 2008;7:146–58.

222. Matthews JC, Hori K, Cormier MJ. Purification and properties of Renilla reniformis luciferase. *Biochemistry*. 1977;16:85–91.

223. Shimomura O, Johnson FH, Saiga Y. Extraction, purification and properties of aequorin, a bioluminescent protein from the luminous hydromedusan, Aequorea. *J Cell Comp Physiol*. 1962;59:223–39.

224. Brennecke J, Hipfner DR, Stark A, Russell RB, Cohen SM. bantam encodes a developmentally regulated microRNA that controls cell proliferation and regulates the proapoptotic gene hid in Drosophila. *Cell*. 2003;113:25–36.

225. Phiwpan K, Guo J, Zhang W, Hu T, Boruah BM, Zhang J, Zhou X. A novel transgenic mouse line for tracing microRNA-155-5p activity in vivo. *PLoS One*. 2015;10:e0128198.

226. Papadopoulou AS, Dooley J, Linterman MA, Pierson W, Ucar O, Kyewski B, Zuklys S, Hollander GA, Matthys P, Gray DHD, De Strooper B, Liston A. The thymic epithelial microRNA network elevates the threshold for infection-associated thymic involution via miR-29a mediated suppression of the IFN-α receptor. *Nat Immunol*. 2012;13:181–187.

227. Wilkins BJ. Calcineurin/NFAT coupling participates in pathological, but not physiological, cardiac hypertrophy. *Circ Res*. 2004;94:110–118.

228. Veeman MT, Slusarski DC, Kaykas A, Louie SH, Moon RT. Zebrafish Prickle, a modulator of noncanonical Wnt/Fz signaling, regulates gastrulation movements. *Curr Biol*. 2003;13:680–685.

229. Rockman HA, Ross RS, Harris AN, Knowlton KU, Steinhelper ME, Field LJ, Ross J, Chien KR. Segregation of atrial-specific and inducible expression of an atrial natriuretic factor transgene in an in vivo murine model of cardiac hypertrophy. *Proc Natl Acad Sci*. 1991;88:9907–9907.

230. Kauffman L, Balatti V, Cascione L, Fadda P, Racke F, Santhanam R, Costinean S. Gradual rarefaction of hematopoietic precursors and atrophy in a depleted microRNA 29a, b and c environment. *PLoS One*. 2015;10:e0131981.

231. Dooley J, Garcia-Perez JE, Sreenivasan J, Schlenner SM, Vangoitsenhoven R, Papadopoulou AS, Tian L, Schonefeldt S, Serneels L, Deroose C, Staats KA, Van der Schueren B, De Strooper B, McGuinness OP, Mathieu C, Liston A. The microRNA-29 family dictates the balance between homeostatic and pathological glucose handling in

diabetes and obesity. *Diabetes*. 2016;65:53–61.

232. Kamran F, Andrade AC, Nella AA, Clokie SJ, Rezvani G, Nilsson O, Baron J, Lui JC. Evidence that up-regulation of microRNA-29 contributes to postnatal body growth deceleration. *Mol Endocrinol*. 2015;29:921–932.

233. Deb A. Cell-cell interaction in the heart via Wnt/ beta-catenin pathway after cardiac injury. *Cardiovasc Res*. 2014;102:214–223.

234. Dawson K, Aflaki M, Nattel S. Role of the Wnt-Frizzled system in cardiac pathophysiology: a rapidly developing, poorly understood area with enormous potential. *J Physiol*. 2013;591:1409–1432.

235. Colston JT, de la Rosa SD, Koehler M, Gonzales K, Mestril R, Freeman GL, Bailey SR, Chandrasekar B. Wnt-induced secreted protein-1 is a prohypertrophic and profibrotic growth factor. *Am J Physiol Circ Physiol*. 2007;293:H1839–H1846.

236. Delviks K a, Pathak VK. Effect of distance between homologous sequences and 3' homology on the frequency of retroviral reverse transcriptase template switching. *J Virol*. 1999;73:7923–32.

237. Salamango DJ, Evans DA, Baluyot MF, Furlong JN, Johnson MC. Recombination can lead to spurious results in retroviral transduction with dually fluorescent reporter genes. *J Virol*. 2013;87:13900–13903.

238. Naso MF, Tomkowicz B, Perry WL, Strohl WR. Adeno-associated virus (AAV) as a vector for gene therapy. *BioDrugs*. 2017;31:317–334.

239. Bish LT, Morine K, Sleeper MM, Sanmiguel J, Wu D, Gao G, Wilson JM, Sweeney HL. Adeno-associated virus (AAV) serotype 9 provides global cardiac gene transfer superior to AAV1, AAV6, AAV7, and AAV8 in the mouse and rat. *Hum Gene Ther*. 2008;19:1359–1368.

240. Guo ZS, Wang LH, Eisensmith RC, Woo SLC. Evaluation of promoter strength for hepatic gene expression in vivo following adenovirus-mediated gene transfer. *Gene Ther*. 1996;3:802–810.

241. Schmidt E V, Christoph G, Zeller R, Leder P. The cytomegalovirus enhancer: a pan-active control element in transgenic mice. *Mol Cell Biol*. 1990;10:4406–11.

242. Kay MA, Baley P, Rothenberg S, Leland F, Fleming L, Ponder KP, Liu T-J, Finegold M, Darlington G, Pokorny W. Expression of human alpha 1-antitrypsin in dogs after autologous transplantation of retroviral transduced hepatocytes. *Proc Natl Acad Sci*. 1992;89:89–93.

243. Hitz C, Wurst W, Kuhn R. Conditional brain-specific knockdown of MAPK using Cre/loxP

regulated RNA interference. *Nucleic Acids Res*. 2007;35:e90–e90.

244. Baens M, Noels H, Broeckx V, Hagens S, Fevery S, Billiau AD, Vankelecom H, Marynen P. The dark side of EGFP: Defective polyubiquitination. *PLoS One*. 2006;1:e54.

245. Zhang J, Rao R V, Spilman P, Mangada J, Xie L, Vitelli C, Gorostiza OF, Madden DT, Zeng X, Jin K, Hart MJ, Bredesen DE, Galvan V. Endogenously EGFP-labeled mouse embryonic stem cells. *Aging Dis*. 2011;2:18–29.

246. Ansari AM, Ahmed AK, Matsangos AE, Lay F, Born LJ, Marti G, Harmon JW, Sun Z. Cellular GFP toxicity and immunogenicity: Potential confounders in in vivo cell tracking experiments. *Stem Cell Rev Reports*. 2016;12:553–559.

247. Montgomery RL, Yu G, Latimer PA, Stack C, Robinson K, Dalby CM, Kaminski N, van Rooij E. MicroRNA mimicry blocks pulmonary fibrosis. *EMBO Mol Med*. 2014;6:1347–1356.

248. Wang J, Chu ES. ., Chen H-Y, Man K, Go MYY, Huang XR, Lan HY, Sung JJY, Yu J. microRNA-29b prevents liver fibrosis by attenuating hepatic stellate cell activation and inducing apoptosis through targeting PI3K/AKT pathway. *Oncotarget*. 2015;6.

249. Wang B, Komers R, Carew R, Winbanks CE, Xu B, Herman-Edelstein M, Koh P, Thomas M, Jandeleit-Dahm K, Gregorevic P, Cooper ME, Kantharidis P. Suppression of microRNA-29 expression by TGF-beta1 promotes collagen expression and renal fibrosis. *J Am Soc Nephrol*. 2012;23:252–265.

250. Lyu G, Guan Y, Zhang C, Zong L, Sun L, Huang X, Huang L, Zhang L, Tian XL, Zhou Z, Tao W. TGF-β signaling alters H4K20me3 status via miR-29 and contributes to cellular senescence and cardiac aging. *Nat Commun*. 2018;9:1–13.

251. Griffiths-Jones S. The microRNA registry. *Nucleic Acids Res*. 2004;32:D109–D111.

252. Kozomara A, Griffiths-Jones S. miRBase: annotating high confidence microRNAs using deep sequencing data. *Nucleic Acids Res*. 2014;42:D68–D73.

253. El-Brolosy MA, Stainier DYR. Genetic compensation: A phenomenon in search of mechanisms. *PLoS Genet*. 2017;13:1–17.

254. Liao J-Y, Ma L-M, Guo Y-H, Zhang Y-C, Zhou H, Shao P, Chen Y-Q, Qu L-H. Deep sequencing of human nuclear and cytoplasmic small RNAs reveals an unexpectedly complex subcellular distribution of miRNAs and tRNA 3′ trailers. *PLoS One*. 2010;5:e10563.

255. Hwang H-W, Wentzel E a, Mendell JT. A hexanucleotide element directs microRNA nuclear import. *Science*. 2007;315:97–100.

256. Shimshek DR, Kim J, Hübner MR, Spergel DJ, Buchholz F, Casanova E, Stewart AF, Seeburg PH, Sprengel R. Codon-improved Cre recombinase (iCre) expression in the mouse. *Genesis*. 2002;32:19–26.

257. Werfel S, Jungmann A, Lehmann L, Ksienzyk J, Bekeredjian R, Kaya Z, Leuchs B, Nordheim A, Backs J, Engelhardt S, Katus HA, Müller OJ. Rapid and highly efficient inducible cardiac gene knockout in adult mice using AAV-mediated expression of Cre recombinase. *Cardiovasc Res*. 2014;104:15–23.

258. Soriano P. Generalized lacZ expression with the ROSA26 Cre reporter strain. *Nat Genet*. 1999;21:70–71.

259. Wiebel FF, Rennekampff V, Vintersten K, Nordheim A. Generation of mice carrying conditional knockout alleles for the transcription factor SRF. *genesis*. 2002;32:124–126.

260. Zhang JCL, Woo YJ, Chen J-A, Swain JL, Sweeney HL. Efficient transmural cardiac gene transfer by intrapericardial injection in neonatal mice. *J Mol Cell Cardiol*. 1999;31:721–732.

261. Chen B, Dodge ME, Tang W, Lu J, Ma Z, Fan C-W, Wei S, Hao W, Kilgore J, Williams NS, Roth MG, Amatruda JF, Chen C, Lum L. Small molecule–mediated disruption of Wnt-dependent signaling in tissue regeneration and cancer. *Nat Chem Biol*. 2009;5:100–107.

262. Aramburu J. Affinity-driven peptide selection of an NFAT inhibitor more selective than Cyclosporin A. *Science*. 1999;285:2129–2133.

263. Michael A, Haq S, Chen X, Hsich E, Cui L, Walters B, Shao Z, Bhattacharya K, Kilter H, Huggins G, Andreucci M, Periasamy M, Solomon RN, Liao R, Patten R, Molkentin JD, Force T. Glycogen Synthase Kinase-3β regulates growth, calcium homeostasis, and diastolic function in the heart. *J Biol Chem*. 2004;279:21383–21393.

264. Stauffer BL. Soy diet worsens heart disease in mice. *J Clin Invest*. 2005;116:209–216.

265. Konhilas JP. Exercise can prevent and reverse the severity of hypertrophic cardiomyopathy. *Circ Res*. 2006;98:540–548.

266. Hardt SE, Sadoshima J. Negative regulators of cardiac hypertrophy. *Cardiovasc Res*. 2004;63:500–509.

267. Kerkelä R, Woulfe K, Force T. Glycogen synthase kinase-3beta - actively inhibiting hypertrophy. *Trends Cardiovasc Med*. 2007;17:91–6.

268. Williams TM, Burlein JE, Ogden S, Kricka LJ, Kant JA. Advantages of firefly luciferase as a reporter gene: application to the interleukin-2 gene promoter. *Anal Biochem*. 1989;176:28–32.

269. Close DM, Xu T, Sayler GS, Ripp S. In vivo bioluminescent imaging (BLI): noninvasive visualization and interrogation of biological processes in living animals. *Sensors*. 2010;11:180–206.

270. Thompson JF, Hayes LS, Lloyd DB. Modulation of firefly luciferase stability and impact on studies of gene regulation. *Gene*. 1991;103:171–7.

271. Corish P, Tyler-Smith C. Attenuation of green fluorescent protein half-life in mammalian cells. *Protein Eng Des Sel*. 1999;12:1035–1040.

272. Shaner NC, Campbell RE, Steinbach PA, Giepmans BNG, Palmer AE, Tsien RY. Improved monomeric red, orange and yellow fluorescent proteins derived from Discosoma sp. red fluorescent protein. *Nat Biotechnol*. 2004;22:1567–1572.

273. Zhang G, Gurtu V, Kain SR. An enhanced green fluorescent protein allows sensitive detection of gene transfer in mammalian cells. *Biochem Biophys Res Commun*. 1996;227:707–711.

274. Wang Z, Ma H-I, Li J, Sun L, Zhang J, Xiao X. Rapid and highly efficient transduction by double-stranded adeno-associated virus vectors in vitro and in vivo. *Gene Ther*. 2003;10:2105–2111.

275. Ellis BL, Hirsch ML, Barker JC, Connelly JP, Steininger RJ, Porteus MH. A survey of ex vivo/in vitro transduction efficiency of mammalian primary cells and cell lines with Nine natural adeno-associated virus (AAV1-9) and one engineered adeno-associated virus serotype. *Virol J*. 2013;10:74.

276. Niwa H, Yamamura K, Miyazaki J. Efficient selection for high-expression transfectants with a novel eukaryotic vector. *Gene*. 1991;108:193–9.

277. McBurney MW, Staines WA, Boekelheide K, Parry D, Jardine K, Pickavance L. Murine PGK-1 promoter drives widespread but not uniform expression in transgenic mice. *Dev Dyn*. 1994;200:278–93.

278. Sladitschek HL, Neveu PA. Bidirectional promoter engineering for single cell microRNA sensors in embryonic stem cells. *PLoS One*. 2016;11:e0155177.

279. Schorpp M, Jager R, Schellander K, Schenkel J, Wagner EF, Weiher H, Angel P. The human Ubiquitin C promoter directs high ubiquitous expression of transgenes in mice. *Nucleic Acids Res*. 1996;24:1787–1788.

280. Fink D, Wohrer S, Pfeffer M, Tombe T, Ong CJ, Sorensen PHB. Ubiquitous expression of the monomeric red fluorescent protein mcherry in transgenic mice. *Genesis*. 2010;48:723–729.

281. Werfel S, Leierseder S, Ruprecht B, Kuster B, Engelhardt S. Preferential microRNA

targeting revealed by in vivo competitive binding and differential Argonaute immunoprecipitation. *Nucleic Acids Res*. 2017;45:10218–10228.

282. Brown BD, Gentner B, Cantore A, Colleoni S, Amendola M, Zingale A, Baccarini A, Lazzari G, Galli C, Naldini L. Endogenous microRNA can be broadly exploited to regulate transgene expression according to tissue, lineage and differentiation state. *Nat Biotechnol*. 2007;25:1457–1467.

283. Beillard E, Ong SC, Giannakakis A, Guccione E, Vardy LA, Voorhoeve PM. miR-sens - A retroviral dual-luciferase reporter to detect microRNA activity in primary cells. *Rna*. 2012;18:1091–1100.

284. Schug J, McKenna LB, Walton G, Hand N, Mukherjee S, Essuman K, Shi Z, Gao Y, Markley K, Nakagawa M, Kameswaran V, Vourekas A, Friedman JR, Kaestner KH, Greenbaum LE. Dynamic recruitment of microRNAs to their mRNA targets in the regenerating liver. *BMC Genomics*. 2013;14:264.

285. Eding JEC, Demkes CJ, Lynch JM, Seto AG, Montgomery RL, Semus HM, Jackson AL, Isabelle M, Chimenti S, van Rooij E. The efficacy of cardiac anti-miR-208a therapy is stress dependent. *Mol Ther*. 2017;25:694–704.

286. Hinkel R, Penzkofer D, Zühlke S, Fischer A, Husada W, Xu Q, Baloch E, van Rooij E, Zeiher AM, Kupatt C, Dimmeler S. Inhibition of microRNA-92a protects against ischemia/reperfusion injury in a large-animal model. *Circulation*. 2013;128:1066–1075.

287. Lucas T, Schäfer F, Müller P, Eming SA, Heckel A, Dimmeler S. Light-inducible antimiR-92a as a therapeutic strategy to promote skin repair in healing-impaired diabetic mice. *Nat Commun*. 2017;8:15162.

288. Shu D, Li H, Shu Y, Xiong G, Carson WE, Haque F, Xu R, Guo P. Systemic delivery of anti-miRNA for suppression of triple negative breast cancer utilizing RNA nanotechnology. *ACS Nano*. 2015;9:9731–9740.

289. Zhou J, Rossi J. Aptamers as targeted therapeutics: Current potential and challenges. *Nat Rev Drug Discov*. 2017;16:181–202.

290. Wagenaar TR, Tolstykh T, Shi C, Jiang L, Zhang J, Li Z, Yu Q, Qu H, Sun F, Cao H, Pollard J, Dai S, Gao Q, Zhang B, Arlt H, Cindhuchao M, Hoffmann D, Light M, Jensen K, Hopke J, Newcombe R, Garcia-Echeverria C, Winter C, Zabludoff S, Wiederschain D. Identification of the endosomal sorting complex required for transport-I (ESCRT-I) as an important modulator of anti-miR uptake by cancer cells. *Nucleic Acids Res*. 2015;43:1204–1215.

291. Liu HY, Gao X. A universal protein tag for delivery of siRNA-aptamer chimeras. *Sci Rep*.

2013;3:3129.

292. Lucas T, Bonauer A, Dimmeler S. RNA therapeutics in cardiovascular disease. *Circ Res*. 2018;123:205–220.

293. Bellera N, Barba I, Rodriguez-Sinovas A, Ferret E, Asín MA, Gonzalez-Alujas M, Pérez-Rodon J, Esteves M, Fonseca C, Toran N, Garcia del Blanco B, Pérez A, Garcia-Dorado D. Single intracoronary injection of encapsulated antagomir-92a promotes angiogenesis and prevents adverse infarct remodeling. *J Am Heart Assoc*. 2014;3:8–10.

294. Li Y, Duo Y, Bi J, Zeng X, Mei L, Bao S, He L, Shan A, Zhang Y, Yu X. Targeted delivery of anti-miR-155 by functionalized mesoporous silica nanoparticles for colorectal cancer therapy. *Int J Nanomedicine*. 2018;13:1241–1256.

8 Acknowledgments

Firstly, I would like to express my sincere gratitude to Prof. Dr. Dr. Stefan Engelhardt for giving me the opportunity to conduct this thesis in his lab. When joining his team I could not have imagined how much I would profit as a scientist but also as a person. I also thank him for the chance to participate in scientific meetings and for his support to apply and acquire a three-years scholarship from the Bayerische Forschungsstiftung.

Besides my first supervisor, I thank Prof. Dr. Arne Skerra, who believed in me and accepted to be my second supervisor. His offer to present my progress in his department of biological chemistry in Weihenstephan gave me the pleasure to interact with scientists from another faculty and scientific background.

My sincere thanks goes also to my mentor concerning my thesis committee, Dr. Bernhard Laggerbauer, whose suggestions improved my research from various perspectives. I would also like to thank him for correcting many of my drafts concerning scientific projects.

I would like to individually thank Prof. Dr. Christos Panagiotidis, who was the one who -with his unique lectures in the university- made me to fall in love with science.

My deepest gratitude goes to Dr. Yassine Sassi, who definitely shaped me as a scientist and became much more than a colleague to me. Working with him was such a pleasure, many times we caught ourselves being in the lab too late without even realizing. His motivation, cleverness, experience, but more than anything else, his moral character, characterize this brilliant scientist.

I thank all my lab mates for their support and the fruitful discussions, as well as for the nice working environment. I would like to particularly thank Dena Esfandyari, Dr. Giulia Felician, and Dr. Anne Dueck for the daily assistance and nice atmosphere in the lab. Moreover, I thank Dr. Deepak Ramanujam for offering help during my first steps in the lab and Dr. Stanislas Werfel for introducing me to the world of microscopy. Thanks to Celia Borja who brought with her Spanish temperament the sunshine to our institute. Dr. Vanessa Philippi saved me a lot of working hours by helping organizing the formalities concerning mice studies. Dr. Andrea Welling was also involved in the revision and submission of respective applications. A special thanks goes to Dr. Ibrahim Bedioune, whose presence in the lab made me re-evaluate the priorities of life, and made it a pleasure working with him. I will definitely miss him.

Moreover, my work has become much easier because of the help of Sabine Brummer, who produced countless viruses for me, Urszula Kremser, who isolated neonatal rat cardiac myocytes on a weekly basis, Lucia Koblitz, who performed Langendorff perfusions from hearts of adult mice and rats, and also always cared that we get a table at the Oktoberfest, Pascal Baclet, Kornelija Sakac, Julia Kerler and Anton Bomhard for operations and echocardiographic

measurements and analysis of mice, Saskia Rausch and Astrid Vens for helping with plasmid preparations and dealing with the lab bureaucracy. Norbert Ertl was always there to fix anything, from a computer to the coffee machine in the kitchen, Selahattin Sahiner, Matija Curkovic, Antonio Sterle and Mehmet Durmaz did a great job looking after the mice and rats, and Michaela Hennig, Hannelore Brand, Selina Weber and Violetta Cavic were always helpful organizing everything - from contracts, holidays and appointments, to the Christmas Party.

In addition I would like to thank all the students that worked with me, Anna Näger, Andreas-David Brunner, Simon Giosele, Theresa Siekmann, Joshua Ludwig and Theresa Hiltner for their help.

Furthermore, I am grateful to Ronald Naumann, group leader of the transgenic core facility at Max Planck institute of molecular cell biology and genetics in Dresden, who performed the blastocyst injections of our recombined embryonic stem cells.

A special thanks goes to the “Bayerische Forschungsstiftung”, who granted me among other international students with a 3-year scholarship and opportunities to interact with other scientists from all over the world. I really enjoyed the trips organized every year!

Last, but not least, I would like to thank my parents and my sister for their love, support, and for the opportunity to study, and my wife, whose love, understanding and encouragement always helped me to find the right way. Without them this dissertation would not be possible.